

**ELG 6369**

**NONLINEAR MICROWAVE DEVICES AND EFFECTS**

**CHAPTER III**

**NONLINEAR CIRCUIT DESIGN**

In the previous chapter, we investigated different models for microwave active components, i.e., diodes and transistors. The next step would be to switch to the circuit level and thus, to include these models in RF/microwave circuits and evaluate how they react in small-signal/large-signal (linear/nonlinear) circuit simulation, optimization, and statistical design.

## A – LINEAR MICROWAVE CIRCUIT DESIGN

Linear circuit design has been widely investigated in the last 50 years and several methods have been proposed to designers. Three of them are now mainly used to design microwave linear and nonlinear circuits and systems namely, the connection-scattering matrix approach, the multiport connection method, and the sub-network method.

### I- Analysis using connection-scattering matrix

This approach is applicable when the network contains arbitrarily interconnected multi-ports and independent generators. Consider a network with  $M$  multiport components. For the  $k^{\text{th}}$  component having  $n_k$  ports, the incoming and outgoing wave vectors ( $[\mathbf{a}_k]$  and  $[\mathbf{b}_k]$ , respectively) at its ports are related by

$$[\mathbf{b}_k] = [\mathbf{S}_k][\mathbf{a}_k] \quad (\text{III-1})$$

This is valid for all the components except the independent generators where

$$[\mathbf{b}_k] = [\mathbf{S}_k][\mathbf{a}_k] + [\mathbf{c}_k] \quad (\text{III-2})$$

where  $[\mathbf{c}_k]$  is the wave vector impressed by the generator. It should be pointed out that no unconnected (i.e., external) ports are allowed in this network.

---

*The materials you receive for this course are protected by copyright and to be used for this course only. You do not have permission to upload the course materials, including any lecture recordings you may have, to any website. If you require clarification, please consult your professor.*

The governing relations for all the  $M$  elements can be put together in the form (Figure III-1)

$$[\mathbf{b}] = [\mathbf{S}][\mathbf{a}] + [\mathbf{c}] \Leftrightarrow \begin{bmatrix} [\mathbf{b}_1] \\ \vdots \\ [\mathbf{b}_M] \end{bmatrix} = \begin{bmatrix} [\mathbf{S}_1] & [\mathbf{0}] & \cdots & [\mathbf{0}] \\ [\mathbf{0}] & \ddots & \ddots & \vdots \\ \vdots & \ddots & \ddots & [\mathbf{0}] \\ [\mathbf{0}] & \cdots & [\mathbf{0}] & [\mathbf{S}_M] \end{bmatrix} \begin{bmatrix} [\mathbf{a}_1] \\ \vdots \\ [\mathbf{a}_M] \end{bmatrix} + \begin{bmatrix} [\mathbf{c}_1] \\ \vdots \\ [\mathbf{c}_M] \end{bmatrix} \quad (\text{III-3})$$

This equation contains the characterizations of individual components but does not take into account the constraints imposed by interconnections. For a pair of connected ports, the outgoing wave variable at one port must equal the incoming wave variable at the other, assuming that the wave variables at the two connected ports are similarly normalized.

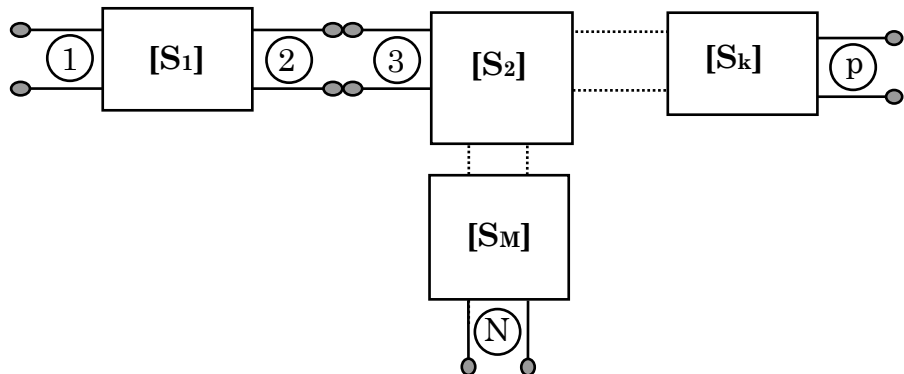


Fig. III-1. Example of a multiport network with  $M$ -elements and  $N$  external ports.

For instance, if port  $j$  of one component is connected to port  $k$  of another component, the wave variables should satisfy to

$$\begin{bmatrix} b_j \\ b_k \end{bmatrix} = \begin{bmatrix} 0 & 1 \\ 1 & 0 \end{bmatrix} \begin{bmatrix} a_j \\ a_k \end{bmatrix} \quad (\text{III-4})$$

---

*The materials you receive for this course are protected by copyright and to be used for this course only. You do not have permission to upload the course materials, including any lecture recordings you may have, to any website. If you require clarification, please consult your professor.*

The elements of the above matrix are "1's" or "0's" because the normalizing impedances for the ports are assumed to be equal. For the overall circuit, we can introduce a connection matrix  $[\Gamma]$ , which describes the topology

$$[\mathbf{b}] = [\Gamma] [\mathbf{a}] \quad (\text{III-5})$$

In each row of  $[\Gamma]$ , all elements are "0" except an entry "1" in the column indicating the interconnection. Substituting for  $[\Gamma]$  from (III-5) to (III-3), we obtain

$$\{ [\Gamma] - [\mathbf{S}] \} [\mathbf{a}] = [\mathbf{W}] [\mathbf{a}] = [\mathbf{c}] \Leftrightarrow [\mathbf{a}] = [\mathbf{W}]^{-1} [\mathbf{c}] \quad (\text{III-6})$$

$[\mathbf{W}]$  is called the connection scattering matrix. The elements in the main diagonal of  $[\mathbf{W}]$  are the negative of the reflection coefficients at the various component ports. This matrix depends only on the topology of the network and does not change with the component characteristics or frequency. It allows to obtain the vector  $[\mathbf{a}]$  and then, using (III-5), to deduce the vector  $[\mathbf{b}]$ . Therefore, the overall scattering matrix of the circuit is totally defined by the following relation

$$[\mathbf{b}] = [\mathbf{S}_g] [\mathbf{a}] \quad (\text{III-7})$$

## II- Multiport connection method

In this method, the scattering matrix of the network is also determined using the individual S-matrices of each component/sub-network. This method is applicable when the network contains arbitrarily interconnected multiport components without independent generators. In this case, incoming and outgoing waves can be separated into two groups; the first is corresponding to the  $p$  external ports, and the second to the  $c$  internally connected ports.

---

*The materials you receive for this course are protected by copyright and to be used for this course only. You do not have permission to upload the course materials, including any lecture recordings you may have, to any website. If you require clarification, please consult your professor.*

We have then

$$\begin{bmatrix} [\mathbf{b}_p] \\ [\mathbf{b}_c] \end{bmatrix} = \begin{bmatrix} [\mathbf{S}_{pp}] & [\mathbf{S}_{pc}] \\ [\mathbf{S}_{cp}] & [\mathbf{S}_{cc}] \end{bmatrix} \begin{bmatrix} [\mathbf{a}_p] \\ [\mathbf{a}_c] \end{bmatrix} \quad (\text{III-8})$$

where  $[\mathbf{S}_{pp}]$ ,  $[\mathbf{S}_{pc}]$ ,  $[\mathbf{S}_{cp}]$  and  $[\mathbf{S}_{cc}]$  are the S sub-matrices determined after separation of ports. As in the previous method, a connection matrix  $[\Gamma]$  allows to take into account the interconnections between the internal blocks (either components or sub-circuits)

$$[\mathbf{b}_c] = [\Gamma] [\mathbf{a}_c] = [\mathbf{S}_{cp}] [\mathbf{a}_p] + [\mathbf{S}_{cc}] [\mathbf{a}_c] \quad (\text{III-9})$$

$\Downarrow$

$$[\mathbf{a}_c] = \{ [\Gamma] - [\mathbf{S}_{cc}] \}^{-1} [\mathbf{S}_{cp}] [\mathbf{a}_p] \quad (\text{III-10})$$

By substitution into (III-8), we obtain

$$[\mathbf{b}_p] = [\mathbf{S}_{pp}] [\mathbf{a}_p] + [\mathbf{S}_{pc}] [\mathbf{a}_c] = \{ [\mathbf{S}_{pp}] + [\mathbf{S}_{pc}] ([\Gamma] - [\mathbf{S}_{cc}])^{-1} [\mathbf{S}_{cp}] \} [\mathbf{a}_p] \quad (\text{III-11})$$

The overall S-matrix is the one that relates between the incoming and the outgoing wave variables of the external ports. It is then equal to

$$[\mathbf{S}_g] = [\mathbf{S}_p] = [\mathbf{S}_{pp}] + [\mathbf{S}_{pc}] ([\Gamma] - [\mathbf{S}_{cc}])^{-1} [\mathbf{S}_{cp}] \quad (\text{III-12})$$

### III- Sub-network growth method

In the two first methods, obtaining the S-matrix of a network requires to invert a matrix of order equals to the number of interconnected ports. When the network contains many interconnected ports, the order of the matrix to be inverted will become quite large. The computational effort of inverting the matrix can be reduced considerably if the entire network is not taken at once, but it portioned into a number of sub-networks. The S-matrices of the sub-networks are obtained separately and are then combined to obtain the overall S-matrix.

### IV- Comparison between the different methods

In order to choose the appropriate method, Gupta *et al.* compared their performance based on a practical example. The multiport connection method requires a huge CPU time and does not take into account the external loads and sources. The sub-network approach is more efficient but it is often difficult to achieve a complete partition of the network. So, based on the above remarks, the first namely, the connection-scattering matrix method, is the most efficient one.

### V- Example: 3-dB rat-race hybrid design

In order to illustrate how to implement this method, let us consider a "3-dB rat-race coupler" designed by Gupta *et al.* at 3 GHz on a microstrip line with a permittivity of 9.8 (Figure III-2). Its decomposition shows eight elementary elements ( $M = 8$ ):

- Four Te junctions (noted TJ1 to TJ4). Their characteristic impedances are  $Z_0$  (for the external line) and  $Z_1$  (for the internal connected lines).
  - Four transmission lines (noted TL1 to TL4). Their characteristic impedances are  $Z_1$ . The three first have a  $\lambda/4$  length and the last  $3\lambda/4$  length.
- 

*The materials you receive for this course are protected by copyright and to be used for this course only. You do not have permission to upload the course materials, including any lecture recordings you may have, to any website. If you require clarification, please consult your professor.*

## B – NONLINEAR APPROACHES TO CIRCUIT ANALYSIS

### I – Experimental approaches

#### 1 – Load pull approach

The early nonlinear models and techniques that attempted to bend linear theory to nonlinear applications were approximate or assumed “black box” characterizations that did not include all the variables or parameters necessary to obtain meaningful results.

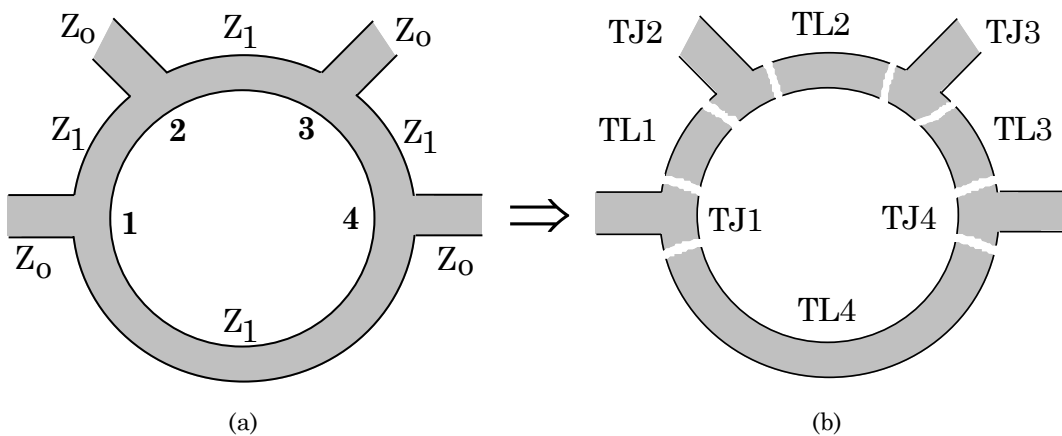


Fig. III-2. Rat-race coupler (a) and its decomposition in elementary elements (b).

One straightforward way to characterize a nonlinear behaviour, such as in a power amplifier, is to graph on a Smith chart the contours of its load impedances that result in prescribed values of gain and output powers. These approximately circular contours can then be used to select output the load impedance that represents the best trade-off of gain against power. The contours are generated empirically by connecting various loads to the amplifier and by measuring the gain and output power at each value of load impedance.

---

*The materials you receive for this course are protected by copyright and to be used for this course only. You do not have permission to upload the course materials, including any lecture recordings you may have, to any website. If you require clarification, please consult your professor.*

This process, called load pulling, has many limitations; the most serious practical one is the difficulty of measuring the load impedances at the device terminals. Load pulling has a major theoretical problem as well: the load impedance at harmonics of the excitation frequency can significantly affect circuit performance, but load pulling is concerned only with the load impedance at the fundamental frequency. Furthermore, load pulling is not useful for determining other important properties of nonlinear circuits (e.g., harmonic levels or effects of multi-tone excitations).

## 2 – S-parameter measurements at large-signal excitation

Another approach to the analysis of nonlinear circuits is to measure a set of two-port parameters, usually S-parameters, at the large-signal excitation level. The standard small-signal equations for S-parameters design are then used to predict the performance characteristics of the circuit. This approach may have limited success if the circuit is not strongly nonlinear. In fact, S-parameters are fundamentally a linear concept and the large-signal S-parameter approach is only a brutal attempt to force nonlinear circuits to obey linear circuit theory under some conditions.

## II – Time domain approaches

An intermediate approach, which is practical for low-frequency analog and digital design, is to use time-domain techniques. This approach is theoretically valid because the use of time-domain differential equations that describe a nonlinear circuit is straightforward in conventional circuit theory. The resulting differential equations in the form of a nonlinear differential system

$$f\left(\left[\mathbf{x}(t)\right], \left[\frac{d\mathbf{x}(t)}{dt}\right], t\right) = 0 \quad \left[\mathbf{x}(0)\right] = \left[\mathbf{x}_0\right] \quad (\text{III-13})$$

---

The materials you receive for this course are protected by copyright and to be used for this course only. You do not have permission to upload the course materials, including any lecture recordings you may have, to any website. If you require clarification, please consult your professor.

and can be solved numerically (here  $\mathbf{x}$  is a vector containing the unknown variables like voltages or currents at the different nodes of the circuit). In fact, time-domain analyses are usually numerical integration methods, which discretize point by point the time variable and then linearize the nonlinear differential system.

The shooting method (which allow obtaining the steady state by optimizing the initial conditions and integrating over only one period) and the successive approximations method (which start from an estimate value of the initial point) are the two most used techniques in nonlinear time domain analyses. These methods present several advantages. First, they allow the analysis of highly nonlinear transient behaviours. Second, the input-output characteristics are already in the time domain. Therefore, the system can have very low dimensions (the number of equations is equal to the number of nodes in the circuit).

Although time-domain techniques are more practical for analyzing circuits that include only lumped elements, they can be used with a limited variety of distributed elements such as ideal transmission lines. In fact, lossy transmission lines cannot be modeled efficiently in time domain (even if some physical/electrical “equivalent” models are available in several time-domain simulators, e.g., *HSpice*).

The two major limitations of time-domain analysis are its inability to handle frequency-domain quantities (e.g., impedances at different frequencies) and the difficulty of applying it to circuits having non-commensurate excitations. However, this technique cannot deal with new circuits where transmission lines can present a significant time delay. In this case, as the integration step must be at least equal to two times the smallest time constant in the circuit, the transient analysis computation may require a huge number of integrations.

---

*The materials you receive for this course are protected by copyright and to be used for this course only. You do not have permission to upload the course materials, including any lecture recordings you may have, to any website. If you require clarification, please consult your professor.*

### III – Frequency domain approaches

Frequency-domain techniques are the most efficient to analyze the nonlinear behaviours of weakly nonlinear circuits having multiple non-commensurate small-signal excitations. The nonlinearities in these circuits are often so weak that they have a negligible effect on their linear response. However, the nonlinear phenomena in such quasi-linear circuits can affect system performance (in terms of intermodulation distortion). The problem of analyzing such circuits is called the *small signal nonlinear problem*.

Two frequency-domain techniques are usually used. The first is *power-series analysis* and the second is *Volterra series analysis*.

#### 1 – Power series analysis

This technique is relatively easy to use but requires a simplifying assumption that is often unrealistic: the circuit should contain only ideal memory-less transfer nonlinearities. However, the power-series approach can give to the designer a good intuitive sense of the behaviour of many types of nonlinear circuits.

Many nonlinear systems can be modeled like filters or other frequency-selective networks followed by a memory-less transfer nonlinearity as shown on Figure III-3. The transfer function of the can be written as

$$w(t) = \sum_{k=1}^N w_k(t) = f(u(t)) = \sum_{k=1}^N a_k u^k(t) = a_1 u(t) + a_2 u^2(t) + a_3 u^3(t) + \dots \quad (\text{III-14})$$

---

The materials you receive for this course are protected by copyright and to be used for this course only. You do not have permission to upload the course materials, including any lecture recordings you may have, to any website. If you require clarification, please consult your professor.

For illustration, let us consider a simplified circuit of a FET (Figure III-4).

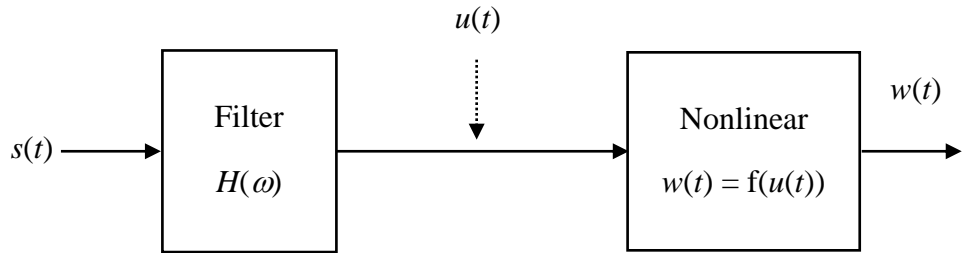


Fig. III-3. Power series model of a nonlinear system.

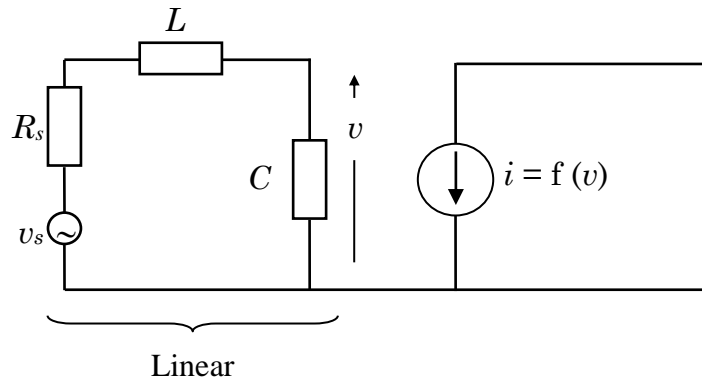


Fig. III-4. Simplified equivalent circuit of a FET.

The input linear transfer function is

$$H(\omega) = \frac{V(\omega)}{V_s(\omega)} = \frac{1}{R_s C j\omega - LC\omega^2 + 1} \quad (\text{III-15})$$

and the nonlinear function is  $\{ i = f(v) \}$  which can be expended in Taylor series around the dc bias voltage  $V_{gs0}$  across the capacitor  $C$

$$f(v) = F(V_{gs0} + v) - F(V_{gs0}) = v \frac{dF(V)}{dV} \Big|_{V=V_{gs0}} + \frac{1}{2} v^2 \frac{d^2 F(V)}{dV^2} \Big|_{V=V_{gs0}} + \frac{1}{6} v^3 \frac{d^3 F(V)}{dV^3} \Big|_{V=V_{gs0}} + \dots \quad (\text{III-16})$$

In the case where the excitation contains at least two non-commensurate frequencies

$$s(t) = v_s(t) = \frac{1}{2} \sum_{q=1}^Q \left\{ V_{s,q} \exp(j\omega_q t) + V_{s,q}^* \exp(-j\omega_q t) \right\} \quad (\text{III-17})$$

$$\rightarrow s(t) = v_s(t) = \frac{1}{2} \sum_{\substack{q=-Q \\ q \neq 0}}^Q V_{s,q} \exp(j\omega_q t) \quad (\text{III-18})$$

the output of the linear circuit is

$$u(t) = v(t) = \frac{1}{2} \sum_{\substack{q=-Q \\ q \neq 0}}^Q V_{s,q} H(\omega_q) \exp(j\omega_q t) \quad (\text{III-19})$$

In these equations  $\{\omega_{-q} = -\omega_q\}$ ,  $\{V_{s,-q} = (V_{s,q})^*\}$  and  $\{H(\omega_{-q}) = H^*(\omega_q)\}$ .

The output of the nonlinear stage is found by substituting  $v(t)$  into equation (III-14).

$$a_n v^n(t) = a_n \left[ \frac{1}{2} \sum_{\substack{q=-Q \\ q \neq 0}}^Q V_{s,q} H(\omega_q) \exp(j\omega_q t) \right]^n \quad (\text{III-20})$$

$$= \sum_{k=1}^N a_k \left\{ \sum_{q_1=-Q}^Q \dots \sum_{q_k=-Q}^Q V_{q_1} \dots V_{q_k} H(\omega_{q_1}) \dots H(\omega_{q_k}) e^{(j\omega_{q_1} + \dots + j\omega_{q_k})t} \right\} \quad (\text{III-21})$$

Therefore, the response is

$$w(t) = i(t) = \sum_{n=1}^N a_n v^n(t) \quad (\text{III-22})$$

In order to illustrate this development, let us consider the case of two-tone excitation ( $Q = 2$ ) and find the part of the response associated with the second-degree component of the output current ( $n = 2$ ). The degree of the nonlinearity refers to the power of  $u(t)$  in the nonlinear transfer characteristic, while the order is defined as one that arises from the sum of  $n$  excitation frequencies.

**Note:** The frequency {  $2\omega_1 - \omega_2$  } appears at first to be the third order, that is

$$2\omega_1 - \omega_2 = \omega_1 + \omega_1 - \omega_2 \quad (\text{III-23})$$

but it could be also the fifth order-mixing product

$$2\omega_1 - \omega_2 = \omega_1 + \omega_1 + \omega_1 - \omega_1 - \omega_2 \quad (\text{III-24})$$


---

Therefore, in complicated circuits, a nonlinearity of degree  $n$  can generate mixing products of order equal to or greater than  $n$ .

Power series analysis is equivalent to Volterra series analysis in the case of memory-less transfer nonlinearities and therefore is a good introduction to the Volterra series.

## 2 – Volterra series analysis

Volterra series analysis or nonlinear transfer function analysis is a very powerful technique that does not require restrictive assumptions. The model used for the Volterra analysis, shown in Figure III-5, is essentially the same of the power series, except that the separation between the memory-less and the reactive parts of the circuit (linear selective circuit) has been eliminated.

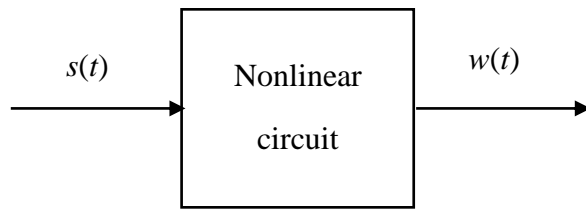


Fig. III-5. Volterra series model of a nonlinear system.

In this case, the nonlinear elements may be either resistive or reactive, and they are characterized by power series having a similar form as in equation (III-14).

$$s(t) = \sum_{k=1}^N \left\{ \sum_{q_1=-Q}^Q \dots \sum_{q_k=-Q}^Q V_{q_1} \dots V_{q_k} H_k(\omega_{q_1}, \dots, \omega_{q_k}) e^{(\omega_{q_1} + \dots + \omega_{q_k})t} \right\} \quad (\text{III-25})$$

The only difference between (III-9) and (III-13) is that (III-13) contains a single transfer function  $H_k(\omega_{q1}, \dots, \omega_{qk})$  instead of a product of elementary linear transfer functions " $a_k \cdot H(\omega_{q1}) \dots H(\omega_{qk})$ ". This function  $H_k$ , called the  $k$ th-order nonlinear transfer function, allows the definition of intermodulation products.

Volterra-series analysis is based on the same assumptions and is subject to almost same limitations as power-series analysis:

- The circuits are weakly nonlinear
- The multiple excitations are small and non-commensurate

In other words, the order  $N$  of the series must be low to avoid the complex algebraic manipulations. This conclusion becomes an imperative condition in the case of multiple excitations ( $M$  input signals)

$$x_i(t) = \sum_{k=1}^N x_k^{(i)}(t) = \sum_{k=1}^N |x_k^{(i)}| \cos(\omega_k t + \varphi_k^{(i)}) \quad i = 1, \dots, m \quad (\text{III-26})$$

that gives the following output response

$$s(t) = \sum_{p_1=0}^{\infty} \dots \sum_{p_M=0}^{\infty} a_{p,q} \prod_{i=1}^M \left( \sum_{k=1}^N \alpha_k^{(i)} x_k^{(i)} (t - \tau_{ki})^i \right) \quad (\text{III-27})$$

where the coefficients  $a_{p,q}$  and  $\alpha_k^{(i)}$  are respectively complex and real and where the time delays  $\tau_{ki}$  depends on the order of the series.

---

Both Volterra- and power-series allow multi-frequency analyses and efficient evaluation of the intermodulation products. Frequency generation process, intermodulation products (like the third intercept point) and power relations are easy to obtain in the frequency domain.

But on the other hand,

- The frequency domain cannot allow easy modeling of device input-output relationships (e.g., the exponential I-V function of a diode),
- The analyzes are limited to weakly nonlinearities,
- The system of equations to solve has high dimensions (the number of equations is equal to the product of the number of nodes by the number of harmonics to consider),
- The mathematical process to expand a given current-voltage relationship into power series or Volterra series is difficult to achieve.

#### IV – Hybrid domain approaches

To overcome the main limitations imposed by the above time- or frequency-domain approaches, two important hybrid techniques can be used.

The first, called *harmonic balance*, is most useful for strongly or weakly nonlinear circuits that have single-tone excitation. It can be applied to a wide variety of circuits such as power amplifiers, frequency multipliers and mixers subjected to local oscillator drive.

The second, called *large-signal small-signal analysis*, is used for nonlinear circuits that are excited by two tones, one of which is very large and the other is vanishingly small. This situation is encountered most frequently in microwave mixers wherein a nonlinear element is excited by a large-signal local oscillator and a much smaller received RF signal. The circuit is first analyzed via harmonic balance, under local oscillator excitation alone, and it converted into a small-signal linear,

---

*The materials you receive for this course are protected by copyright and to be used for this course only. You do not have permission to upload the course materials, including any lecture recordings you may have, to any website. If you require clarification, please consult your professor.*

time-varying equivalent. The time-varying circuit is then analyzed as a quasi-linear circuit under small-signal RF excitation.

## V – Summary of various nonlinear approaches

In table III-I, we have summarized the most used frequency- and time-domain approaches in microwave CAD.

Table III-I: Classification of nonlinear analysis techniques.

NON LINEAR NETWORK			
		Time Domain	Frequency Domain
L I N E A R	Time Domain	Extrapolation methods Direct integration methods	X
	Frequency Domain	Harmonic Balance [ Direct Methods, relaxation and optimum methods, ...]	Volterra Series Power Series Descriptive Functions

---

The materials you receive for this course are protected by copyright and to be used for this course only. You do not have permission to upload the course materials, including any lecture recordings you may have, to any website. If you require clarification, please consult your professor.

## C – HARMONIC BALANCE ANALYSIS

### I – Introduction

A general circuit that describes many of nonlinear circuits is shown on Figure III-6.

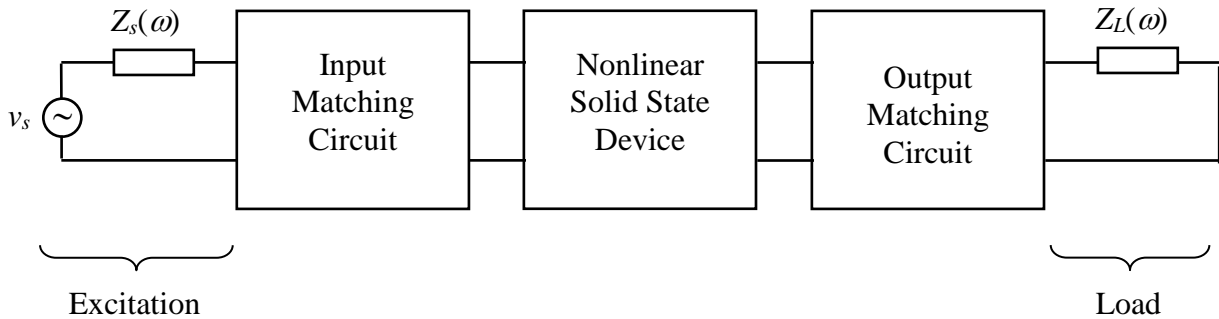


Fig. III-6. Equivalent circuit of a general nonlinear two-port device.

The circuit consists of a nonlinear solid-state component (often a transistor or a diode) that is connected to a load and a source of signal frequency large-signal excitation. Matching networks are used at the input and output to optimize the circuit performance, to couple bias voltages to the device, to filter and terminate various harmonics appropriately (filters, matching cells, bias circuits, ...). The matching networks are invariably linear and the problem of analyzing this type of circuit does not seem too difficult (these circuits are usually LC circuits).

One could start by writing a set of time domain differential equations describing the combined nonlinear device and matching networks, solving them to obtain the steady-state voltage waveform across the load, and Fourier-transforming to obtain the frequency component corresponding to the desired output harmonic. As the differential equations would be nonlinear and have to be solved numerically, three problems often occur that can make such time-domain techniques impractical

---

*The materials you receive for this course are protected by copyright and to be used for this course only. You do not have permission to upload the course materials, including any lecture recordings you may have, to any website. If you require clarification, please consult your professor.*

- The matching circuits may contain elements such as dispersive transmission lines and transmission-line discontinuities that are difficult to analyze in time domain. The best is to use a set of S-parameters at each harmonic. However, these parameters are frequency domain quantities and cannot be used to characterize the other part of the overall circuit, namely the nonlinear device.
- The circuit may have time constants that are large compared to the inverse of the fundamental excitation frequency. When these exist, it becomes necessary to continue the numerical integration of the equations through many excitation cycles until the transient part of the response has decayed and only the steady-state part remains. As the number of iterations can be very high (perhaps thousands), this long integration is an extravagant use of computer time and a source of large numerical errors that reduce the accuracy of the solution. Although algorithms exist to ameliorate this difficulty, their implementation is an extra complication.
- Each linear and nonlinear reactive element in the circuit adds a differential equation to the set of equations that describes the circuit. A large system can have many reactive elements, so the set of equations that must be solved may be very large.

It is then preferable to use multiport circuit theory to simplify at least part of the circuit by lumping all the linear reactances, impedances, transmission lines, and other linear elements into a single matrix of limited size. By describing the linear part of the circuit as one multiport, it need be evaluated only once at each harmonic, with the results stored as matrices, and no further evaluation is necessary.

## II – Harmonic balance approach

To overcome the above limitations of pure time- or frequency-domain approaches, Nakhla and Vlach introduced an alternative approach, called "Harmonic Balance technique".

---

*The materials you receive for this course are protected by copyright and to be used for this course only. You do not have permission to upload the course materials, including any lecture recordings you may have, to any website. If you require clarification, please consult your professor.*

This hybrid approach is based on the principle of dividing the nonlinear circuit into two sub-circuits:

- The first sub-circuit, called linear sub-network, will contain all linear elements (bias networks, filters, matching networks and all linear elements of active device equivalent circuits).
- The second, called nonlinear sub-network, will contain all nonlinear elements.

In fact, the circuit elements in Figure III-6 can be regrouped as shown in Figure III-7, so that they form a linear sub-circuit and a number of nonlinear elements (the nonlinear elements, as a group, are called the nonlinear sub-circuit).

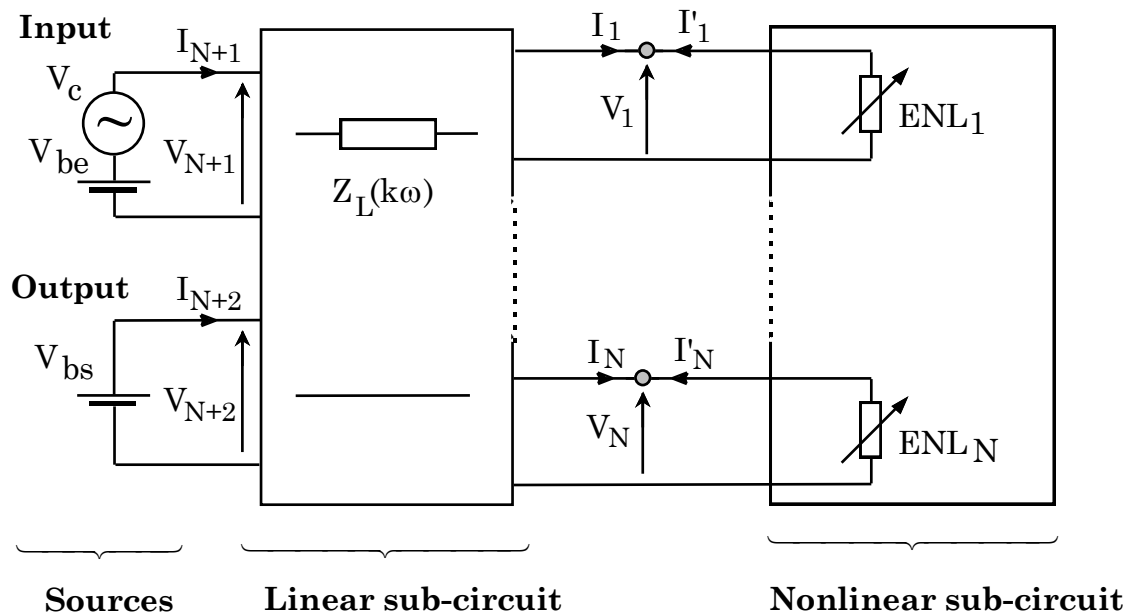


Fig. III-7. Nonlinear microwave circuit, divided into linear and nonlinear sub-circuits, with the source and load impedances absorbed into the linear sub-circuit.

*The materials you receive for this course are protected by copyright and to be used for this course only. You do not have permission to upload the course materials, including any lecture recordings you may have, to any website. If you require clarification, please consult your professor.*

The linear sub-circuit can be treated as a linear multiport and described by its  $Y$ -,  $Z$ -, or  $S$ -parameters (frequency domain). The nonlinear elements are modeled by their global  $I$ - $V$  or  $Q$ - $V$  characteristics, and must be analyzed in the time domain. Thus the circuit is reduced to an  $N+2$  port network, with nonlinear elements connected to  $N$  of the ports and voltages sources connected to the other two ports. The  $N+1^{\text{th}}$  and  $N+2^{\text{th}}$  ports represent the input and output ports in a two-port network, respectively.

Usually, a sinusoidal source is connected to only one of those ports. However, sources are shown at both ports for complete generality. The source and load impedances, respectively  $Z_s(\omega_p)$  and  $Z_L(\omega_p)$ , are included into the linear sub-circuit where  $\omega_p$  is the excitation pulsation.

The voltages and currents at each port can be expressed in the time or the frequency domain. For numerical purposes, only a finite number  $M$  of harmonics is considered ( $k = 1, \dots, M$ ). The circuit is analyzed when either the steady-state voltage or current waveforms at each port are known.

The idea of harmonic balance is to find sets of port voltage waveforms (or alternatively, the harmonic voltage components) that give the same currents in both the linear sub-circuit equations and the nonlinear sub-circuit equations.

If we express the port-current frequency components as vectors, Kirchhoff's current law requires that:

$$\begin{bmatrix} I_{1,0} \\ \vdots \\ I_{1,M} \\ \vdots \\ I_{N,0} \\ \vdots \\ I_{N,M} \end{bmatrix} + \begin{bmatrix} I'_{1,0} \\ \vdots \\ I'_{1,M} \\ \vdots \\ I'_{N,0} \\ \vdots \\ I'_{N,M} \end{bmatrix} = \begin{bmatrix} 0 \\ \vdots \\ 0 \\ \vdots \\ 0 \\ \vdots \\ 0 \end{bmatrix} \quad (\text{III-28})$$

where  $I_{n,k}$ , a phasor quantity, is the  $k^{\text{th}}$  harmonic component of the current at port  $n$ , calculated via the port voltages and the admittance matrix  $[\mathbf{Y}]$  of the linear sub-circuit;  $I'_{n,k}$  is the current component calculated via the same port voltages and the nonlinear elements. This general notation will be used for all voltage and current vectors.

The vectors include only positive-frequency components because the negative-frequency components, being the complex conjugates of the positive-frequency components, can be found immediately if needed.

First the admittance matrix of the linear sub-circuit should satisfy the following equation:

$$\begin{bmatrix} [\mathbf{I}_1] \\ [\mathbf{I}_2] \\ [\mathbf{I}_3] \\ \vdots \\ [\mathbf{I}_N] \\ [\mathbf{I}_{N+1}] \\ [\mathbf{I}_{N+2}] \end{bmatrix} = \begin{bmatrix} [\mathbf{Y}_{1,1}] & [\mathbf{Y}_{1,2}] & \cdots & [\mathbf{Y}_{1,N}] & [\mathbf{Y}_{1,N+1}] & [\mathbf{Y}_{1,N+2}] \\ [\mathbf{Y}_{2,1}] & [\mathbf{Y}_{2,2}] & \cdots & [\mathbf{Y}_{2,N}] & [\mathbf{Y}_{2,N+1}] & [\mathbf{Y}_{2,N+2}] \\ [\mathbf{Y}_{3,1}] & [\mathbf{Y}_{3,2}] & \cdots & [\mathbf{Y}_{3,N}] & [\mathbf{Y}_{3,N+1}] & [\mathbf{Y}_{3,N+2}] \\ \vdots & \vdots & \vdots & \cdots & \vdots & \vdots \\ [\mathbf{Y}_{N,1}] & [\mathbf{Y}_{N,2}] & \cdots & [\mathbf{Y}_{N,N}] & [\mathbf{Y}_{N,N+1}] & [\mathbf{Y}_{N,N+2}] \\ [\mathbf{Y}_{N+1,1}] & [\mathbf{Y}_{N+1,2}] & \cdots & [\mathbf{Y}_{N+1,N}] & [\mathbf{Y}_{N+1,N+1}] & [\mathbf{Y}_{N+1,N+2}] \\ [\mathbf{Y}_{N+2,1}] & [\mathbf{Y}_{N+2,2}] & \cdots & [\mathbf{Y}_{N+2,N}] & [\mathbf{Y}_{N+2,N+1}] & [\mathbf{Y}_{N+2,N+2}] \end{bmatrix} \begin{bmatrix} [\mathbf{V}_1] \\ [\mathbf{V}_2] \\ [\mathbf{V}_3] \\ \vdots \\ [\mathbf{V}_N] \\ [\mathbf{V}_{N+1}] \\ [\mathbf{V}_{N+2}] \end{bmatrix} \quad (\text{III-29})$$

where each sub-vector  $[\mathbf{I}_k]$  and  $[\mathbf{I}_k]$  represent the harmonic currents and voltages at the  $k^{\text{th}}$  port,

$$[\mathbf{I}_k] = \begin{bmatrix} I_{k,0} \\ I_{k,1} \\ \vdots \\ I_{k,M} \end{bmatrix} \quad (\text{III-30})$$

and

$$[\mathbf{V}_k] = \begin{bmatrix} V_{k,0} \\ V_{k,1} \\ \vdots \\ V_{k,M} \end{bmatrix} \quad (\text{III-31})$$


---

*The materials you receive for this course are protected by copyright and to be used for this course only. You do not have permission to upload the course materials, including any lecture recordings you may have, to any website. If you require clarification, please consult your professor.*

The elements of the admittance matrix  $[\mathbf{Y}]$  as given in (III-29) are all matrices; each sub-matrix is diagonal, whose elements  $Y_{m,n}$  are the admittances  $\{ Z_L(k\omega_p) \}^{-1}$  between ports  $m$  and  $n$  at each harmonic  $k$  of the fundamental frequency  $\omega_p$

$$[\mathbf{Y}_{\mathbf{m},\mathbf{n}}] = \text{diag} \{ Y_{m,n}(k\omega_p) \} \quad k = 0, \dots, M \quad (\text{III-32})$$

$$[\mathbf{Y}_{\mathbf{m},\mathbf{n}}] = \begin{bmatrix} Y_{m,n}(0) & 0 & 0 & \cdots & 0 \\ 0 & Y_{m,n}(\omega_p) & 0 & \cdots & 0 \\ 0 & 0 & Y_{m,n}(2\omega_p) & \cdots & 0 \\ \vdots & \vdots & \vdots & \cdots & \vdots \\ 0 & 0 & 0 & \cdots & Y_{m,n}(M\omega_p) \end{bmatrix} \quad (\text{III-33})$$

In (III-29),  $[\mathbf{V}_{N+1}]$  and  $[\mathbf{V}_{N+2}]$ , the excitation vectors, have the form

$$[\mathbf{V}_{N+1}] = \begin{bmatrix} V_{be} \\ V_c \\ 0 \\ \vdots \\ 0 \end{bmatrix} \quad (\text{III-34})$$

$$[\mathbf{V}_{N+2}] = \begin{bmatrix} V_{bs} \\ 0 \\ 0 \\ \vdots \\ 0 \end{bmatrix} \quad (\text{III-35})$$

where  $V_{be}$  and  $V_{bs}$  are the dc voltages at ports  $N+1$  and  $N+2$ , respectively;  $V_c$  is the excitation voltage at port  $N+1$ . Partitioning the admittance matrix gives an expression for the current vector,

$$\begin{bmatrix} [\mathbf{I}_1] \\ \vdots \\ [\mathbf{I}_N] \end{bmatrix} = \begin{bmatrix} [\mathbf{Y}_{1,N+1}] & [\mathbf{Y}_{1,N+2}] \\ \vdots & \vdots \\ [\mathbf{Y}_{N,N+1}] & [\mathbf{Y}_{N,N+2}] \end{bmatrix} \begin{bmatrix} [\mathbf{V}_{N+1}] \\ [\mathbf{V}_{N+2}] \end{bmatrix} + \begin{bmatrix} [\mathbf{Y}_{1,1}] & [\mathbf{Y}_{1,N}] \\ \vdots & \vdots \\ [\mathbf{Y}_{N,1}] & [\mathbf{Y}_{N,N}] \end{bmatrix} \begin{bmatrix} [\mathbf{V}_1] \\ \vdots \\ [\mathbf{V}_N] \end{bmatrix} \quad (\text{III-36})$$

$$\rightarrow [\mathbf{I}] = [\mathbf{I}_s] + [\mathbf{Y}_{NxN}][\mathbf{V}] \quad (\text{III-37})$$

where  $[\mathbf{Y}_{NxN}]$  is the  $N \times N$  sub-matrix of  $[\mathbf{Y}]$  corresponding to its first  $N$  rows and columns.  $[\mathbf{I}_s]$  represents a set of current sources in parallel with the first  $N$  ports. The first matrix term of (III-24) transforms the input- and output-port excitations into this set of current sources, so the  $N+1^{\text{th}}$  and  $N+2^{\text{th}}$  ports need not to be considered further leading to the circuit shown in Figure III-8.

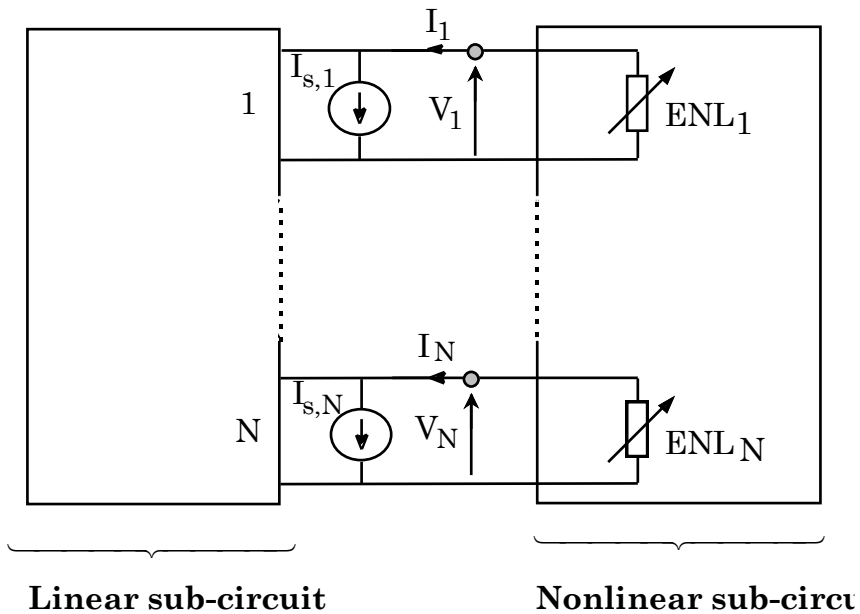


Fig. III-8. Nonlinear microwave circuit in which the excitation voltage sources at Ports  $N+1$  and  $N+2$  has been transformed into current sources at ports 1 to  $N$ .

This transformation allows us to express the harmonic balance equations as functions of currents at only the first through  $N^{\text{th}}$  ports, the ones connected to nonlinear elements.

The nonlinear element currents, represented by the current vector  $[\mathbf{I}']$ , can result from nonlinear capacitors or resistors.

Let  $\{ v_o(t), \dots, v_N(t) \}$  be the time voltage waveforms given by the inverse Fourier transforming  $\mathbf{F}^{-1}$  of the voltages at each port of the nonlinear sub-circuit:

$$\{ \mathbf{F}^{-1} ([\mathbf{V}_k]) \rightarrow v_k(t) \} \quad (\text{III-38})$$

---

*The materials you receive for this course are protected by copyright and to be used for this course only. You do not have permission to upload the course materials, including any lecture recordings you may have, to any website. If you require clarification, please consult your professor.*

The nonlinear capacitors will be treated first. Because the port voltages uniquely determine all voltages in the network, a capacitor's charge waveforms  $\{ q_0(t), \dots, q_N(t) \}$  can be expressed as a function of these voltages:

$$q_k(t) = f_{qk} (v_o(t), \dots, v_N(t)) \quad (\text{III-39})$$

Fourier transforming the charge waveform at each port gives the charge vectors for the capacitors at each port (and the related charge vector  $[\mathbf{Q}]$ ):

$$\{ \mathbf{F}(q_k(t)) \rightarrow [\mathbf{Q}_k] \} \quad (\text{III-40})$$

$$[\mathbf{Q}] = \begin{bmatrix} [\mathbf{Q}_1] \\ [\mathbf{Q}_2] \\ [\mathbf{Q}_3] \\ \vdots \\ [\mathbf{Q}_N] \end{bmatrix} = \begin{bmatrix} [\mathbf{Q}_{1,0}] \\ \vdots \\ [\mathbf{Q}_{1,M}] \\ \vdots \\ [\mathbf{Q}_{N,0}] \\ \vdots \\ [\mathbf{Q}_{N,M}] \end{bmatrix} \quad (\text{III-41})$$

The nonlinear capacitor current is the time derivative of the charge waveform. Taking the time derivative corresponds to multiplying by  $\{ j\omega_p \}$  in the frequency domain, so

$$i_{c,k}(t) = \frac{dq_k(t)}{dt} \leftrightarrow j m \omega_p Q_{k,m} \quad (\text{III-42})$$


---

*The materials you receive for this course are protected by copyright and to be used for this course only. You do not have permission to upload the course materials, including any lecture recordings you may have, to any website. If you require clarification, please consult your professor.*

This equation can be written as

$$[\mathbf{I}_c] = j [\Omega] [\mathbf{Q}] \quad (\text{III-43})$$

where  $[\Omega]$  is a diagonal matrix where elements are the pulsations  $k\omega_p$ :

$$[\Omega] = \begin{bmatrix} 0 & 0 & 0 & 0 & \cdots & \cdots & \cdots & \cdots & 0 \\ 0 & \omega_p & 0 & 0 & \cdots & \cdots & \cdots & \cdots & 0 \\ 0 & 0 & 2\omega_p & 0 & \cdots & \cdots & \cdots & \cdots & 0 \\ \vdots & \vdots \\ 0 & 0 & 0 & \cdots & M\omega_p & 0 & 0 & \cdots & 0 \\ 0 & 0 & 0 & \cdots & 0 & \omega_p & 0 & \cdots & 0 \\ 0 & 0 & 0 & \cdots & 0 & 0 & 2\omega_p & \vdots & \vdots \\ 0 & 0 & 0 & \cdots & 0 & 0 & 0 & \cdots & 0 \\ 0 & 0 & \cdots & \cdots & 0 & 0 & 0 & \cdots & 0 \\ \vdots & \vdots \\ 0 & 0 & 0 & \cdots & \cdots & \cdots & \cdots & \cdots & M\omega_p \end{bmatrix}$$

This matrix has  $N$  cycles of  $(0, \dots, M)\omega_p$  along the main diagonal. Similarly, the current in a nonlinear conductance is

$$i_{g,k}(t) = f_k(v_o(t), \dots, v_N(t)) \quad (\text{III-44})$$


---

Fourier transforming these gives

$$\{ \mathbf{F}(i_{g,k}(t)) \rightarrow [\mathbf{I}_{G,k}] \} \quad (\text{III-45})$$

and the vector  $[\mathbf{I}_G]$

$$[\mathbf{I}_G] = \begin{bmatrix} [\mathbf{I}_{G1}] \\ [\mathbf{I}_{G2}] \\ [\mathbf{I}_{G3}] \\ \vdots \\ [\mathbf{I}_{GN}] \end{bmatrix} \quad (\text{III-46})$$

Substituting (III-46), (III-43), and (III-37) into (III-28) gives the expression

$$[\mathbf{B}[\mathbf{V}]] = [\mathbf{I}_s] + [\mathbf{Y}_{N \times N}][\mathbf{V}] + [\mathbf{I}_g] + j[\mathcal{Q}][\mathbf{Q}] = [\mathbf{0}] \quad (\text{III-47})$$

This equation, *called the harmonic balance equation*, represents a test to determine whether a trial set of port voltage components is the correct one; that is if  $\{ [\mathbf{B}[\mathbf{V}]] = [\mathbf{0}] \}$ , then  $[\mathbf{V}]$  is a valid solution.  $[\mathbf{B}[\mathbf{V}]]$ , also *called the current-error vector*, represents the difference between the current calculated from the linear and nonlinear sub-circuits, at each port and at each harmonic, for a trial-solution vector  $[\mathbf{V}]$ .

### **III - Algorithms**

A number of algorithms have been proposed for solving harmonic balance equation. Initiated by Kryloff and Bogoliuboff, the harmonic balance technique was applied to microwave circuit CAD by Egami who utilized an iterative technique, namely the Newton algorithm, to minimize the error. Afterwards, many authors like Kerr, Hicks and Khan, and Camacho-Penalosa developed several relaxation methods to solve the harmonic balance equation.

The selection of an algorithm depends upon a number of factors, including computational efficiency, computer memory requirements, convergence properties, the need for an initial estimate of the solution, etc.

#### *1- Optimization methods*

Since solving (III-35) looks like an optimization problem, it is possible to solve it by minimizing the magnitude of the current-error function. An advantage of this approach is that optimization routines are widely used by designers. However most optimization routines are relatively slow and may have convergence problems.

#### *2- Newton's method*

Newton's method (or its variant the Newton-Raphson method) is a very powerful algorithm for finding the zeros of a multivariate function. It is an iterative technique: it finds the zero of a function by using its first derivative to extrapolate to the axis of the independent variable and repeating the process until the zero is found.

From an initial point  $x_o$  we can estimate the function using the linear extrapolation (Figure III-9). If the function and its derivative are known at the initial point  $x_o$ , (III-48) can estimate the value of  $\Delta x$ . Then, a new estimate of the zero is found at the new point {  $x_I = x_o + \Delta x$  } and the process is repeated until the zero is determined.

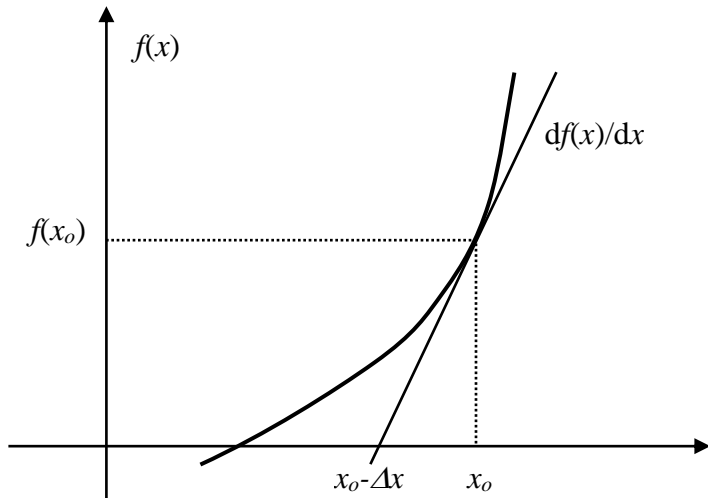


Fig. III-9. Newton's method applied to a one-dimensional problem.

For the multidimensional case, we have at the  $k^{\text{th}}$  iteration

$$[B[\mathbf{V}^k] - [\partial \mathbf{V}] \frac{[\partial B[\mathbf{V}]]}{[\partial \mathbf{V}]}]_{[\mathbf{V}][\mathbf{v}^k]} = [\mathbf{0}] \quad (\text{III-49})$$

$$f(x_o) = -\Delta x \left. \frac{df}{dx} \right|_{x=x_o} \quad (\text{III-48})$$

where  $[\mathbf{V}^k]$  is the  $k^{\text{th}}$  estimate of the solution vector. With

$$[\mathbf{V}^{k+1}] - [\mathbf{V}^k] = [\Delta \mathbf{V}] \quad (\text{III-50})$$

The updated vector  $[\mathbf{V}^{k+1}]$  is

$$[\mathbf{V}^{k+1}] = [\mathbf{V}^k] - \left[ \frac{\partial B[\mathbf{V}]}{\partial \mathbf{V}} \right]_{[\mathbf{V}]=[\mathbf{V}^k]}^{-1} B[\mathbf{V}^k] \quad (\text{III-51})$$

where the derivative of  $B[\mathbf{V}]$  is called the jacobian of  $B$

$$[\mathbf{J}_B] = \left[ \frac{\partial B[\mathbf{V}]}{\partial \mathbf{V}} \right] = [\mathbf{Y}_{N \times N}] + \left[ \frac{\partial \mathbf{I}_G[\mathbf{V}]}{\partial \mathbf{V}} \right] + j[\mathcal{Q}] \left[ \frac{\partial \mathbf{Q}[\mathbf{V}]}{\partial \mathbf{V}} \right] \quad (\text{III-52})$$

which can be written as

$$[\mathbf{J}_B] = \begin{bmatrix} \frac{\partial B_{1,0}}{\partial V_{1,0}} & \frac{\partial B_{1,0}}{\partial V_{1,1}} & \frac{\partial B_{1,0}}{\partial V_{1,2}} & \dots & \frac{\partial B_{1,0}}{\partial V_{1,M}} & \frac{\partial B_{1,0}}{\partial V_{2,0}} & \frac{\partial B_{1,0}}{\partial V_{2,1}} & \frac{\partial B_{1,0}}{\partial V_{2,2}} & \dots & \frac{\partial B_{1,0}}{\partial V_{N,M}} \\ \frac{\partial B_{1,1}}{\partial V_{1,0}} & \frac{\partial B_{1,1}}{\partial V_{1,1}} & \frac{\partial B_{1,1}}{\partial V_{1,2}} & \dots & \frac{\partial B_{1,1}}{\partial V_{1,M}} & \frac{\partial B_{1,1}}{\partial V_{2,0}} & \frac{\partial B_{1,1}}{\partial V_{2,1}} & \frac{\partial B_{1,1}}{\partial V_{2,2}} & \dots & \frac{\partial B_{1,1}}{\partial V_{N,M}} \\ \vdots & \vdots & \vdots & \dots & \vdots & \vdots & \vdots & \vdots & \dots & \vdots \\ \frac{\partial B_{1,M}}{\partial V_{1,0}} & \frac{\partial B_{1,M}}{\partial V_{1,1}} & \frac{\partial B_{1,M}}{\partial V_{1,2}} & \dots & \frac{\partial B_{1,M}}{\partial V_{1,M}} & \frac{\partial B_{1,M}}{\partial V_{2,0}} & \frac{\partial B_{1,M}}{\partial V_{2,1}} & \frac{\partial B_{1,M}}{\partial V_{2,2}} & \dots & \frac{\partial B_{1,M}}{\partial V_{N,M}} \\ \frac{\partial B_{2,0}}{\partial V_{1,0}} & \frac{\partial B_{2,0}}{\partial V_{1,1}} & \frac{\partial B_{2,0}}{\partial V_{1,2}} & \dots & \frac{\partial B_{2,0}}{\partial V_{1,M}} & \frac{\partial B_{2,0}}{\partial V_{2,0}} & \frac{\partial B_{2,0}}{\partial V_{2,1}} & \frac{\partial B_{2,0}}{\partial V_{2,2}} & \dots & \frac{\partial B_{2,0}}{\partial V_{N,M}} \\ \frac{\partial B_{2,1}}{\partial V_{1,0}} & \frac{\partial B_{2,1}}{\partial V_{1,1}} & \frac{\partial B_{2,1}}{\partial V_{1,2}} & \dots & \frac{\partial B_{2,1}}{\partial V_{1,M}} & \frac{\partial B_{2,1}}{\partial V_{2,0}} & \frac{\partial B_{2,1}}{\partial V_{2,1}} & \frac{\partial B_{2,1}}{\partial V_{2,2}} & \dots & \frac{\partial B_{2,1}}{\partial V_{N,M}} \\ \vdots & \vdots & \vdots & \dots & \vdots & \vdots & \vdots & \vdots & \dots & \vdots \\ \frac{\partial B_{2,M}}{\partial V_{1,0}} & \frac{\partial B_{2,M}}{\partial V_{1,1}} & \frac{\partial B_{2,M}}{\partial V_{1,2}} & \dots & \frac{\partial B_{2,M}}{\partial V_{1,M}} & \frac{\partial B_{2,M}}{\partial V_{2,0}} & \frac{\partial B_{2,M}}{\partial V_{2,1}} & \frac{\partial B_{2,M}}{\partial V_{2,2}} & \dots & \frac{\partial B_{2,M}}{\partial V_{N,M}} \\ \vdots & \vdots & \vdots & \dots & \vdots & \vdots & \vdots & \vdots & \dots & \vdots \\ \frac{\partial B_{N,M}}{\partial V_{1,0}} & \frac{\partial B_{N,M}}{\partial V_{1,1}} & \frac{\partial B_{N,M}}{\partial V_{1,2}} & \dots & \frac{\partial B_{N,M}}{\partial V_{1,M}} & \frac{\partial B_{N,M}}{\partial V_{2,0}} & \frac{\partial B_{N,M}}{\partial V_{2,1}} & \frac{\partial B_{N,M}}{\partial V_{2,2}} & \dots & \frac{\partial B_{N,M}}{\partial V_{N,M}} \end{bmatrix} \quad (III-53)$$

The terms of  $[\mathbf{J}_B]$  are

$$\frac{\partial B_{n,k}}{\partial V_{m,l}} = Y_{m,n} (k = l) + \frac{\partial I_{Gn,k}}{\partial V_{m,l}} + j k \omega_p \frac{\partial Q_{n,k}}{\partial V_{m,l}} \quad (III-54)$$

where the  $n$  and  $m$  subscripts refer to the port number and the  $k$  and  $l$  subscripts indicate the harmonic number. The term  $Y_{m,n}$  ( $k = l$ ) is  $Y_{m,n}(k\omega_p)$  when  $\{ k = l \}$  and zero when  $\{ k \neq l \}$ . It is possible to show that

$$\frac{\partial I_{Gn,k}}{\partial V_{m,l}} = \frac{1}{T} \int_{-\frac{1}{2T}}^{\frac{1}{2T}} \frac{\partial i_{gn}(t)}{\partial V_m(t)} e^{-j(k-l)\omega_p t} dt \quad (\text{III-55})$$

$$\frac{\partial Q_{n,k}}{\partial V_{m,l}} = \frac{1}{T} \int_{-\frac{1}{2T}}^{\frac{1}{2T}} \frac{\partial q_n(t)}{\partial V_m(t)} e^{-j(k-l)\omega_p t} dt \quad (\text{III-56})$$

where  $T$  is the fundamental excitation period. If the main advantage of Newton's method is that it makes full use of all the derivatives of the error function with respect to each variable at each port, its main disadvantage is in the large amount of computer memory and computation time required to generate the jacobian and to solve the matrix equation.

As an illustration, if we have three nonlinear elements and eight harmonics (plus dc), the jacobian is  $N*(M+1) = 27*27$ . Because the jacobian is complex, solving the system involves solving a  $54*54$  set of real equations, knowing that the derivatives are evaluated numerically. Also, the entire matrix, the solution, and updated vectors must remain in memory simultaneously so this requires a large segment of computer memory.

Even, if many works have been proposed to minimize the memory requirements and to speed up the process (Kundert *et al.*, Heron and Steer, Chang *et al.*, Rhodes and Perlman), convergence problems are often encountered in the algorithm, especially in circuits having large excitations.

---

*The materials you receive for this course are protected by copyright and to be used for this course only. You do not have permission to upload the course materials, including any lecture recordings you may have, to any website. If you require clarification, please consult your professor.*

### 3- Splitting methods

A number of relaxation methods, which are both simple to implement and intuitively satisfying, have been proposed. Two of the most popular are those of Hicks and Khan, and Kerr (also called the reflection algorithm).

#### a. Method of Hicks and Khan

In the method proposed by Hicks and Khan, the algorithm

- Estimate the initial voltage vector  $[V^o]$  of the linear sub-circuit,
- Inverse-Fourier transform  $[V^o]$  to get the time-domain waveforms of the initial point:

$$\{ F^{-1} ([V^o]) \rightarrow [V(t)^o] \},$$

- Deduce the time-domain waveforms of the current vector  $[I'(t)^o]$  for the nonlinear sub-circuit,
- Fourier transform  $[I'(t)^o]$  to obtain the frequency domain current vector  $[I'^o]$

$$\{ F ([I'(t)^o]) \rightarrow [I'^o] \},$$

- Assume the current vector  $[I^o]$  of the linear sub-circuit is equal to  $\{ -[I'^o] \}$ ,
- The linear sub-circuit having an impedance matrix  $[Z_{NxN}]$ , the voltage vector  $[V']$  of the nonlinear sub-circuit is then equal to

$$[V'] = [Z_{NxN}] \{ [I^o] - [I_s] \} \quad (\text{III-57})$$

- Form the new estimate voltage vector  $[\mathbf{V}^1]$  of the linear sub-circuit as

$$[\mathbf{V}^1] = s [\mathbf{V}'] + (1-s) [\mathbf{V}^0] \quad (\text{III-58})$$

where  $s$  is a real positive constant ( $0.0 < s < 1.0$ ). The vector  $[\mathbf{V}^0]$  is then replaced by  $[\mathbf{V}^1]$  and the process is repeated until minimal change in the voltage vector is observed between iterations.

The method is simple to implement but the variable  $s$ , called the splitting coefficient, is a constant that must be determined empirically. Small values of  $s$  favour slow but monotonic convergence; increasing  $s$  gives faster convergence up to the point at which oscillation begins. Typically,  $s = 0.2$ .

#### *b. Reflection algorithm*

All the above methods are based on mathematical aspects, without any direct relation with the physical meaning of the problem. The reflection algorithm solves the harmonic balance equations via a process that mimics the turn-on process of a real circuit. To implement the reflection algorithm, the equivalent circuit of Figure III-8 is redrawn as shown in Figure III-10.

The greatest difference between the two circuits is the set of transmission lines between the respective ports of the linear and nonlinear sub-circuits. These transmission lines are assumed to be ideal, as well as to be a large integer number of wavelengths long ( $n\lambda$ ) at the fundamental excitation frequency; thus, they do not affect the circuit's steady-state response (infinite ideal transmission lines).

When the circuit is turned on, voltage waveforms appear at the  $N$  ports and incident waves are impressed on the transmission lines. These propagate towards, and eventually reach, the respective

---

*The materials you receive for this course are protected by copyright and to be used for this course only. You do not have permission to upload the course materials, including any lecture recordings you may have, to any website. If you require clarification, please consult your professor.*

ports of the nonlinear sub-circuit. The waves excite the nonlinear elements, and reverse-traveling waves are generated. These return to the ports of the linear sub-circuit, are again reflected, and add to the incident wave; then, the process is repeated.

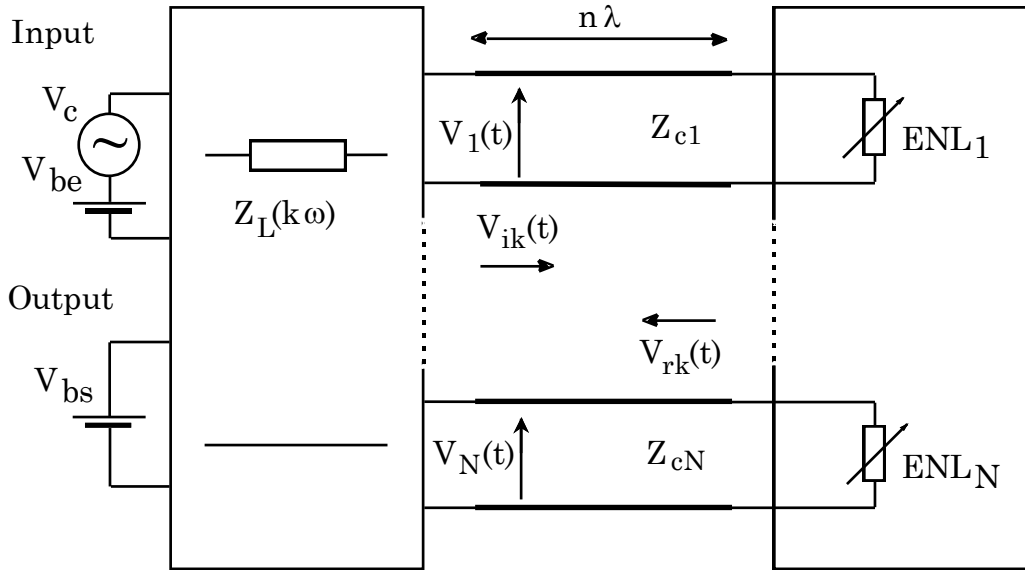


Fig. III-10. General nonlinear microwave circuit, with fictitious ideal transmission lines, for analysis via the reflection algorithm.

The ruse of the ideal transmission lines allows the circuit to be separated into two parts as shown in Figure III-11.

At the instant the circuit is turned on, no reflected wave exists, so the input impedance of the transmission line is equal to its characteristic impedance. When the incident wave reaches the nonlinear sub-circuit, the transmission line interface has the equivalent circuit shown on the right side of Figure III-11.

---

*The materials you receive for this course are protected by copyright and to be used for this course only. You do not have permission to upload the course materials, including any lecture recordings you may have, to any website. If you require clarification, please consult your professor.*

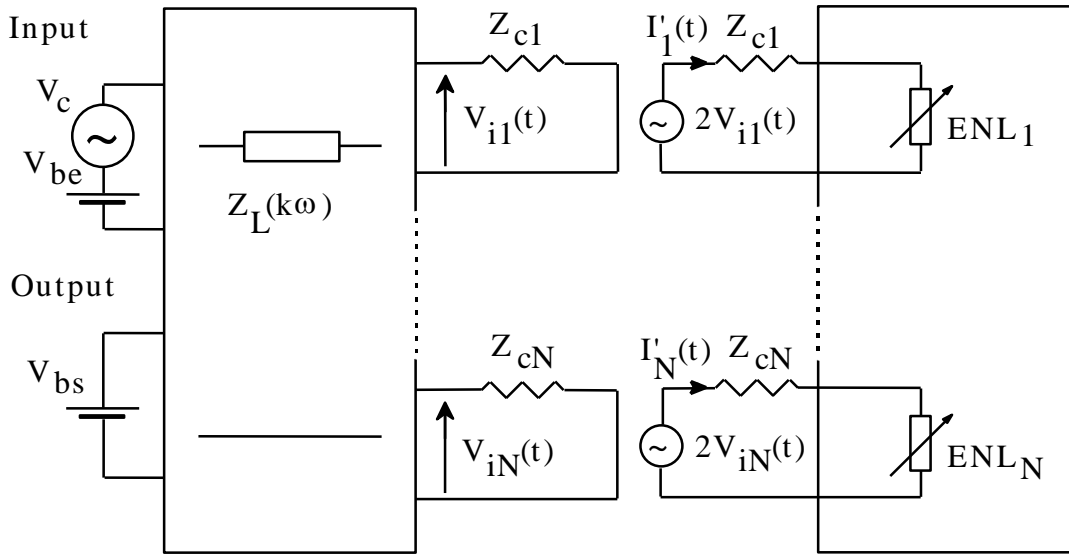


Fig. III-11. Nonlinear microwave circuit with fictitious ideal transmission lines. Incident wave circuit equivalent to that of Figure III-10.

The process is as follows:

- The frequency-domain initial incident voltage vector  $[V_i^0]$  of the linear sub-circuit is obtained by a straightforward analysis of the linear sub-circuit starting from dc and ac sources. Therefore, the original incident wave vector  $[V_i(t)^0]$  at the  $N$  ports  $\{ v_{n,i}(t), n = 1, \dots, N \}$  can be found by inverse-Fourier transforming

$$\{ F^{-1} ([V_i^0]) \rightarrow [V_i(t)^0] \},$$

Notice here that the initial point is not *estimated* but *calculated*.

- Applied to the nonlinear sub-circuit, the initial vector  $\{ [V_i(t)^0] = [V'_i(t)^0] \}$  allows to find the initial reverse wave  $[V'_r(t)^0]$   $\{ v'_{n,r}(t), n = 1, \dots, N \}$  by analyzing the nonlinear network. Then, the initial current wave  $[I'(t)^0]$  of the nonlinear sub-circuit is deduced.

We have then

$$[V_r(t)^0] = [V_i(t)^0] - [Z_c] [I'(t)^0] \quad (\text{III-59})$$

where  $[Z_c]$  is a diagonal matrix whose elements are the characteristic impedances  $Z_{cn}$  of the  $N$  ideal transmission lines.

- Let  $Z_n(k\omega_p)$  be the source impedance seen by the  $n^{\text{th}}$  ideal transmission line and let  $\Gamma_n(k\omega_p)$  be its reflection coefficient.

$$\Gamma_n(k\omega_p) = \frac{Z_n(k\omega_p) - Z_{cn}}{Z_n(k\omega_p) + Z_{cn}} \quad (\text{III-60})$$

- By Fourier transforming we obtain the reflected vector of the linear sub-circuit.

$$\{ \mathbf{F}([V_r(t)^0]) \rightarrow [V_r^0] \},$$

Notice that the element  $V_{n,r}(0)$  is twice the dc value.

- To form the new incident wave vector  $[V_i(t)^1]$ , the reflected wave is multiplied by the source reflection coefficient at the linear-circuit end of the line. Thus,

$$V_{i,n}^1(t) = V_{i,n}^0(t) + \frac{1}{2} \sum_{k=0}^M \Gamma_n(k\omega) V_{r,n}^0(t) e^{jk\omega t} \quad (\text{III-61})$$


---

*The materials you receive for this course are protected by copyright and to be used for this course only. You do not have permission to upload the course materials, including any lecture recordings you may have, to any website. If you require clarification, please consult your professor.*

After the  $p^{\text{th}}$  iteration, the new incident wave is

$$V_{i,n}^{p+1}(t) = V_{i,n}^o(t) + \frac{1}{2} \sum_{k=0}^M \Gamma_n(k\omega) V_{r,n}^p(t) e^{jk\omega t} \quad (\text{III-62})$$

Note that the summation term is added to the initial incident wave, not to the previous one.

- The process convergence is reached when the difference between successive incident wave vectors  $[\mathbf{V}^{p+1}]$  and  $[\mathbf{V}^p]$  is minimized

$$\left| [\mathbf{V}^{p+1}] - [\mathbf{V}^p] \right| = \left| \left\{ [\mathbf{V}_i^{p+1}] + [\mathbf{V}_r^{p+1}] \right\} - \left\{ [\mathbf{V}_i^p] + [\mathbf{V}_r^p] \right\} \right| < \varepsilon \quad (\text{III-63})$$

Two complications often arise in the implementation of the reflection algorithm. The first concerns the selection of the characteristic impedances  $Z_{cn}$ . The algorithm usually is not very sensitive to the choice of  $Z_{cn}$ , but it does affect convergence rate. Equations (III-61) to (III-63) indicate that  $Z_{cn}$  could be selected to minimize the reflection coefficients at the lower harmonics of the excitation frequency. This choice improves the speed of convergence, because the lower harmonics invariably dominate the convergence process.

The second complication is that the dc source impedance at each port, in most circuits, is usually equal to zero. Thus, the dc component  $V_n(0)$  of the transmission line waves changes polarity with each iteration, converging only very slowly to its correct value.

The wide variation often introduces numerical instability; it can also force some of the voltages in the nonlinear circuit, during intermediate iterations, to exceed the range of the model. The simplest way to avoid this problem is artificially to set the dc source impedance at each port equal

---

*The materials you receive for this course are protected by copyright and to be used for this course only. You do not have permission to upload the course materials, including any lecture recordings you may have, to any website. If you require clarification, please consult your professor.*

to  $Z_{cn}$  making the reflection coefficient zero. This change will affect the dc values of the voltages at the nonlinear elements, so the bias source value will have to be offset to compensate.

## D – LARGE-SIGNAL SMALL-SIGNAL ANALYSIS

Large-signal - small-signal analysis, or conversion matrix analysis, is the second nonlinear approach for analyzing nonlinear circuits.

It is useful for a large class of problems wherein a nonlinear device is pumped by a single large sinusoidal signal and another signal, which is assumed to be much smaller, is also applied.

The most common application of this technique is in the design of microwave mixers, but it is also applicable to circuits like modulators, parametric amplifiers, and parametric up-converters. The process involves *first* analyzing the nonlinear device under large-signal excitation *only*, usually via the harmonic-balance method. *This is called the large signal analysis.*

The nonlinear element or elements in the device's equivalent circuit are then converted to small-signal, linear, time-varying elements and the small-signal analysis is performed, without further consideration of the large-signal excitation. *This is called the small signal analysis.*

The assumption of small-signal linearity requires that the quasi-linear response be of primary interest, but these techniques are also useful, with significant modifications, to circuits wherein quasi-linearity is not assumed.

## I – Mixing process

In general, a nonlinear element excited by two tones supports currents and voltages at the mixing frequencies

$$\omega_{m,n} = m\omega_1 + n\omega_2 \quad (\text{III-64})$$

where  $m$  and  $n$  can be positive and negative integers, including zero. In the present case, one of the tones,  $\omega_{RF}$ , is at such a low level that it does not generate harmonics, and the other is a large-signal sinusoid at  $\omega_p$ . Then, the mixing frequencies are

$$\omega = \pm \omega_{RF} + n\omega_p \quad (\text{III-65})$$

This equation represents the set of frequency components shown in Figure III-12 which consists of two tones on either side of each large-signal harmonic frequency, separated by  $\{\omega_o = / \omega_p - \omega_{RF} / \}$ . A more convenient representation of the mixing frequencies is

$$\omega_n = \omega_o + n\omega_p \quad (\text{III-66})$$

The frequency domain currents and voltages in a time varying circuit element are related by a conversion matrix.

The small-signal voltage and current can be expressed in the frequency notation as follows

$$V(t) = \sum_{k=-\infty}^{\infty} V_k e^{jk\omega t} = \sum_{k=-\infty}^{\infty} V_k e^{j\omega_k t} \quad (\text{III-67})$$


---

*The materials you receive for this course are protected by copyright and to be used for this course only. You do not have permission to upload the course materials, including any lecture recordings you may have, to any website. If you require clarification, please consult your professor.*

and

$$I(t) = \sum_{k=-\infty}^{\infty} I_k e^{jk\omega t} = \sum_{k=-\infty}^{\infty} I_k e^{j\omega_k t} \quad (\text{III-68})$$

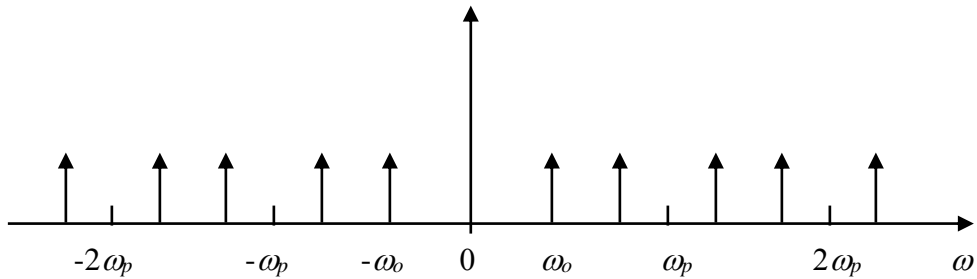


Fig. III-12. Spectrum of small-signal mixing frequencies in the pumped nonlinear element.

## II – Diode circuit analysis

In order to illustrate this process, we will consider the case of a mixing diode, e.g. the Schottky diode (Figure III-13).

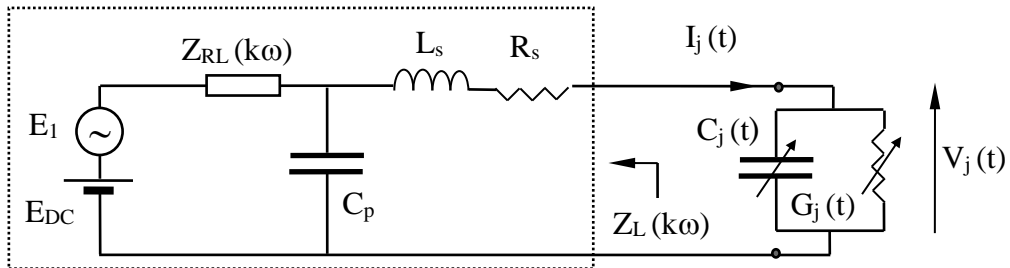


Fig. III-13. Equivalent circuit of a nonlinear Schottky diode network.

### 1– Large signal analysis

The goal of the large signal analysis is to determine the Fourier coefficients of the nonlinear elements. Assuming that the parasitic elements  $R_s$ ,  $L_s$  and  $C_p$  are constant up to the millimetre range, they can be included in the linear sub-circuit. Therefore, the nonlinear elements are the junction capacitance  $C_j$  and the junction conductance  $G_j$ . For each harmonic  $k\omega_p$  of the excitation signal, the junction voltage  $V_j(t)$  and current  $I_j(t)$  can be found by expending

$$V_j(t) = \sum_{k=-\infty}^{\infty} V_{jk} e^{jk\omega_p t} \quad ; \quad I_j(t) = \sum_{k=-\infty}^{\infty} I_{jk} e^{jk\omega_p t} \quad (\text{III-69})$$

Let us define  $Z_L(k\omega_p)$  as the impedance of Thevenin seen by the junction and constituted by the impedance  $Z_{RL}(k\omega_p)$  of the linear sub-circuit and the parasitic elements of the diode. Let  $E_{DC}$  and  $E_I$  be the bias and the excitation voltages respectively. We have then the following system

$$\left. \begin{array}{l} V_{j0} = E_{DC} - I_{j0} Z_L(0) \quad \text{for } k=0 \\ V_{j1} = E_I - I_{j1} Z_L(\pm\omega) \quad \text{for } k=\pm 1 \\ V_{jk} = -I_{jk} Z_L(k\omega) \quad \text{for } k=\pm 2, \pm 3, \dots \end{array} \right\} \quad (\text{III-70})$$

Its resolution allows characterizing the nonlinear elements

$$C_j(t) = \sum_{k=-\infty}^{\infty} C_{jk} e^{jk\omega_p t} \quad (\text{III-71})$$

$$G_j(t) = \sum_{k=-\infty}^{\infty} G_{jk} e^{jk\omega_p t} \quad (\text{III-72})$$

The Fourier coefficients represent the element values at the different harmonics. They allow obtaining the transfer matrix of the diode at each harmonic of the excitation signal. Therefore, the circuit parameters can be determined.

## 2– Small signal analysis

In the small-signal analysis, the circuit is represented by a multifrequency multiport network as shown in Figure III-14 (see the definition in Chapter I). By adding the small input signal (RF excitation) to the large signal of the pump, we obtain

$$V_j(t) = \sum_{k=-\infty}^{\infty} V_{jk} e^{j(\omega_o + k\omega_p)t} ; \quad I_j(t) = \sum_{k=-\infty}^{\infty} I_{jk} e^{j(\omega_o + k\omega_p)t} \quad (\text{III-73})$$

As the Fourier representation of a time-varying resistor  $R_j(t)$  is defined by

$$R_j(t) = \frac{V_j(t)}{I_j(t)} = \sum_{q=-N}^N R_{jq} e^{jq\omega_p t} \quad (\text{III-74})$$

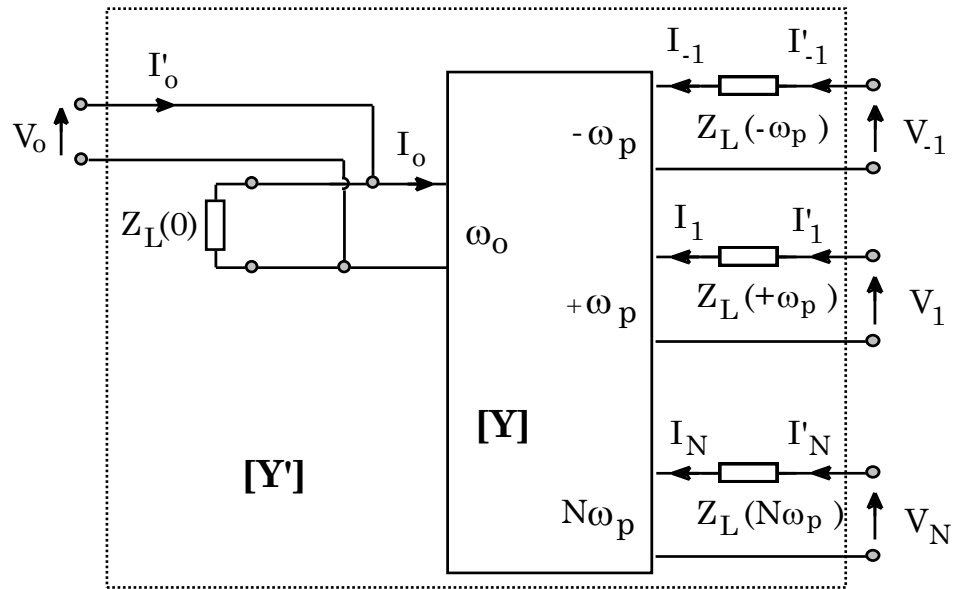


Fig. III-14. Multifrequency multiport network representation of the circuit on Figure III-13.

Therefore, we obtain

$$\sum_{k=-N}^N V_k e^{j(\omega_0 + k\omega_p)t} = \sum_{q=-N}^N \sum_{m=-N}^N R_q I_m e^{j(\omega_0 + (q+m)\omega_p)t} \quad (\text{III-75})$$

This equation can be reordered to show the nonlinear conversion matrix **[R]** of a resistor:

$$\begin{bmatrix} V_{-N} \\ \vdots \\ V_0 \\ \vdots \\ V_N \end{bmatrix} = \begin{bmatrix} R_0 & \cdots & R_{-N} & \cdots & R_{-2N} \\ \vdots & & \vdots & & \vdots \\ R_N & \cdots & R_0 & \cdots & R_{-N} \\ \vdots & & \vdots & & \vdots \\ R_{2N} & \cdots & R_N & \cdots & R_0 \end{bmatrix} \begin{bmatrix} I_{-N} \\ \vdots \\ I_0 \\ \vdots \\ I_N \end{bmatrix} \quad (\text{III-76})$$

The elements are the Fourier components of the resistance. Note that the vectors have been truncated to a limit  $\pm N$  for both current and voltage, and  $\pm 2N$  for the resistor to prevent the occurrence of infinite vectors and matrices ( $V_k$ ,  $I_k$  and  $R_k$  are assumed to be negligible beyond this limit).

Note also that the negative-frequency components (where  $k < 0$ ) are shown as conjugate. Positive and negative-frequency components are related by

$$V_{-k}^* = V_k \quad ; \quad I_{-k}^* = I_k \quad ; \quad R_{-k}^* = R_k \quad (\text{III-77})$$

Then, (III-76) becomes

$$\begin{bmatrix} V_{-N}^* \\ \vdots \\ V_0 \\ \vdots \\ V_N \end{bmatrix} = \begin{bmatrix} R_0 & \cdots & R_{-N} & \cdots & R_{-2N} \\ \vdots & & \vdots & & \vdots \\ R_N & \cdots & R_0 & \cdots & R_{-N} \\ \vdots & & \vdots & & \vdots \\ R_{2N} & \cdots & R_N & \cdots & R_0 \end{bmatrix} \begin{bmatrix} I_{-N}^* \\ \vdots \\ I_0 \\ \vdots \\ I_N \end{bmatrix} \quad (\text{III-78})$$

Similarly, for a capacitor, we start from the basic equation:

$$I(t) = \frac{dQ(t)}{dt} = C(t) \frac{dV(t)}{dt} + V(t) \frac{dC(t)}{dt} \quad (\text{III-79})$$



$$\sum_{k=-N}^N I_k e^{j(\omega_o + k\omega_p)t} = \sum_{q=-N}^N \sum_{m=-N}^N j(\omega_o + (q+m)\omega_p) V_q C_m e^{j(\omega_o + (q+m)\omega_p)t} \quad (\text{III-80})$$

Therefore, we can deduce the conversion matrix  $[\mathbf{C}]$  of a capacitor

$$\begin{bmatrix} I_{-N}^* \\ \vdots \\ I_0 \\ \vdots \\ I_N \end{bmatrix} = \begin{bmatrix} \omega_{-N} C_o & \cdots & \omega_{-N} C_{-N} & \cdots & \omega_{-N} C_{-2N} \\ \vdots & & \vdots & & \vdots \\ \omega_o C_N & \cdots & \omega_o C_o & \cdots & \omega_o C_{-N} \\ \vdots & & \vdots & & \vdots \\ \omega_N C_{2N} & \cdots & \omega_N C_N & \cdots & \omega_N C_o \end{bmatrix} \begin{bmatrix} V_{-N}^* \\ \vdots \\ V_0 \\ \vdots \\ V_N \end{bmatrix} \quad (\text{III-81})$$



$$[\mathbf{I}] = j [\boldsymbol{\Omega}] [\mathbf{C}] [\mathbf{V}] \quad (\text{III-82})$$

where  $[\boldsymbol{\Omega}]$  is a diagonal matrix whose elements are the frequencies  $\omega_{-N}$  to  $\omega_N$ . Conversion matrices can be treated as in all ways like multiport admittance or impedance matrices. So, we can determine the admittance matrix  $[\mathbf{Y}]$  whose elements should be on the following form

$$Y_{mn} = G_{m-n} + j(\omega_o + m\omega_p)C_{m-n} \quad \omega_m = \omega_o + m\omega_p \quad (\text{III-83})$$

The dimensions are  $2N \times 2N$  and each  $k^{\text{th}}$  line (or column) refers to the  $k^{\text{th}}$  harmonic of the excitation

$$[\mathbf{Y}] = \begin{array}{c} \text{Line\#} \\ \vdots \\ 1 \\ 0 \\ -1 \\ \vdots \\ \dots \end{array} \begin{bmatrix} \vdots & \vdots & \vdots & \vdots \\ \cdots & Y_{11} & Y_{10} & Y_{1-1} & \cdots \\ \cdots & Y_{01} & Y_{00} & Y_{0-1} & \cdots \\ \cdots & Y_{-11} & Y_{-10} & Y_{-1-1} & \cdots \\ \vdots & \vdots & \vdots & \vdots \\ \dots & 1 & 0 & -1 & \cdots \end{bmatrix} \begin{array}{c} \text{Column\#} \\ \dots \end{array} \quad (\text{III-84})$$

From this matrix, we can deduce the overall admittance matrix  $[\mathbf{Y}']$  of the circuit shown on Figure III-13 by including the equivalent impedances  $Z_L(k\omega_p)$ . These impedances are formed by the impedances  $Z_{RL}(k\omega_p)$  of the linear sub-circuit *plus* the linear parasitic elements of the diode:

$$[\mathbf{Y}'] = [\mathbf{Y}] + \text{diag} \left\{ \frac{1}{Z_L(k\omega_p)} \right\} \quad (\text{III-85})$$

This circuit matrix allows obtaining the circuit parameters. Therefore, the conversion loss from an input frequency  $nf$  (e.g. the RF input signal) to an output frequency  $mf$  (e.g. the IF frequency) and the corresponding input-output impedances are

$$L_{mn} = 4|Y'_{mn}|^2 \operatorname{Re}\{Z_L(m\omega_p)\} \operatorname{Re}\{Z_L(n\omega_p)\} \quad (\text{III-86})$$

$$Z_{input} = 1/Y_{mm} - Z_L(m\omega_p) \quad (\text{III-87})$$

$$Z_{output} = 1/Y_{nn} - Z_L(n\omega_p) \quad (\text{III-88})$$

## II – Transistor circuit analysis

Usually for nonlinear purposes, the optimized performances are achieved when the RF signal and the pump (local oscillator) are applied to the gate of the pumped transistor. The output signal is on the drain. In this case, the capacitances and drain-resistance variations are minimized while the excursion over the trans-conductance is maximized.

These conditions lead to a bias point closed to the saturation region during the pump signal cycle. This saturation is assured by quasi-constant value of the drain voltage (by shunting the drain

at the frequency pump and its harmonics). Therefore, the operating conditions are similar to those of a Class B amplifier.

### 1– Large signal analysis

For a transistor (e.g. a FET), the large signal analysis purpose is to find the Fourier coefficients of the input port (noted  $V_i$  and  $I_i$  respectively), namely the gate, and the output port or drain (noted  $V_o$  and  $I_o$  respectively)

$$V_i(t) = \sum_{k=-N}^N V_{ik} e^{jk\omega_p t} ; \quad I_i(t) = \sum_{k=-N}^N I_{ik} e^{jk\omega_p t} \quad (\text{III-89})$$

and

$$V_o(t) = \sum_{k=-N}^N V_{ok} e^{jk\omega_p t} ; \quad I_o(t) = \sum_{k=-N}^N I_{ok} e^{jk\omega_p t} \quad (\text{III-90})$$

Then, similarly to the diode, the coefficients of all nonlinear elements can be deduced (drain current source, capacitances, ..).

### 2– Small signal analysis

The process is similar to the one used for the diode circuit. The only difference is that the multifrequency multiport will have  $\{ 2(N+1) \}$  ports instead of  $\{ N+1 \}$ .

---

Let  $[\mathbf{R}_a]$ ,  $[\mathbf{G}_m]$ ,  $[\mathbf{C}_s]$  and  $[\mathbf{C}_d]$  be the conversion matrices of  $R_{ds}$ ,  $G_m$ ,  $C_{gs}$  and  $C_{ds}$  respectively. The admittance matrix of the transistor circuit is given by

$$[\mathbf{Y}] = \left[ \{ [\mathbf{Z}_1] + [\mathbf{Z}_c][\mathbf{Z}_6] \} \{ [\mathbf{Z}_A]^{-1} [\mathbf{Z}_B] \} + [\mathbf{Z}_c][\mathbf{Z}_5] + [\mathbf{Z}_2] \right]^{-1} \quad (\text{III-91})$$

with

$$[\mathbf{Z}_A] = [\mathbf{Z}_3][\mathbf{Z}_7]^{-1}[\mathbf{Z}_6] + [\mathbf{Z}_4]$$

$$[\mathbf{Z}_B] = [\mathbf{R}_a] - [\mathbf{Z}_3][\mathbf{Z}_7]^{-1}[\mathbf{Z}_5]$$

$$[\mathbf{Z}_c] = [\mathbf{R}_a][\mathbf{Z}_7]^{-1}$$

$$[\mathbf{Z}_1] = [\mathbf{Z}_{ni}] + [\mathbf{C}_s]^{-1} + j [\boldsymbol{\Omega}] L_s + (R_s + R_i) [\mathfrak{J}]$$

$$[\mathbf{Z}_2] = +j [\boldsymbol{\Omega}] L_s + R_s [\mathfrak{J}]$$

$$[\mathbf{Z}_3] = [\mathbf{C}_d]^{-1} + R_i [\mathfrak{J}] + \{ [\mathfrak{J}] + [\mathbf{R}_a][\mathbf{G}_m] \} [\mathbf{C}_s]^{-1} + [\mathbf{R}_a]$$

$$[\mathbf{Z}_4] = R_i [\mathfrak{J}] + \{ [\mathfrak{J}] + [\mathbf{R}_a][\mathbf{G}_m] \} [\mathbf{C}_s]^{-1}$$

$$[\mathbf{Z}_5] = [\mathbf{Z}_{no}] + j [\boldsymbol{\Omega}] L_s + [\mathbf{R}_a] + R_s [\mathfrak{J}]$$

and

$$[\mathbf{Z}_6] = j [\boldsymbol{\Omega}] L_s + R_s [\mathfrak{I}] - [\mathbf{R}_a] [\mathbf{G}_m] [\mathbf{C}_s]^{-1}$$

$$[\mathbf{Z}_7] = [\mathbf{R}_a] \left\{ [\mathbf{G}_m] [\mathbf{C}_s]^{-1} + [\mathfrak{I}] \right\}$$

$$[\mathbf{Z}_{ni}] = \text{diag} \{ Z_{Le}(k\omega_p) \} \quad \text{and} \quad [\mathbf{Z}_{no}] = \text{diag} \{ Z_{Ls}(k\omega_p) \}$$

where  $[\mathfrak{I}]$  is the identity matrix. From this formulation, it is possible to deduce the circuit gain  $G_{mn}$  from an input frequency  $nf$  to an output frequency  $mf$ ,

$$G_{mn} = 4|Y_{mn}|^2 \operatorname{Re} \{ Z_{Le}(m\omega_p) \} \operatorname{Re} \{ Z_{Ls}(n\omega_p) \} \quad (\text{III-92})$$

and the corresponding input impedance while the output is matched:

$$[\mathbf{Z}_{in}] = [\mathbf{Z}_1] + \{ [\mathbf{Z}_2] + [\mathbf{Z}_C] [\mathbf{Z}_5] \} \left\{ [\mathbf{Z}_B]^{-1} [\mathbf{Z}_A] \right\} + [\mathbf{Z}_C] [\mathbf{Z}_6] - [\mathbf{Z}_{ni}] \quad (\text{III-93})$$

and the output impedance while the input port is matched

$$[\mathbf{Z}_{out}] = [\mathbf{Z}_{out1}] + \{ [\mathbf{Z}_{out2}] [\mathbf{Z}_{out3}]^{-1} [\mathbf{Z}_{out4}] \} - [\mathbf{Z}_{no}] \quad (\text{III-94})$$

with

$$[\mathbf{Z}_{out1}] = [\mathbf{Z}_5] + [\mathbf{Z}_7] [\mathbf{R}_a]^{-1} [\mathbf{Z}_2]$$

---

*The materials you receive for this course are protected by copyright and to be used for this course only. You do not have permission to upload the course materials, including any lecture recordings you may have, to any website. If you require clarification, please consult your professor.*

and

$$[\mathbf{Z}_{out2}] = [\mathbf{Z}_6] + [\mathbf{Z}_7][\mathbf{R}_a]^{-1}[\mathbf{Z}_1] \quad [\mathbf{Z}_{out3}] = [\mathbf{Z}_4] - [\mathbf{Z}_3][\mathbf{R}_a]^{-1}[\mathbf{Z}_1]$$

$$[\mathbf{Z}_{out4}] = [\mathbf{R}_d] + [\mathbf{Z}_3][\mathbf{R}_a]^{-1}[\mathbf{Z}_2]$$

## E- PROPOSED ALGORITHM FOR THE HARMONIC BALANCE

The large-signal / small-signal analysis is quite similar to nonlinear / linear circuit analysis. For that purpose, we can propose a general framework for both linear and nonlinear circuit design in the form of the algorithm shown on Figure III-15. This algorithm is based on the analysis using connection-scattering matrix for the circuit design and on the harmonic balance algorithm for the nonlinear part.

An outer optimization loop can be added to the process to improve the circuit performance. For linear circuits, the optimization loop will change some element values in order to reach the desired requirements. But for nonlinear circuits, the problem is more complicated.

In fact, the optimized elements are function not only of the fundamental excitation frequency but also of all harmonics. Then the question is:

What should be the new circuit topology after optimization  
to match the new input-output impedances *for each harmonic?*

To clarify the meaning of this question, let us consider a diode mixer proposed by Maas and shown on Figure III-16.

---

*The materials you receive for this course are protected by copyright and to be used for this course only. You do not have permission to upload the course materials, including any lecture recordings you may have, to any website. If you require clarification, please consult your professor.*

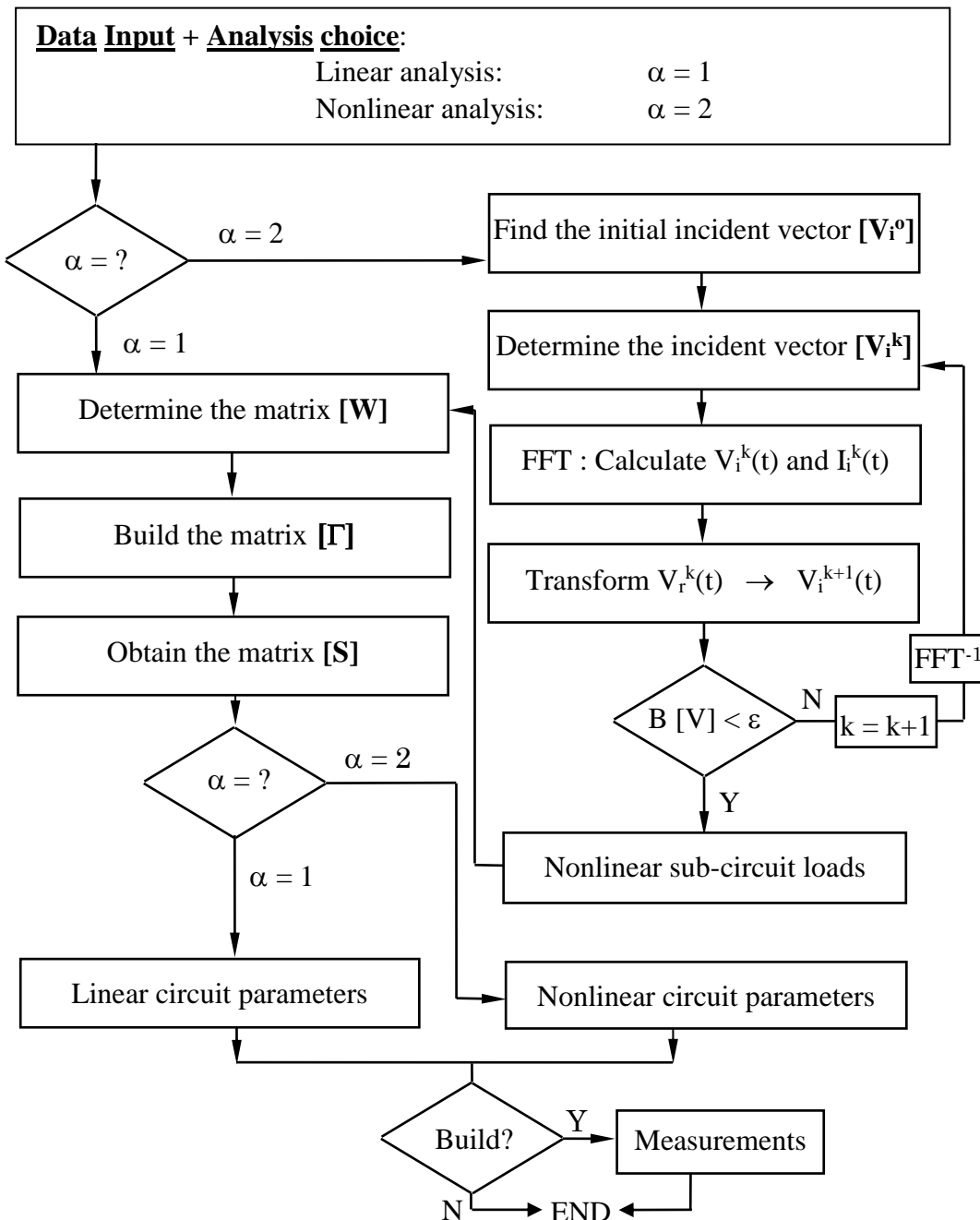


Fig. III-15. General linear-nonlinear circuit analysis algorithm.

The materials you receive for this course are protected by copyright and to be used for this course only. You do not have permission to upload the course materials, including any lecture recordings you may have, to any website. If you require clarification, please consult your professor.

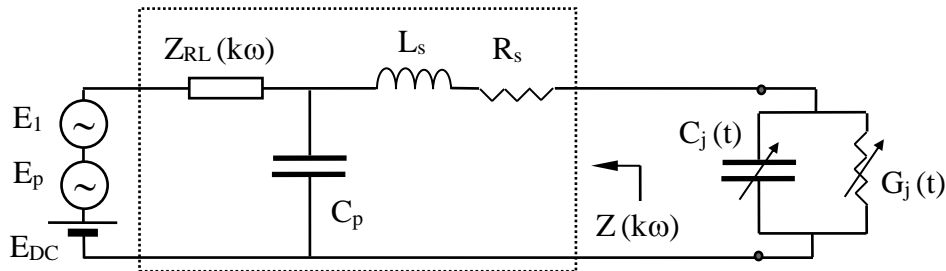


Fig. III-16. Equivalent circuit of a mixer proposed by Maas.

. By varying the loads impedances  $Z(k\omega_p)$ , we can notice that the optimization loop reduces the conversion loss (Table III-II), but what is the conclusion for the new circuit topology? Should we change the matching cells topology, the filters input-output impedances, the bias network, ....?

Table III-II. Diode mixer parameters before and after optimization.

	Before Optimization	After Optimization
Conversion Loss L (dB)	4.33 dB	3.48 dB
Large-signal impedances ( $\Omega$ )	$Z(\omega_p)$ $50.0 + j 20.0$ $Z(2\omega_p)$ $10.0 + j 0.0$	$49.9 + j 28.0$ $9.98 + j 0.01$
Small-signal impedances ( $\Omega$ )	$Z(\omega_{FI} + \omega_p)$ $35.0 + j 20.0$ $Z(\omega_{FI} + 2\omega_p)$ $1.0 + j 0.0$	$48.0 + j 56.0$ $1.01 + j 0.0$

**The answer to this question remains open for all researchers.**

## **APPENDIX III-1**

### **EQUIVALENT NETWORKS**

## **A – EQUIVALENT NETWORKS FOR LINEAR CIRCUITS**

Let  $M$  an  $N$ -port network defined by its reduced impedance matrix  $[z]$ . If at each port  $k$ , we connect a coupling two-port  $Q_k$  of which the chain matrix is  $[T^k]$ , the impedance matrix of the overall network  $M' = \{ (M, Q_k) \}$  will be noted  $[z']$ .

Let the incident and reflected waves vectors of network  $M$  and  $M'$  be  $\{ [a], [b] \}$  and  $\{ [a'], [b'] \}$  respectively. Then, from the definition of scattering matrices, the corresponding chain matrix between  $M$  and  $M'$  is defined as

$$\begin{aligned} [b] &= [S][a] \\ [b'] &= [S'][a'] \end{aligned} \quad \xrightarrow{\quad} \quad \begin{bmatrix} [b'] \\ [a'] \end{bmatrix} = \begin{bmatrix} [T_{11}] & [T_{12}] \\ [T_{21}] & [T_{22}] \end{bmatrix} \begin{bmatrix} [b] \\ [a] \end{bmatrix} \quad (\text{AIII1-1})$$

where  $[S]$  and  $[S']$  are the scattering matrices of  $M$  and  $M'$  respectively and where the  $[T_{ij}]$  are diagonal chain sub-matrices of elements  $T_{ij}^k$ . It can be shown that the scattering matrix  $[S']$  can be written as

$$[S'] = \{ [T_{11}] + [T_{12}][S][T_{21}] \{ [T_{21}] + [T_{22}][S] \}^{-1} \} \quad (\text{AIII1-2})$$

---

*The materials you receive for this course are protected by copyright and to be used for this course only. You do not have permission to upload the course materials, including any lecture recordings you may have, to any website. If you require clarification, please consult your professor.*

Moreover, if all the two-port  $Q_k$  are reciprocal and lossless, then the chain matrix is symmetric and the sub-matrices  $[T_{ij}]$  can be noted as:

$$[T_{11}] = [T_{22}]^* = [\alpha] \quad \text{and} \quad [T_{21}] = [T_{12}]^* = [\beta] \quad (\text{AIII1-3})$$

where the symbol "\*" indicates the conjugate matrix. If we note the unit matrix as  $[\mathfrak{I}]$ , then the sub-matrices satisfy to

$$[\alpha][\alpha]^* - [\beta][\beta]^* = [\mathfrak{I}]$$

$$\Rightarrow [S'] = \left\{ [\alpha] + [\beta][S] \right\} \left\{ [\beta]^* + [\alpha]^*[S] \right\}^{-1} \quad (\text{AIII1-4})$$

The invariance of  $M$  defines its intrinsic properties independently of the  $Q_k$  (assumed to be the embedding sub-network of  $M$ ). These are the functions of  $S_{ij}$  which do not vary with the transformation (AIII1-4). In this case, the networks  $M$  and  $M'$  are called "equivalent networks" and then, have the same properties and performance.

This conclusion implies that the performance of a particular component assumed to be  $M$  (generally an active component like a diode or a transistor) and the corresponding circuit ( $M'$ ) can be the same if the circuit topology is well defined.

This remark means that the embedding sub-network of the active component (corresponding to all coupling two-port) must be lossless and reciprocal.

Then, under this condition, the optimization of a circuit performance can be reduced to the optimization of each active component parameters.

In order to apply this notion of equivalent networks to linear electronic circuits, let us consider the following relation between the incident and reflected waves of  $M$  and  $M'$  at each port  $k$

$$\begin{bmatrix} b'_k \\ a'_k \end{bmatrix} = \begin{bmatrix} \lambda_k & 0 \\ 0 & \lambda_k \end{bmatrix} \begin{bmatrix} a_k \\ b_k \end{bmatrix} \quad (\text{AIII1-5})$$

with  $\lambda_k > 0$ . In this case, the chain matrix  $[T^k]$  permits to obtain the following identity

$$[T^k] [\lambda^k] [T^k]^* = [\lambda^k] \quad (\text{AIII1-6})$$

which is independent of the corresponding two-port  $Q_k$ . From these results, the combination of (AIII1-1) and (AIII1-6) gives the general form

$$[\lambda] - [S'][\lambda][S] = [0] \quad (\text{AIII1-7})$$

and the solution of this system of equations is given by :

$$\det \{ [\lambda] - [S'][\lambda][S] \} = 0 \quad \text{or} \quad \det \{ [\lambda][Z] + [Z'][\lambda] \} = 0 \quad (\text{AIII1-8})$$

The only relations between  $[Z]$  and  $[Z']$  are under the general forms

$$[Z'] = -[R]^{-1}[Z][R] \quad [Z'] = -[R]^{-1}[Z]^t[R] \quad (\text{AIII1-9-a})$$


---

and

$$[\mathbf{z}'] = -[\mathbf{R}]^{-1} [\mathbf{z}]^* [\mathbf{R}] \quad [\mathbf{z}'] = -[\mathbf{R}]^{-1} [\mathbf{z}]^+ [\mathbf{R}] \quad (\text{AIII1-9-b})$$

where the superscripts "  $[ ]^t$ " and "  $[ ]^+$ " indicate respectively the transpose matrix and the complex conjugate transpose matrix and where  $[\mathbf{R}]$  is the reference matrix (for example the characteristic impedance matrix in the case of distributed elements). We can demonstrate that the two first relations (AIII1-9-a) represent the properties of non reciprocity in a network and that the two last relations (AIII1-9-b) are the most interesting. In fact, they are used for determining stability and maximum efficiency of networks [10]. For example, the last equation, which is the most general form

$$\det \left\{ [\lambda] [\mathbf{z}] + [\mathbf{z}]^+ [\lambda] \right\} = \det \left\{ [\mathbf{G}] \right\} = 0 \quad (\text{AIII1-10})$$

allow defining the maximum circuit efficiency. In fact, if  $I_k$  and  $P_k$  are respectively the current and the allowed power at a given port  $k$ , (AIII1-10) can be written as a power relation

$$[I_1 \ \dots \ I_N]^* [\mathbf{G}] \begin{bmatrix} I_1 \\ \vdots \\ I_N \end{bmatrix} = [\mathbf{0}] \quad \Rightarrow \quad \sum_{k=1}^N \lambda_k P_k = 0 \quad (\text{AIII1-11})$$

A port "0" can be added to take into account the eventual bias port of the active component. The volume defined by (AIII1-11) is enclosed by a surface characterized by canceling with a sign change of an eigenvector of  $[\mathbf{G}]$ . This surface is called the "characteristic surface" of the linear network. In order to determine the maximum efficiency, let us load the ports (2) to (N) of the network  $M$  (active component) by passive reactive impedances  $\{P_k \leq 0, k = 2, \dots, N\}$  and connect

---

*The materials you receive for this course are protected by copyright and to be used for this course only. You do not have permission to upload the course materials, including any lecture recordings you may have, to any website. If you require clarification, please consult your professor.*

the first port to a source  $\{P_1 \geq 0\}$ . A variation of the impedance values is equivalent to change the above network  $M$  by an equivalent network  $M'$  which of the loads would be identical.

So, if  $\lambda_2, \dots, \lambda_N$  are maintained constant, it is necessary that  $\lambda_1$  and  $\lambda'_1$  should be different in order to verify the following power relation

$$\lambda'_1 P'_1 + \sum_{k=2}^N \lambda_k P'_k = 0 \quad (\text{AIII112})$$

As shown in Fig. 1, let us consider in the  $\lambda_k$  N-dimensions space, the points  $A'(\lambda_1, \lambda_2, \dots, \lambda_N)$  and  $A''(\lambda'_1, \lambda_2, \dots, \lambda_N)$  as the intersection points  $A_1$  and  $A_2$  of the line  $A'A''$  with the contour  $C_k(\lambda)$  of the characteristic surface.

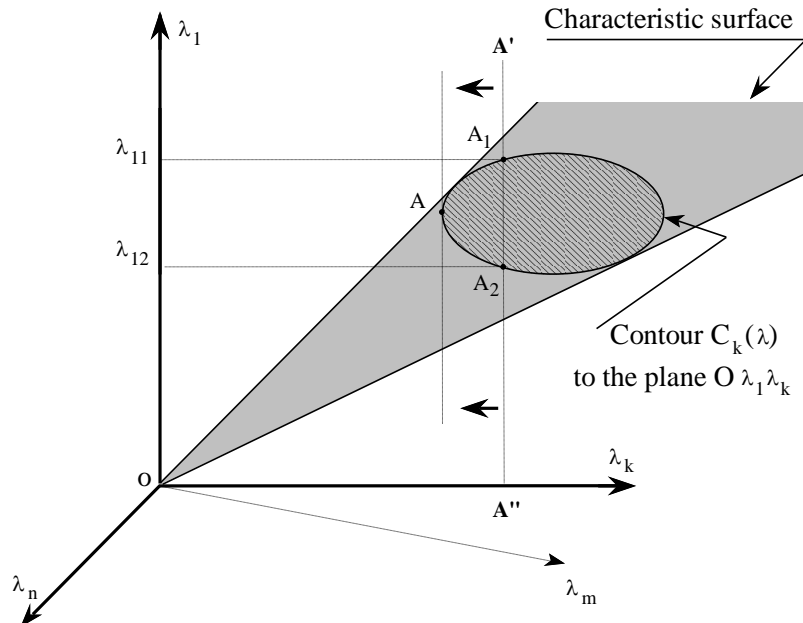


Fig. AIII1-1. Characteristic surface of a linear network.

The materials you receive for this course are protected by copyright and to be used for this course only. You do not have permission to upload the course materials, including any lecture recordings you may have, to any website. If you require clarification, please consult your professor.

Since A' and A" cannot be between A<sub>1</sub> and A<sub>2</sub>, the coordinates λ<sub>11</sub> and λ<sub>12</sub> of λ<sub>1</sub> are the extrema of the function:

$$\frac{-\sum_{k=2}^N \lambda_k P_k}{P_1} = 0 \quad (\text{AIII1-13})$$

Thus, if { μ<sub>N1</sub> = - P<sub>N</sub> / P<sub>1</sub> } is the partial efficiency between the ports (1) and (N), find the maximum of μ<sub>N1</sub> implies to determine the solutions of { λ<sub>2</sub> P<sub>2</sub> + ... + λ<sub>N-1</sub> P<sub>N-1</sub> = 0 } under the conditions { P<sub>k</sub> ≤ 0, λ<sub>k</sub> > 0, k = 2, ..., N-1 }.

The condition { λ<sub>k</sub> = 0, k = 2, ..., N-1 } is not acceptable because it implies that { λ<sub>1</sub> = λ<sub>N</sub> = 0 }. So, the only possible solution is to put { P<sub>k</sub> = 0, ∀ λ<sub>k</sub>, k = 2, ..., N-1 }, then, to assemble the points A<sub>1</sub> and A<sub>2</sub> in an unique point A in order to obtain the maximum efficiency.

In conclusion, the maximum efficiency between two ports *i* and *j* of a linear network is then equal to the slope of the tangent to the contour C<sub>k</sub>(λ) over the plane Oλ<sub>i</sub>λ<sub>j</sub>. Now, the aim is to extend this notion of characteristic surface to nonlinear lossy networks.

## B – OPTIMIZATION OF NONLINEAR CIRCUITS

Under large-signal time-periodic regime, a nonlinear device can be simulated as a multifrequency multiport network where each port *k* corresponds to the *k*<sup>th</sup> harmonic of the fundamental input frequency (refer to Chapter I).

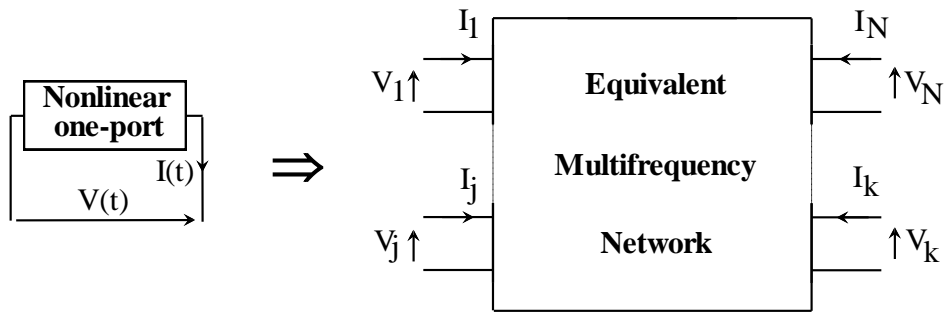


Fig. AIII1-2. Equivalent representation of a nonlinear one-port as a multifrequency N-port.

Let  $V_k$  and  $I_k$  be respectively the voltage and current at port  $k$ , the characteristics of such a diode, for a finite number  $N$  of harmonics, can be expressed by means of the  $N$  equations

$$I_k = f_k(V_1, \dots, V_N) \quad k = 1, \dots, n \quad (\text{AIII1-14})$$

Let us consider  $d$  as the distance to the origin of any plane ( $\mathbf{D}$ ) cutting the characteristic surface. The coordinates of the normal to the plane are noted  $\lambda_k$  (Fig. AIII1-3 presents a 2-D graphic illustration).

Any variation of voltage implies a variation of the distance  $d$ . Now on the contour of the characteristic surface, at contact point  $M_0$ , this distance has a maximum  $d_0$ . So, the points of this contour represent allowed powers independent of any variation of voltage. These maximum powers verify the equation of any tangent plane ( $\mathbf{D}_0$ ) to the surface:

$$\sum_{k=1}^N \lambda_k P_k = d(V_1, \dots, V_n) \quad (\text{AIII1-15})$$

---

*The materials you receive for this course are protected by copyright and to be used for this course only. You do not have permission to upload the course materials, including any lecture recordings you may have, to any website. If you require clarification, please consult your professor.*

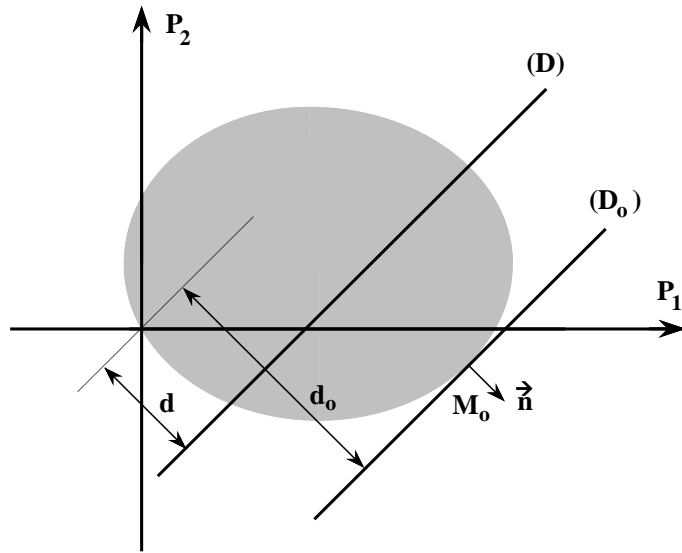


Fig. AIII1-3. Characteristic surface of a nonlinear two-port network.

Moreover, from (AIII1-14), it is possible to deduce an admittance matrix  $[\partial Y]$  which the element  $\partial Y_{jk}$  is the derivative of jth harmonic current  $I_j$  with respect to kth harmonic voltage  $V_k$  :

$$\partial Y_{jk} = \frac{\partial I_j}{\partial V_k} \quad \rightarrow \quad [\partial I_1, \dots, \partial I_N]^t = [\partial Y] [\partial V_1, \dots, \partial V_N]^t \quad (\text{AIII1-16})$$

Furthermore, with the fact that powers must be limited, conditions of extremum operation should be taken into consideration. So, a supplementary relation is added to the system in the form of a constraint condition

$$\sum_{m=1}^N V_m \sum_{n=1}^N I_n^* \leq \bar{P}_{\max} \quad (\text{AIII1-17})$$

---

*The materials you receive for this course are protected by copyright and to be used for this course only. You do not have permission to upload the course materials, including any lecture recordings you may have, to any website. If you require clarification, please consult your professor.*

where  $\bar{P}_{\max}$  is the mean output maximum power of the one-port active component. The combination of relations (AIII1-15) and (AIII1-16) gives, independently of any arbitrary variation of voltage  $\delta V_k$  (at any port of the network), the following system of  $N$  nonlinear equations

$$\mathbf{Re} \{ [\mathbf{I}]^+ [\lambda] + [\mathbf{V}]^+ [\lambda] [\mathbf{Y}] \} = \mathbf{0} \quad (\text{AIII1-18})$$

where **Re** denotes the real part. This system describes the combinations of extremum allowed powers available at the different ports of the nonlinear active component. To each set of values  $\lambda_k$  corresponds a solution of voltage vector and therefore a combination of extremum allowed powers. So, the intersection points of the characteristic surface with the tangent planes are obtained by variation of the  $\lambda_k$ . Since relations (AIII1-14) allow writing the harmonic currents in function of voltages, the unknown vector is the harmonic voltage vector. The determination of the voltages for the different harmonics allows deducing the optimum loads for the nonlinear component. Then, the large-signal optimum efficiency between the input power  $P_j$  and the output power  $P_k$ , defined as  $\{\mu_{jk\text{opt}} = P_{k\text{max}} / P_{j\text{opt}}\}$  is deduced from the characteristic surface (Fig. AIII1-4 shows the large-signal optimum efficiency of a nonlinear two-port network).

In the case of a two-port, like a transistor, the current-voltage characteristics can be expressed by

$$I_{1k} = f_{1k}(V_{11}, \dots, V_{1N}, V_{21}, \dots, V_{2N}); \quad I_{2k} = f_{2k}(V_{11}, \dots, V_{1N}, V_{21}, \dots, V_{2N}) \quad (\text{AIII1-19})$$

Then, with the same reasoning, we will have a nonlinear system of  $2N$  equations similar to the one described by (AIII1-18).

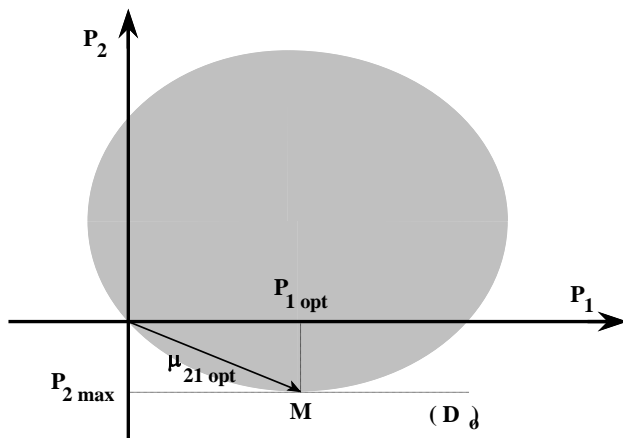


Fig. AIII1-4. Large-signal optimum efficiency  $\mu_{21\text{opt}}$  of a nonlinear frequency two-port network.

## B – APPLICATION TO TRANSISTORS

To apply the above method to a MEtal-Semiconductor Field Effect Transistor (MESFET), we must beforehand express the I-V relationships. Then, the equations governing the model

$$\left. \begin{aligned} -V_{gs} + Z_g I_{gs} + V_{gd} - Z_d I_{ds} + V_{ds} &= 0 \\ -V_{gs} + Z_g I_{gs} + V_g + R_i(I_{gs} - I_{gd}) + Z_s(I_{ds} + I_{gs}) &= 0 \\ -V_{ds} + Z_d I_{ds} + \mu V_g + R_{ds}(I_{ds} + I_{gd}) + Z_s(I_{ds} + I_{gs}) &= 0 \end{aligned} \right\} \quad (\text{AIII1-20})$$

allow deducing an admittance matrix  $[Y]$  which relies input and output currents respectively  $I_{gs}$  and  $I_{ds}$  to input gate-source voltage  $V_{gs}$  and output drain-source voltage  $V_{ds}$  :

$$\begin{bmatrix} \mathbf{I}_{gs} \\ \mathbf{I}_{ds} \end{bmatrix} = [\mathbf{Y}] \begin{bmatrix} \mathbf{V}_{gs} \\ \mathbf{V}_{ds} \end{bmatrix} \quad (\text{AIII1-21})$$

*The materials you receive for this course are protected by copyright and to be used for this course only. You do not have permission to upload the course materials, including any lecture recordings you may have, to any website. If you require clarification, please consult your professor.*

and then their corresponding harmonic coefficients:

$$\begin{bmatrix} \mathbf{I}_{gso} \\ \vdots \\ \mathbf{I}_{gsN} \\ \mathbf{I}_{dso} \\ \vdots \\ \mathbf{I}_{dsN} \end{bmatrix} = \begin{bmatrix} [\mathbf{Y}_{11}] & \vdots & [\mathbf{Y}_{12}] \\ \dots & \dots & \vdots & \dots & \dots \\ [\mathbf{Y}_{21}] & \vdots & [\mathbf{Y}_{22}] \end{bmatrix} \begin{bmatrix} \mathbf{V}_{gso} \\ \vdots \\ \mathbf{V}_{gsN} \\ \mathbf{V}_{dso} \\ \vdots \\ \mathbf{V}_{dsN} \end{bmatrix}$$

$$\Rightarrow \begin{cases} I_{gsk} = f_{gk}(V_{gso}, \dots, V_{gsN}, V_{dso}, \dots, V_{dsN}) \\ I_{dsk} = f_{dk}(V_{gso}, \dots, V_{gsN}, V_{dso}, \dots, V_{dsN}) \end{cases} \quad (\text{AIII1-22})$$

It is the same for the derivatives of drain-source and gate-source harmonic currents with respect to drain-source and gate-source voltage vectors:

$$\begin{bmatrix} \partial \mathbf{I}_{gso} \\ \vdots \\ \partial \mathbf{I}_{gsN} \\ \partial \mathbf{I}_{dso} \\ \vdots \\ \partial \mathbf{I}_{dsN} \end{bmatrix} = \begin{bmatrix} [\partial \mathbf{Y}_{11}] & \vdots & [\partial \mathbf{Y}_{12}] \\ \dots & \dots & \vdots & \dots & \dots \\ [\partial \mathbf{Y}_{21}] & \vdots & [\partial \mathbf{Y}_{22}] \end{bmatrix} \begin{bmatrix} \partial \mathbf{V}_{gso} \\ \vdots \\ \partial \mathbf{V}_{gsN} \\ \partial \mathbf{V}_{dso} \\ \vdots \\ \partial \mathbf{V}_{dsN} \end{bmatrix} \quad (\text{AIII1-23})$$

where the elements of the submatrices are

$$\mathcal{Y}_{11}(k, m) = \frac{\partial I_{gsk}}{\partial V_{gsm}} ; \quad \mathcal{Y}_{12}(k, m) = \frac{\partial I_{gsk}}{\partial V_{dsm}}$$

$$\mathcal{Y}_{21}(k, m) = \frac{\partial I_{dsk}}{\partial V_{gsm}} ; \quad \mathcal{Y}_{22}(k, m) = \frac{\partial I_{dsk}}{\partial V_{dsm}}$$

---

The materials you receive for this course are protected by copyright and to be used for this course only. You do not have permission to upload the course materials, including any lecture recordings you may have, to any website. If you require clarification, please consult your professor.

## REFERENCES

### *General references*

- [1] H.J. Carlin, "The scattering matrix in network theory," *IRE Trans. Circuit Theory*, Vol 3, 88-97, June 1956.
- [2] K. Kurokawa, "Power waves and the scattering matrix," *IEEE Trans. Microwave Theory Tech.*, Vol 13, 194-202, Mar. 1965.
- [3] Hewlett-Packard, *S-Parameters, circuit analysis and design*, Application note N° 95, 1968.
- [4] T.C. Laverghetta, *Handbook of microwave testing*, London : Artech House, 1981.
- [5] K.C. Gupta, R. Garg, R. Chadha, *Computer aided design of microwave circuits*, Dedham MA : Artech House, 1981.
- [6] S.A. Maas, *Nonlinear microwave circuits*, Norwood MA: Artech House, 1988.
- [7] J. Fitzpatrick, T. Cutler, "From CAE to measurements and documentation - one program in the 90's," *Applied Microwave*, 88-96, May 1989.
- [8] G.D. Vendelin, A.M. Pavio, U.L. Rohde, *Microwave circuit design using linear and nonlinear techniques*, New York : Wiley & Sons, 1990.
- [9] S.A. Maas, *C/NL: linear and nonlinear microwave circuit analysis and optimization software*, Butler WI: Artech House, 1990.

### *Linear circuit analysis*

- [10] R.W. Newcomb, *Linear multiport synthesis*, New York: Mc Graw-Hill, 1956.
  - [11] W.F. Tinney, Walker J.W., "Direct solutions of sparse network equations by optimally ordered triangular factorization," *Proc. IEEE*, Vol 55, 1801-1809, Nov. 1967.
  - [12] G.D. Hachtel, R.K. Brayton, F.G. Gustavson, "The sparse tableau approach to network analysis and design," *IEEE Trans. Circuit Theory*, Vol 18, 101-113, Jan. 1971.
- 

*The materials you receive for this course are protected by copyright and to be used for this course only. You do not have permission to upload the course materials, including any lecture recordings you may have, to any website. If you require clarification, please consult your professor.*

- [13] G.C.S. Bown, G.V. Geiger, "Design and optimization of circuits by computer," *Proc. IEEE*, Vol 118, 649-661, May 1971.
  - [14] P. Bodharamik, L. Besser, R.W. Newcomb, "Two scattering matrix programs for active circuit analysis," *IEEE Trans. Microwave Theory Tech.*, Vol 18, 610-618, Nov. 1971.
  - [15] R.N. Gadenz, G.C. Temes, "Efficient hybrid and state space analysis of the adjoint network," in *IEEE Int. Symp. Circuit Theory*, Los Angeles, 184-188, 1972.
  - [16] G.C. Temes, R.M. Ebers, R.N. Gadenz, "Some applications of the adjoint network concept in frequency domain analysis and optimization," *Computer Aided Design*, Vol 4, 129-134, April 1972.
  - [17] Fairchild Semiconductor, *SPEEDY: a Computer aided design program for RF and microwave circuits*, User manual, 1973.
  - [18] L.W. Nagel, D.O. Pederson, *SPICE: Simulation Program with Integrated Circuit Emphasis*, Memo ERL-M382, Berkeley University, CA, 1973.
  - [19] E. Sánchez-Sinencio, T.N. Trick, "CADMIC - Computer-aided design of microwave integrated circuits," *IEEE Trans. Microwave Theory Tech.*, Vol 22, 309-316, Mar. 1974.
  - [20] V.A. Monaco, P. Tiberio, "Computer-aided analysis of microwave circuits," *IEEE Trans. Microwave Theory Tech.*, Vol 22, 249-263, Mar. 1974.
  - [21] F. Bonfatti, V.A. Monaco, P. Tiberio, "Microwave circuit analysis by sparse-matrix techniques," *IEEE Trans. Microwave Theory Tech.*, Vol 22, 264-269, Mar. 1974.
  - [22] W.A. Rytand, "OPNODE: interactive linear circuit design and optimization," *Hewlett-Packard J.*, 28-31, Mar. 1977.
  - [23] Compact Inc., *COMPACT : Computerized Optimization of Microwave Passive and Active CircuiTs*, User manual, 1978.
  - [24] P.F. Combes, J. Graffeuil, J.F. Sautereau, *Composants, dispositifs et circuits actifs en micro-ondes*, Paris : Dunod Université, 1985.
  - [25] L.O. Chua, C.A. Desoer, E.S. Kuh, *Linear and nonlinear circuits*, New-York : Mc Graw-Hill, 1987.
- 

The materials you receive for this course are protected by copyright and to be used for this course only. You do not have permission to upload the course materials, including any lecture recordings you may have, to any website. If you require clarification, please consult your professor.

### **Nonlinear circuit analysis**

- [26] G.L. Heiter, "Characterization of nonlinearities in microwave devices and systems," *IEEE Trans. Microwave Theory Tech.*, Vol 21, 797-805, Dec. 1973.
  - [27] D. Frey, "A simple generalised modelling technique for non-linear networks," in *IEEE Int. Symp. on Circuit Syst.*, Montreal, 1984.
  - [28] V. Rizzoli, A. Neri, "State of the art and present trends in nonlinear microwave CAD techniques," *IEEE Trans. Microwave Theory Tech.*, Vol 36, 343-365, Feb. 1988.
  - [29] M.I. Sobhy, E.A. Hosny, Y.A.R. El-Sawy, A.A. Nasser, A.K. Jastrzebski, "Recent results in non-linear microwave circuit analysis," in *20th European Microwave Conf.*, Budapest, Sept. 1990.
  - [30] M.B. Steer, "Simulation of nonlinear microwave circuits - an historical perspective and comparisons," in *IEEE Int. Microwave Symp. Dig.*, Boston, 599-602, 1991.
  - [31] M. Nakhla, J. Vlach, "A piecewise harmonic balance technique for determination of periodic response of nonlinear systems," *IEEE Trans. Circuits Syst.*, Vol 23, 85-91, Feb. 1976.
  - [32] J. Lenkowski, "Transients in periodically time-varying circuits," *IEEE Trans. on Circuit Theory*, Vol 14, 426-429, Dec. 1967.
  - [33] L. Gustafsson, G.H.B. Hansson, K.I. Lundstroem, "On the use of describing functions in the study of nonlinear active microwave circuits," *IEEE Trans. Microwave Theory Tech.*, Vol 20, 402-409, June 1972.
  - [34] S. Skelboe, "Computation of the periodic steady-state response of nonlinear networks by extrapolation methods," *IEEE Trans. Circuits Syst.*, Vol 27, 161-175, Mar. 1980.
  - [35] M.I. Sobhy, A.K. Jastrzebski, "Direct integration methods of non-linear microwave circuits," in *15th European Microwave Conf.*, Paris, Sept. 1985.
  - [36] M.I. Sobhy, Y.A.R. El-Sawy, "Parallel processing application to nonlinear microwave network design," *IEEE Trans. Microwave Theory Tech.*, Vol 37, 2067-2073, Dec. 1989.
- 

*The materials you receive for this course are protected by copyright and to be used for this course only. You do not have permission to upload the course materials, including any lecture recordings you may have, to any website. If you require clarification, please consult your professor.*

- [37] M.I. Sobhy, E.A. Hosny, M.W.R. Ng, E.A. Bakkar, "Nonlinear system and subsystem modeling in time domain," *IEEE Trans. Microwave Theory Tech.*, Vol 44, 2571-2579, Dec. 1996.
- [38] J. Kunisch, A. Bahr, M. Rittweger, I. Wolff, "Analysis of nonlinear microwave circuits using the compression approach," in *IEEE MTT-S Int. Microwave Symp. Dig.*, Atlanta, 637-640, 1993.
- [39] V. Volterra, *Theory of functionals and of integral and integro-differential equations*, New-York: Dover, 1959.
- [40] R.G. Sea, A.G. Vacroux, "On the computation of intermodulation products for a power series nonlinearity," *Proc. IEEE*, Vol 57, 337-338, Mar. 1969.
- [41] E. Bedrosian, S.O. Rice, "The output properties of Volterra system (nonlinear system with memory) driven by harmonic and gaussian inputs," *Proc. IEEE*, Vol 59, 1688-1707, Dec. 1971.
- [42] D.D. Weiner, G.H. Naditch, "A scattering variable approach to the Volterra analysis of nonlinear systems," *IEEE Trans. Microwave Theory Tech.*, Vol 24, 422-433, July 1976.
- [43] V. Rizzoli, A. Lipparini, E. Marazzi, "A general purpose program for nonlinear microwave circuit design," *IEEE Trans. Microwave Theory Tech.*, Vol 31, 762-770, Sept. 1983.
- [44] K.S. Kundert, A. Sangiovanni-Vincentelli, "Simulation of nonlinear circuits in the frequency domain," *IEEE Trans. Computer-Aided Design*, Vol 5, 521-535, Oct. 1986.
- [45] S.A. Maas, "A general-purpose computer program for the Volterra-series analysis of nonlinear microwave circuits," in *IEEE MTT-S Int. Microwave Symp. Dig.*, New-York, 311-314, 1988.
- [46] G.W. Rhyne, M.B. Steer, B.D. Bates, "Frequency-domain nonlinear circuit analysis using generalized power series," *IEEE Trans. Microwave Theory Tech.*, Vol 36, 379-387, Feb. 1988.

---

*The materials you receive for this course are protected by copyright and to be used for this course only. You do not have permission to upload the course materials, including any lecture recordings you may have, to any website. If you require clarification, please consult your professor.*

- [47] J.W. Bandler, Q.J. Zhang, R.M. Biernacki, "A unified theory for frequency-domain simulation and sensitivity analysis of linear and nonlinear circuits," *IEEE Trans. Microwave Theory Tech.*, Vol 36, 1661-1669, Dec. 1988.
  - [48] Y. Hu, J.J. Obregon, J.C. Mollier, "Nonlinear analysis of microwave FET oscillators using Volterra series," *IEEE Trans. Microwave Theory Tech.*, Vol 37, 1689-1693, Nov. 1989.
  - [49] P.J. Lunsford II, G.W. Rhyne, M.B. Steer, "Frequency-domain bivariate generalized power series analysis of nonlinear analog circuits," *IEEE Trans. Microwave Theory Tech.*, Vol 38, 815-818, June 1990.
  - [50] C.R. Chang, M.B. Steer, "Frequency-domain nonlinear microwave circuit simulation using the arithmetic operator method," *IEEE Trans. Microwave Theory Tech.*, Vol 38, 1139-1143, Aug. 1990.
  - [51] M.B. Steer, C.R. Chang, G.W. Rhyne, "Computer aided analysis of nonlinear microwave circuits using frequency domain spectral balance techniques: the state of the art," *Int. J. on Microwave and Millimeter CAE*, Vol 1, Apr. 1991.
  - [52] T. Larsen, "Determination of Volterra Transfer functions of non-linear multiport networks", *Int. Journal of Circuit Theory and Applications*, Vol 21 (2), 107-131, 1993.
  - [53] T. Nähri, "Frequency-domain analysis of strongly nonlinear circuits using a consistent large-signal model," *IEEE Trans. Microwave Theory Tech.*, Vol 44, 182-192, Feb. 1996.
  - [54] M. Gayral, *Simulation des circuits microondes par la méthode d'équilibrage harmonique et spectral*, Thèse de Doctorat, Université de Limoges, France, 1987.
  - [55] W.R. Curtice, "Nonlinear analysis of GaAs MESFET amplifiers, mixers and distributed amplifiers using the harmonic balance technique," *IEEE Trans. Microwave Theory Tech.*, Vol 35, 441-447, April 1987.
  - [56] U.L. Rohde, "Harmonic balance method handles nonlinear microwave CAD problems," *Microwave J.*, Vol 30, 203-210, Oct. 1987.
- 

*The materials you receive for this course are protected by copyright and to be used for this course only. You do not have permission to upload the course materials, including any lecture recordings you may have, to any website. If you require clarification, please consult your professor.*

- [57] J.W. Bandler, Q.J. Zhang, R.M. Biernacki, "A unified framework for harmonic balance simulation and sensitivity analysis," in *IEEE Int. Microwave Symp. Dig.*, New-York, 1041-1044, 1988.
  - [58] R.J. Gilmore, M.B. Steer, "Nonlinear circuit analysis using the method of harmonic balance - a review of the art : Part I, Introductory concepts; Part II, Advanced concepts," *Int. J. on Microwave and Millimeter CAE*, Vol 1, Jan. / Apr. 1991.
  - [59] N. Kryloff, N. Bogoliuboff, *Introduction to nonlinear mechanics*, Princeton: University Press, 1943.
  - [60] S. Egami, "Nonlinear, linear analysis and computer aided design of resistive mixers," *IEEE Trans. Microwave Theory Tech.*, Vol 22, 270-275, Mar. 1974.
  - [61] A.R. Kerr, "A technique for determining the local oscillator waveforms in a microwave mixer," *IEEE Trans. Microwave Theory Tech.*, Vol 23, 828-831, Oct. 1975.
  - [62] R.G. Hicks, P.J. Khan, "Numerical analysis of nonlinear solid-state device excitation in microwave circuits," *IEEE Trans. Microwave Theory Tech.*, Vol 30, 251-259, Mar. 1982.
  - [63] C. Camacho-Penalosa, "Numerical steady-state analysis of nonlinear microwave circuits with periodic excitation," *IEEE Trans. Microwave Theory Tech.*, Vol 31, 724-730, Sept. 1983.
  - [64] R.J. Gilmore, "Nonlinear circuit design using the modified harmonic balance algorithm," *IEEE Trans. Microwave Theory Tech.*, Vol 34, 1294-1307, Dec. 1986.
  - [65] K.S. Kundert, G.B. Sorkin, A. Sangiovanni-Vincentelli, "Applying harmonic balance to almost-periodic circuits," *IEEE Trans. Microwave Theory Tech.*, Vol 36, 366-378, Feb. 1988.
  - [66] M. Gayral, E. Ngoya, R. Quere, J. Rousset, J.J. Obregon, "Un outil pour la CAO des circuits microondes non linéaires attaqués par des générateurs non harmoniques", *Ann. Télécommun.*, Vol 43 (5-6), 306-313, 1988.
  - [67] V. Rizzoli, A. Neri, "Harmonic-balance analysis of multitone autonomous nonlinear microwave circuits", in *IEEE MTT-S Int. Microwave Symp. Dig.*, Boston, 107-110, 1991.
- 

*The materials you receive for this course are protected by copyright and to be used for this course only. You do not have permission to upload the course materials, including any lecture recordings you may have, to any website. If you require clarification, please consult your professor.*

- [68] V. Rizzoli, A. Lipparini, A. Costanzo, F. Mastri, C. Cecchetti, A. Neri, D. Masotti, "State-of-the-art harmonic-balance simulation of forced nonlinear microwave circuits by the piecewise technique," *IEEE Trans. Microwave Theory Tech.*, Vol 40, 12-28, Jan. 1992.
  - [69] V. Rizzoli, A. Lipparini, V.D. Esposti, F. Mastri, C. Cecchetti, "Simultaneous thermal and electrical analysis of nonlinear microwave circuits," *IEEE Trans. Microwave Theory Tech.*, Vol 40, 1446-1455, July 1992.
  - [70] V. Rizzoli, F. Mastri, F. Sgallari, G. Spaletta, "Harmonic-balance simulation of strongly nonlinear very large-size microwave circuits by inexact Newton methods," in *IEEE MTT-S Int. Microwave Symp. Dig.*, San Francisco, 1357-1360, 1996.
  - [71] Y. Thodesen, K. Kundert, "Parametric harmonic balance," in *IEEE MTT-S Int. Microwave Symp. Dig.*, San Francisco, 1361-1364, 1996.
  - [72] V. Borish, J. East, G. Haddad, "An efficient Fourier transform algorithm for multitone harmonic balance," *IEEE Trans. Microwave Theory Tech.*, Vol 47, 182-188, Feb. 1999.
  - [73] H. Nussbaumer, *Fast Fourier Transform and convolution algorithms*, Berlin: Springer-Verlag, 1981.
  - [74] S. Vajda, *Theory of linear and nonlinear programming*, London: Longman, 1974.
  - [75] V.A. Monaco, P. Tiberio, "Computer-aided analysis of microwave circuits," *IEEE Trans. Microwave Theory Tech.*, Vol 22, 249-263, Mar. 1974.
  - [76] J. Vignes, *Algorithmes numériques*, Tome II, Paris: Technip, 1980.
  - [77] Jr. Denis, R.B. Schnabel, *Numerical methods of unconstrained optimization and nonlinear equations*, Englewood Cliffs NJ: Prentice Hall, 1983.
  - [78] W. Press, B.P. Flannery, S.A. Teukolsky, W.T. Vetterling, *Numerical Recipes*, 2nd Ed., New-York: University Press, 1990.
  - [79] M.C.E. Yagoub, *Contribution à l'optimisation des circuits micro-ondes non linéaires*, Ph.D. Thesis, INP, Toulouse, France, 1994.
- 

*The materials you receive for this course are protected by copyright and to be used for this course only. You do not have permission to upload the course materials, including any lecture recordings you may have, to any website. If you require clarification, please consult your professor.*

- [80] P.L. Heron, M.B. Steer, "Jacobian calculation using the multidimensional fast Fourier transform in the harmonic-balance analysis of nonlinear circuits," *IEEE Trans. Microwave Theory Tech.*, Vol 38, 429-431, April 1990.
- [81] C.R. Chang, P.L. Heron, M.B. Steer, "Harmonic-balance and frequency-domain simulation of nonlinear microwave circuits using the block Newton method," *IEEE Trans. Microwave Theory Tech.*, Vol 38, 431-434, April 1990.
- [82] D.L. Rhodes, B.S. Perlman, "Parallel computation for microwave circuit simulation," *IEEE Trans. Microwave Theory Tech.*, Vol 45, 587-592, May 1997.

---

*The materials you receive for this course are protected by copyright and to be used for this course only. You do not have permission to upload the course materials, including any lecture recordings you may have, to any website. If you require clarification, please consult your professor.*

# State of the Art and Present Trends in Nonlinear Microwave CAD Techniques

VITTORIO RIZZOLI, MEMBER, IEEE, AND ANDREA NERI

(*Invited Paper*)

**Abstract** — The paper presents a survey of modern nonlinear CAD techniques as applied to the specific field of microwave circuits. A number of fundamental aspects of the nonlinear CAD problem, including simulation, optimization, intermodulation, frequency conversion, stability, and noise, are addressed and developed. For each one it is shown that either well-established CAD solutions are available, or at least a solution approach suitable for implementation in a general-purpose CAD environment can be outlined. Also, the discussion shows that the various subjects are not just separate items, but rather can be chained in a strictly logical sequence. Finally an elementary treatment of vector processing is given, to show that supercomputers can handle the involved large-size numerical problems in a most efficient way.

## I. INTRODUCTION

THIS PAPER surveys the application of computer-aided techniques to the problem of nonlinear microwave circuit simulation for engineering purposes.

For years, the general topic of nonlinear networks has been a favorite among circuit theorists, as is clearly shown by the large amount of related technical literature. As an example, a search in the INSPEC data base revealed no less than 4000 papers devoted to this subject in the last eight years. More recently the interest in nonlinear circuit techniques has begun to spread inside the microwave community, so that at present one or more nonlinear sessions usually show up in the technical programs of all major microwave meetings. The reasons for this increasing popularity are not difficult to understand, and are closely linked to the advance of microwave technology.

One first obvious aspect is that the ever-increasing miniaturization of microwave circuits, with reduced ability to trim, calls for more powerful and general design capa-

Manuscript received February 25, 1987; revised August 31, 1987. This work was supported by the Italian Ministry of Public Education and by the Istituto Superiore delle Poste e delle Telecomunicazioni (ISPT). The development of vectorized software tools for nonlinear microwave circuit CAD is currently being pursued as a joint research effort by the Electronics Department of the University of Bologna, Fondazione Ugo Bordoni, and Fondazione Guglielmo Marconi. This paper was first given as an invited presentation at the Workshop on Trends in Microwave CAD, held in conjunction with the 1986 IEEE MTT-S International Microwave Symposium (Baltimore, MD, June 5, 1986).

V. Rizzoli is with the Dipartimento di Elettronica, Informatica e Sistemistica, University of Bologna, Villa Griffone, 40044 Pontecchio Marconi, Bologna, Italy.

A Neri is with the Fondazione Ugo Bordoni, Roma, Italy.

IEEE Log Number 8718989.

bilities. In this respect, nonlinear circuit CAD may be essentially viewed as the extension of classic CAD to problems that have traditionally been treated by semiempirical approaches.

There is, however, another aspect, which is more promising, though more projected into the future. The maturation and spread of MMIC technology are facing us with a dramatic evolution of the traditional concepts of circuits and systems, which tend to be identified as long as more and more interconnected subsystems tend to merge into a single chip. At the same time it becomes increasingly difficult, if possible at all, to treat subsystems as individual items that can be separately specified and designed. Not surprisingly, a major impulse to the development of monolithic gallium arsenide circuits is being given by systems firms. In order to be useful, CAD techniques must obviously keep pace with technological reality, which means that conventional circuit-oriented CAD must evolve into modern system-oriented CAD. This involves the need for nonlinear capabilities, since system performance always requires nonlinear functions, and the ability to deal with very large size problems. From this viewpoint, nonlinear circuit CAD marks an essential step toward the technological update of computer-aided techniques.

In the authors' opinion, this clearly establishes the present trends in nonlinear microwave CAD. On the one hand, we have the circuit design problem, an intriguing one with several interrelated aspects, a tentative list of which is given below:

- analysis (simulation) of a known circuit;
- optimization of a nonlinear circuit;
- multiple-frequency excitation (intermodulation);
- frequency conversion (mixing);
- stability analysis;
- noise analysis.

Some of these are very popular, while others have seldom been touched on in the technical literature. What the paper tries to do in this respect is to show that the state of the art of nonlinear microwave CAD allows us to envisage a complete set of software tools covering all these aspects within the framework of a substantially unique philosophy. These tools are truly general-purpose in the CAD sense,

which means there are no restrictions on circuit topologies, device representations, or electrical functions. To a certain extent this requires some anticipation, since some of the problems already have well-established solutions, while others are still at the stage of conceptual development.

On the other hand, the extension of circuit CAD to cover system requirements may be expected to introduce at least one major new difficulty, that is, the very large size of the related numerical problems. This may arise both from the complexity of circuit topologies including several interacting subsystems, and from the need to deal with broad frequency spectra, possibly encompassing the MHz as well as the GHz regions. In this respect, we try to demonstrate that a key tool for the solution of this additional problem can be provided by one of the best-known concepts of modern computer science, namely parallel processing, and by its most common present-day implementation, represented by supercomputers. Supercomputers have the potential of extending to the nonlinear CAD domain all of the design issues that are now commonplace in linear CAD, and of making them as handy as their linear counterparts.

Of course, for this to become possible, all aspects of the general simulation problem should be consistently developed, especially passive and active device modeling. However, this paper is not going to touch on such aspects since they are covered by specialized presentations in this same issue, but rather will be devoted to methodology.

## II. SIMULATION

The simulation of nonlinear circuits is by far the most popular aspect of the entire job. Considerable effort and considerable ingenuity have been spent in devising new nonlinear analysis methods or improvements to existing ones. During the 15th European Microwave Conference, in Paris, an entire tutorial session was devoted to this subject [1]; thus to avoid duplications as far as possible, only a schematic classification and a brief highlight of some of the best-known approaches will be reported here.

In Table I a number of analysis algorithms are organized according to the type of description they adopt for the two fundamental kinds of circuit components, the linear and the nonlinear ones. Attention here is restricted to those methods that we could name "quasi-exact," i.e., that address the problem in a rigorous way except for numerical approximation, and do not rely upon *a priori* limiting assumptions such as weak nonlinearity or almost-monochromatic operation.

### A. Time-Domain Methods

A huge amount of technical literature is available on the general topic of nonlinear circuit simulation in the time domain, concerning both theoretical and computational aspects. Generally speaking, this work is not oriented toward microwave applications; thus it is beyond the scope of this paper to survey it. For the present purposes it will be sufficient to quote a number of special issues of the IEEE TRANSACTIONS ON CIRCUITS AND SYSTEMS [2]–[5],

TABLE I  
QUASI-EXACT ANALYSIS APPROACHES

	NONLINEAR COMPONENTS DESCRIPTION	
	TIME DOMAIN	FREQUENCY DOMAIN
LINEAR	DIRECT INTEGRATION SHOOTING METHODS EXTRAPOLATION METHODS	
NONLINEAR	HARMONIC BALANCE SYSTEM SOLVING OPTIMIZATION CONTINUATION METHODS RELAXATION METHODS SAMPLE BALANCE	POWER SERIES

where several review papers and a very extensive bibliography on the subject can be found. In particular, a review of the best-known time-domain simulation programs is given in [6].

A specific effort aimed at the extension of time-domain techniques to cover microwave applications is currently being made by several research groups [7]–[13]. An example of a microwave-oriented time-domain computational scheme is briefly outlined below. The use of suitable models of nonlinear capacitors and inductors leads to an equivalent circuit containing resistors and controlled sources as the only nonlinear components [13]. The circuit may thus be described in terms of a state vector of capacitor voltages, inductor currents, voltages at the transmission-line ports, and nonlinear resistor control variables. Combining Kirchhoff's laws with the voltage-current relationships of the circuit components results in the following set of coupled differential-difference and algebraic equations with constant coefficients:

$$\begin{aligned} \frac{dx_1}{dt} &= A_1x + B_1u + C_1 \frac{du}{dt} \\ x_2 &= A_2x(t - T_i) + B_2u(t - T_i) \\ 0 &= A_{31}x_1 + A_{32}x_2 + B_3u + F(x, u, t) \\ y &= A_4x + B_4u + C_4 \frac{du}{dt} \end{aligned} \quad (1)$$

where

- $x_1$  vector of lumped state variables,
- $x_2$  vector of distributed state variables,
- $x_3$  vector of nonlinear resistor control variables,
- $x$  overall state vector,

<b>A, B, C</b>	time-independent circuit matrices,
<b>u</b>	source vector,
$T_i$	transmission-line delays,
<b>F</b>	vector of nonlinear resistor characteristics,
<b>y</b>	output vector.

The system (1) is directly solved in the time domain by a suitable integration scheme [14], [15], requiring the solution of a set of nonlinear algebraic equations at each iterative step. The starting point is usually chosen as the result of a dc analysis.

Apparently, methods that work entirely in the time domain should represent the most natural and straightforward approach to the simulation problem. As a matter of fact, real-world circuits do work in the time domain, and semiconductor devices are naturally described in the time domain, too. However, such methods generally suffer from two major inconveniences. First of all, the only available means of accurately computing and measuring linear microwave components is to work in the frequency domain under sinusoidal excitation, except of course for elementary ones. Thus the difficulties come from the time-domain analysis of the linear subnetwork whenever realistic component models are to be dealt with. For instance, the description of a device as simple as a microstrip line with frequency-dependent propagation constant and characteristic impedance still represents a problem in the time domain. Of course, in principle one could think of such approaches as frequency-domain to time-domain conversions and convolution integrals [16], [17], but the practical feasibility of this still has to be demonstrated. The second point is numerical efficiency. An analysis based on the direct integration of the time-domain network equations would typically spend most of its computational effort on transient evaluation, while most of the user's interest is concentrated on steady-state information. To give a representative idea of what this means quantitatively, let us consider, for instance, some of the numerical results presented in [12]. Fig. 3 of this paper shows that the analysis of a circuit as simple as a biased FET without anything else requires the consideration of at least ten RF periods to reach steady state when using SPICE, one of the best-known time-domain simulators [18]. Similar conclusions are reached in [19]. Also, the situation may be definitely worse for more complicated circuits, not to mention special cases involving high-*Q* components, such as dielectric resonators.

For this reason, considerable effort has been spent by circuit theorists in devising techniques allowing the calculation of the transient to be at least partially bypassed and the steady state to be reached quickly. The basic concept is usually the evaluation of a set of initial conditions from which the network starts in periodic steady state. The so-called shooting methods [20]–[23] consist of a direct search for such initial conditions by a Newton iteration or some other nonlinear optimization technique. An alternative approach is to compute the state of the circuit at a number of instants by time-domain integration, and then

to extrapolate from these by algebraic methods the state from which the network starts in time-periodic regime [24]. We limit ourselves to this brief mention because the application of these approaches to microwave circuits has been only marginal.

A limiting form of the same ideas is represented by those methods that completely disregard the transient and directly focus on the steady state. The physical unknowns of the problem are still represented by state-variable waveforms, but the formulation is such that these waveforms are *a priori* guaranteed to be time-periodic. For numerical purposes the waveforms are approximately described by a discrete set of scalar unknowns; if the discretization is carried out in the frequency domain this leads to harmonic-balance methods.

### B. Harmonic-Balance Techniques

A quick review of the fundamentals of this approach is worthwhile because of the key role it plays in modern nonlinear CAD techniques. The network is first decomposed into a linear and a nonlinear multiport subnetwork having the same number of ports,  $n_D$ . The subdivision criterion usually represents a tradeoff between two opposite needs: on the one hand,  $n_D$  should be kept to a minimum for optimum numerical efficiency, while on the other, increasing the number of ports usually makes for an easier description of the nonlinear subnetwork.

The latter is represented by a set of time-domain nonlinear equations. Although this can be done in a number of ways, for the sake of generality and for later convenience we shall make use of the following system of parametric equations:

$$\begin{aligned} \mathbf{v}(t) &= \phi \left[ \mathbf{x}(t), \frac{d\mathbf{x}}{dt}, \dots, \frac{d^n \mathbf{x}}{dt^n} \right] \\ \mathbf{i}(t) &= \psi \left[ \mathbf{x}(t), \frac{d\mathbf{x}}{dt}, \dots, \frac{d^n \mathbf{x}}{dt^n} \right] \end{aligned} \quad (2)$$

where  $\mathbf{v}$  and  $\mathbf{i}$  are vectors of instantaneous voltages and currents at the nonlinear subnetwork ports, and  $\mathbf{x}$  is a set of time-dependent quantities used as state variables.  $\phi$  and  $\psi$  are nonlinear and analytically or numerically known.

The linear subnetwork is described in the frequency domain. For maximum generality its equations are written in the form

$$\mathbf{A}(\omega)\mathbf{V}(\omega) + \mathbf{B}(\omega)\mathbf{I}(\omega) + \mathbf{D}(\omega) = 0 \quad (3)$$

where  $\mathbf{A}$  and  $\mathbf{B}$  are circuit matrices,  $\mathbf{V}$  and  $\mathbf{I}$  are vectors of voltage and current phasors at the network ports, and  $\mathbf{D}$  is a set of driving functions. For a well-conditioned network all vector quantities appearing in (2) and (3) have the same size  $n_D$ .

In steady state, the state-variable waveforms are approximated by

$$\mathbf{x}(t) = \sum_{k=-N_H}^{N_H} \mathbf{X}_k \exp(jk\omega_0 t) \quad (4)$$

( $\mathbf{X}_{-k}^* = \mathbf{X}_k$ , \* = complex conjugate), where  $\omega_0$  is the

fundamental angular frequency of the time-periodic regime. Thus the steady state is completely identified by the vector  $\mathbf{X}$  of all  $X_k$ 's (state vector).

The circuit analysis problem now consists of finding the state vector  $\mathbf{X}$  in such a way that the time-domain voltages and currents obtained from (2) through (4) have spectral components satisfying (3) at  $\omega = k\omega_0$  ( $0 \leq k \leq N_H$ ). Making use of the fast Fourier transform, one obtains the nonlinear solving system

$$\mathbf{E}(\mathbf{X}) = 0 \quad (5)$$

where the  $k$ th subvector of  $\mathbf{E}$ , namely

$$\mathbf{E}_k(\mathbf{X}) = \mathbf{A}(k\omega_0)\Phi_k(\mathbf{X}) + \mathbf{B}(k\omega_0)\Psi(\mathbf{X}) + \mathbf{D}(k\omega_0) \quad (6)$$

( $0 \leq k \leq N_H$ ) is a set of harmonic-balance errors at  $k\omega_0$ . Note that (5) is equivalent to a system of

$$N = n_D(2N_H + 1) \quad (7)$$

real equations in as many real unknowns. Thus for a forced or nonautonomous circuit, the problem is well posed from a mathematical viewpoint. For an autonomous circuit of given topology ( $\mathbf{D}(k\omega_0) = 0$  for  $k \neq 0$ ,  $\mathbf{A}, \mathbf{B}$  *a priori* assigned), only dc solutions will exist in general. Nonstatic solutions may, of course, exist for some values of the fundamental, so that  $\omega_0$  must be regarded as an additional real unknown in (5). As a consequence, one of the remaining real unknowns (e.g., the phase of one of the harmonics) may be arbitrarily chosen, and the electrical regime is invariant with respect to a shift of the time origin. Note, however, that this situation is somewhat unusual in microwave engineering practices: most often one is faced with oscillator *design* problems whereby  $\omega_0$  is *a priori* fixed as a design goal. The required degree of freedom must then be available under the form of a free circuit parameter, so that the problem becomes one of circuit optimization from the CAD viewpoint (see Section III).

The method outlined above is known as the "piecewise" harmonic-balance technique [25], and has the advantage that the required number of state variables is equal to the number of linear subnetwork ports, no matter what the actual number of lumped or distributed reactive components. Thus the problem size is considerably reduced with respect to time-domain techniques and to earlier implementations of the harmonic-balance concept [26]. As an alternative to the piecewise harmonic-balance technique, a nodal analysis approach has also been proposed in [27]. The same reference also provides an in-depth review of harmonic-balance concepts.

Note that the harmonic-balance method takes advantage of the most accurate and straightforward approach to the simulation of both linear and nonlinear circuit components.

Harmonic-balance techniques have been used very extensively in the technical literature to analyze virtually any kind of nonlinear microwave subsystem. Most applications are based on the general guidelines presented above, except for minor details. On the other hand, a number of

different strategies have been developed in order to solve numerically the system (5). Some of these deserve a brief discussion because of their conceptual importance and widespread acceptance.

1) *Direct Methods*: The conceptually simplest way to solve the problem is to directly apply to (5) any numerical system-solving algorithm. Such solution routines are available in virtually all mathematical libraries (e.g., CERN, IMSL). For well-behaved circuits (e.g., weakly nonlinear), a simple Newton iteration is often sufficient to quickly achieve convergence: this is usually the case for circuits containing only FET's as the active elements.

As a more robust, but less efficient, alternative [28], one can use a nonlinear optimization scheme to minimize the objective function

$$E(\mathbf{X}) = \|E(\mathbf{X})\| \quad (8)$$

representing a combined harmonic-balance error ( $\|\cdot\|$  indicates the norm). Of course, some care must be taken in choosing the numerical algorithm. In the user-oriented CAD perspective, it is absolutely mandatory that the analysis algorithm be able to reach convergence starting from initial values automatically set by the program in a conventional way; this means that there is no starting-point information available. An effective though obvious way to obtain this result is to approach the solution by a direct search scheme and then to refine it by a Newton iteration. Excellent results have been reached by Powell's method [29]. Quasi-Newton methods [30] also yield satisfactory performance: in a sense they represent a different implementation of the same concept, since they also rely upon a combination of one-dimensional searches and gradient iterations. The starting point may be just taken as zero for nonautonomous circuits; for self-oscillating networks it is usually better to initially set to a suitable nonzero value the magnitude of the harmonic that most directly affects the circuit output power. This has the effect of avoiding the static solution, which generally exists in the autonomous case.

2) *Continuation Methods*: Convergence of direct iterative approaches may sometimes be improved by continuation methods [31], which have been successfully applied to nonlinear microwave circuit problems by several authors [32]–[35]. In this case, the original problem (5) is replaced by an auxiliary one of the form

$$\mathbf{F}(\mathbf{X}, \rho) = 0 \quad (9)$$

where  $\mathbf{F}$  is continuously dependent on a parameter  $\rho$ . The auxiliary problem (9) is defined in such a way that a solution  $\mathbf{X}^0$  is known for a certain value, say 0, of the continuation parameter, and that the original problem is reobtained for a different value, say 1. Thus

$$\begin{aligned} \mathbf{F}(\mathbf{X}^0, 0) &= 0 \\ \mathbf{F}(\mathbf{X}, 1) &= E(\mathbf{X}). \end{aligned} \quad (10)$$

The required solution  $\mathbf{X}$  can now be generated starting from the known vector  $\mathbf{X}^0$  by a step-by-step mechanism, through a sequence of intermediate solutions corresponding to increasing values of  $\rho$ . Each intermediate step is

obtained by solving a nonlinear problem which is very well conditioned, because its starting point and solution can be made as close as desired by making correspondingly small the step of the continuation parameter. Multiple solutions can be found by extending the generation of the solution curve beyond the first operating point, of course in the case where the curve itself bends back towards the  $\rho = 1$  position. Very sophisticated algorithms available in the literature allow the path to be followed across the turning points [36].

It is not easy to establish in general whether or not the use of a continuation method does yield a consistent performance improvement with respect to the corresponding direct solution approach. The authors' experience tends to show that they are roughly equivalent from the viewpoint of computational efficiency. In principle, continuation methods guarantee that a solution can always be reached by taking sufficiently small steps of the continuation parameter, while obviously direct methods do not provide the same assurance. On the other hand, direct methods are very simple and flexible, and lend themselves nicely to the implementation of circuit optimization schemes, as will be shown later on.

In both cases, a key step for obtaining good computational efficiency is to make use of the gradient evaluation algorithm outlined below [27], [37]. This mechanism is based on the assumption that the Jacobians of the nonlinear subnetwork equations (2) with respect to the state variables and to their time derivatives are available in closed form and can be represented by Fourier expansions:

$$\begin{aligned}\frac{\partial \Phi}{\partial y_m} &= \sum_p C_{m,p} \exp(jp\omega_0 t) \\ \frac{\partial \Psi}{\partial y_m} &= \sum_p D_{m,p} \exp(jp\omega_0 t)\end{aligned}\quad (11)$$

where  $y_m = d^m x / dt^m$ ,  $0 \leq m \leq n$ . As we shall see, these expansions play an important role in the solution of the generalized mixer problem and of the related problems of stability and noise analysis. Once the coefficients  $C_{m,p}$ ,  $D_{m,p}$  have been found by the FFT, the Jacobians of the harmonics  $\Phi_k$ ,  $\Psi_k$  with respect to the state-variable harmonics may be expressed as [37]

$$\begin{aligned}\frac{\partial \Phi_k}{\partial X_s} &= \sum_{m=0}^n (js\omega_0)^m C_{m,k-s} \\ \frac{\partial \Psi_k}{\partial X_s} &= \sum_{m=0}^n (js\omega_0)^m D_{m,k-s}.\end{aligned}\quad (12)$$

Note that all vector quantities appearing in (11), (12) have the same size  $n_D$  (i.e., the number of nonlinear subnetwork ports).

3) *Relaxation Methods:* As an alternative to the search strategies described above, the harmonic-balance equations may be solved by relaxation methods [40]–[45]. In the simplest approach, the vector of state variables  $x(t)$  is chosen as a set of  $n_D$  voltages or currents at the nonlinear

subnetwork ports, and it is assumed that the corresponding circuit matrix of the linear subnetwork exists.

Let the complementary set of voltages and currents be denoted by  $y(t)$ , and its vector of harmonics by  $Y$ . The time-domain analysis of the nonlinear subnetwork by (4) and (2), and the subsequent use of the FFT then establish a relationship of the form

$$Y = T(X) \quad (13)$$

where  $T$  is a (numerically defined) nonlinear vector operator. The frequency-domain equations of the linear subnetwork are now written as

$$X = HY + D \quad (14)$$

where  $H$  is a hybrid matrix and  $D$  represents a set of driving functions ( $D \neq 0$ ). Combining (14) with (13) leads to the solving system

$$X = HT(X) + D = F(X) \quad (15)$$

which is now formulated as a fixed-point problem of the vector nonlinear operator  $F$ . This is naturally suited for a relaxation approach; if the  $i$ th estimate of the state vector is denoted by  $X^{(i)}$ , the most obvious iteration scheme is defined by

$$X^{(i+1)} = F[X^{(i)}]. \quad (16)$$

It is quite clear that this approach is potentially attractive because of its reduced computational cost; however, its reliability is limited because convergence cannot be *a priori* guaranteed [38].

To improve the rather poor convergence properties of the direct iteration (16), more sophisticated iteration schemes have been proposed. An effective and popular one, which was successfully applied to diode and FET circuits [40]–[42] uses the following update mechanism:

$$X^{(i+1)} = P^{(i)}F[X^{(i)}] + [1 - P^{(i)}]X^{(i)} \quad (17)$$

where  $P^{(i)}$  is a diagonal matrix of iteration-dependent convergence parameters, and  $\mathbf{1}$  is an identity matrix.

Although (17) can be brought to perform much better than (16) by a suitable choice of the convergence parameters, its convergence properties still remain critically related to the specific aspects of each individual problem, and in particular to the impedance level of the nonlinear subnetwork [41]. Low impedances improve convergence when voltages are chosen as the independent variables, and conversely. This criticality can be easily inferred, for instance, from [41, fig. 6]. In this case a 5- $\Omega$  change of the nonlinear subnetwork impedance separates a condition of optimum convergence rate from one where convergence is not achieved at all. An important consequence of this situation is that the choice of the state variables is usually not free, but rather is dictated by the frequency behavior of the linear subnetwork. In turn, this implies that the time-domain analysis of the nonlinear subnetwork may require the integration of a set of differential equations

[41]. Think, for instance, of a varactor diode for which the current rather than the voltage has to be used as the state variable in order to obtain convergence. In such cases, the computational advantage of relaxation methods with respect to direct solution methods becomes questionable.

It is noteworthy that the convergence properties may be improved by resorting to even more complex iteration strategies. As an example,  $x(t)$  and  $y(t)$  could be defined as two independent combinations of *all* voltages and currents at the nonlinear subnetwork ports, which of course can lead to considerably increased complication in the numerical definition of the nonlinear operator  $F$ . A good choice turns out to be the use of incident and reflected waves, rather than voltages and currents, as the state variables, since this takes advantage of the subunitary nature of the scattering matrix [43]. A very well known approach falling within this class is Kerr's multiple-reflection method [39].

The above discussion makes it clear that relaxation methods are not ideal candidates for general-purpose CAD applications or for nonlinear circuit optimization because of a certain lack of reliability. Furthermore, they are usually not very well suited for analyzing nonlinear circuits having multiple operating points, such as oscillators or frequency dividers. On the other hand, relaxation methods can represent an excellent choice for specialized applications, or as a backup to conventional harmonic-balance techniques in general-purpose programs.

### C. Other Analysis Approaches

To conclude this brief and by necessity incomplete survey of nonlinear analysis methods, we would like to mention two other approaches that are potentially interesting, but of course do not share the maturity and widespread acceptance of the previously described ones.

One of them is referred to as the "power-series" method in Table I [45]. It is a harmonic-balance technique, but is based on a generalized power-series description of the nonlinear components [46], [47]. Once this has been developed, which is not necessarily an easy job, all required calculations may be carried out in the frequency domain, thus avoiding any time-consuming Fourier transforms.

The other one, which was arbitrarily named the "sample-balance" method in Table I, may be viewed in a sense as the dual of harmonic-balance techniques. It relies upon a direct time-domain approximation of the state-variable waveforms by suitable basis functions such as periodic cubic splines [48], [49], and uses time-domain samples as problem unknowns. The errors to be minimized are produced by comparing time-domain samples of the linear and nonlinear subnetwork responses. The linear subnetwork is analyzed in the frequency domain and its time-domain response to an elementary excitation is found once for all by Fourier transformation; at any subsequent step the time-domain response to a general driving force is simply found by linear superposition.

### III. OPTIMIZATION

From the general CAD viewpoint, circuit optimization obviously represents a most important goal, and a natural follow-up to the analysis problem. In the linear CAD case, the transition from the latter to the former is stepless: once a suitable analysis algorithm has been developed, this can be coupled to a minimization program—in the simplest case an off-the-shelf one—to produce an optimization-based design capability. Unfortunately this is not true in the nonlinear case, which could give a possible explanation of the striking disproportion between the considerable number of studies in the technical literature devoted to analysis methods and the sporadic attention paid to optimization. According to the authors' experience, there are a few basic reasons for this, which can be synthesized as follows.

As a first point, a full analysis of a nonlinear microwave circuit is typically too time-consuming to be effectively used as the objective-function generation mechanism within an optimization loop. A straightforward consequence is that the conventional linear optimization scheme is not applicable to nonlinear circuits: in fact, using a steady-state analysis to generate the objective function to be minimized would result in exceedingly large computer costs. Nonlinear circuit optimization thus requires the development of specialized algorithms based on the integration of the two fundamental aspects of circuit analysis and function minimization. The general rule is that the approach adopted should not require a full nonlinear analysis to be carried out at each step of the optimization loop. If we accept this viewpoint, we can go over the various analysis algorithms to understand whether or not they are potentially useful for optimization purposes. The most obvious candidates are those methods treating the analysis itself as an optimization problem, since any constraint arising from electrical specifications can be added to the objective function in a simple and straightforward way.

One of the first attempts to apply these principles in conjunction with time-domain methods, and more precisely shooting methods, was reported by Director and Wayne Current in 1976 [50]. Their approach is briefly described below. As in conventional shooting methods [20]–[23], the unknowns are a set of initial conditions from which the network starts in periodic steady state. If the vector of state variables is denoted by  $\mathbf{x}(t)$ , such conditions will be represented by  $\mathbf{x}(0)$ . These unknowns are now complemented by a set of linear circuit parameters, namely  $\mathbf{p}$ , so that the overall set of designable parameters is given by

$$\mathbf{U} = [\mathbf{x}^T(0), \mathbf{p}^T]^T \quad (18)$$

the superscript  $T$  denoting transposition. The objective function to be minimized is defined as [48]

$$F(\mathbf{U}) = \int_0^{T_0} \{ E_1[\mathbf{x}(t), \mathbf{U}, t] + E_2[\mathbf{x}(t), \mathbf{U}, t] \} dt \quad (19)$$

where  $T_0 = 2\pi/\omega_0$  is the steady-state period. In (19),  $E_2$

represents a suitable performance function arising from the design specifications, while  $E_1$  has the expression

$$E_1[\mathbf{x}(t), \mathbf{U}, t] = [\mathbf{x}(t) - \mathbf{x}(0)]^T \frac{d\mathbf{x}}{dt} \quad (20)$$

and thus introduces the steady-state condition. The state  $\mathbf{x}(t)$  is obtained by a time-domain integration of the usual circuit equations with starting point  $\mathbf{x}(0)$ . To solve the problem, the objective  $F$  is simultaneously minimized with respect to the whole set of unknowns  $\mathbf{U}$ .

Note, however, that this attempt was partially unable to meet its main goal, that is, the elimination of any complete steady-state nonlinear analysis within the optimization loop. In fact it was found [50] that a steady-state analysis had to be performed before every gradient evaluation of the quasi-Newton algorithm adopted. Otherwise the iteration would often converge upon a set of initial conditions that were found not to represent a steady state after running a time-domain analysis over many cycles.

This experience clearly suggests that the aforementioned optimization concepts can only be brought to a fully satisfactory implementation in conjunction with those methods that *a priori* guarantee the periodicity of the electrical regime, such as harmonic-balance techniques.

An approach to nonlinear circuit optimization based on the harmonic-balance concept is outlined below [51], [52]. This time the set of designable parameters is

$$\mathbf{U} = [\mathbf{X}^T, \mathbf{p}^T]^T \quad (21)$$

where  $\mathbf{X}$  is the vector of all state-variable harmonics. The objective function arises from two contributions, one of which is the harmonic-balance error, while the other originates from the design specifications. We thus have

$$F(\mathbf{U}) = [\|\mathbf{E}(\mathbf{U})\|^2 + E_2^2(\mathbf{U})]^{1/2} \quad (22)$$

which appears as an extension of the objective (8) used for a plane analysis. The second term,  $E_2$ , is defined in such a way that  $E_2 = 0$  when all specifications are met, and  $E_2 > 0$  otherwise [51].

Once again, to solve the problem,  $F$  is minimized with respect to  $\mathbf{U}$  by any nonlinear programming algorithm. However, this time the numerical procedure turns out to be very robust and reliable, and to be successfully applicable to both forced and autonomous circuits [53], [54]. The need for repeated nonlinear analyses is completely eliminated, and the gap between analysis and design CPU time requirements is effectively bridged. This partly happens because the number of unknown circuit parameters is usually small with respect to the number of harmonics in a well-posed problem, and partly because the availability of some degrees of freedom in the linear subnetwork often makes it easier for the minimization algorithm to reach the harmonic balance.

It is worth mentioning that the ability to carry out a constrained harmonic-balance analysis also allows some typical limitations of this class of techniques to be easily overcome. As an example, in an autonomous circuit the static solution of the circuit equations may be eliminated

just by requiring a finite output power. Similarly, multiple operating points may be detected by adding suitable performance specifications [37], even if they do not belong to the same solution path from the viewpoint of continuation methods [35].

The high degree of maturity achieved by the technique described above leads to the easy prediction that any other conceptually related analysis algorithm may be successfully used in a quite similar way for optimization purposes. This is obvious, for instance, for the power-series method that was mentioned previously, since this is still a harmonic-balance approach, making use of a frequency-domain, rather than time-domain, device description. Another good candidate is what we called the "sample-balance" technique: in this case the unknowns to be simultaneously optimized would be represented by linear network parameters and time-domain samples of the state-variable waveforms.

Continuation methods have also been shown to be usable for nonlinear circuit optimization [32]–[34]. The underlying idea is still to avoid any full nonlinear analysis to be carried out within the minimization loop; however, this is now obtained by the typical philosophy of this kind of approach. The objective is optimized by a sequence of one-dimensional minimizations making use of a direct-search strategy such as Powell's method [29]. A regular analysis of the starting point is first performed by the standard stepped-parameter approach. In all subsequent objective-function evaluations the parameter is kept constant. Continuation is applied with respect to the circuit variables to generate the required steps of each one-dimensional search: the basic concept is essentially to keep small enough the steps along the search direction.

In this way every objective-function evaluation does require a nonlinear analysis, but this can be performed much more quickly than a regular one because a starting point very close to the solution is always available. The result is an order-of-magnitude speedup with respect to a brute-force optimization approach. However, the overall procedure is less efficient than the direct optimization described earlier, because the computation of the objective function is slower, and the one-dimensional search strategy is not optimal due to the limitations on step size.

#### *An Example of Application*

At this stage, we would like to discuss a simple example which is intended to give a feeling of what a powerful design tool a harmonic-balance optimization program may represent, and how deep an insight into circuit behavior can be obtained by this kind of technique. We consider the circuit depicted in Fig. 1 and we assume for the time being that the feedback branch  $AB$  is cut away so that we are simply left with a biased FET with input and output matching networks. It is quite clear that this topology can be used to do almost anything provided that the matching sections are suitably chosen. We assume that the circuit has to work as a regenerative frequency divider by two. For this purpose the input section is designed as a band-

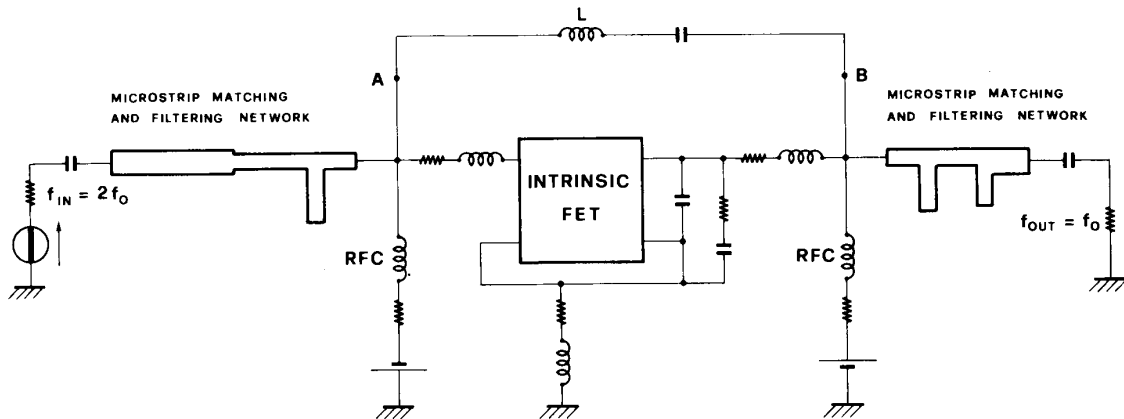


Fig. 1. Schematic topology of a microstrip regenerative frequency divider.

stop filter at the output frequency, and conversely, and the remaining degrees of freedom are optimized together with six gate and drain voltage harmonics for a conversion gain of 0 dB with an input power level of 6 mW at 9.4 GHz. What happens is that the optimization fails to converge, even though more complicated matching network topologies and different input drive levels are tried. An inspection of the results clearly shows the reason for this: the output frequency components cannot be balanced at the FET gate, because the device has an input impedance with a significant real part but is reactively loaded by the input filter. The two possible solutions are to suppress the input filter, which is obviously undesirable, or to introduce some degree of parallel feedback, such as connecting nodes *A*, *B* by an *LC* branch, as shown in Fig. 1. Once this has been done, the circuit can be designed with no further complications, and a behavior in agreement with experimental observations [55] can be predicted.

Of course, in this case the answer was *a priori* known, but the general principle still remains valid: even an unsuccessful optimization may provide useful design information, because the available circuit description is so detailed as to make it normally easy to find out where the difficulties come from. It is worth mentioning that the application of time-domain techniques to the same problem would only lead to the obvious result that the initial topology behaves as a low-efficiency frequency multiplier, with no indications on how the final goal could be met.

#### IV. MULTIPLE-FREQUENCY EXCITATION

The preceding discussion referred to nonlinear circuits supporting strictly time-periodic electrical regimes, described by a truncated Fourier expansion of the form (4). However, all results are equally valid for a quasi-periodic regime containing all possible intermodulation products of a number of non-harmonically related "exciting tones." In this case the mathematical representation (4) of the steady state is replaced by

$$x(t) = \sum_{\mathbf{k}} X_{\mathbf{k}} \exp\left(j \sum_i k_i \omega_i t\right) \quad (23)$$

( $X_{-\mathbf{k}}^* = X_{\mathbf{k}}$ ), where  $\omega_i$  is the angular frequency of the *i*th exciting tone. Truncation is now performed by taking into account only those intermodulation products whose order does not exceed a prescribed integer [56], that is,

$$\sum_i |k_i| \leq N_H. \quad (24)$$

It is worth mentioning that the term "exciting tone" should be interpreted here in the very broad sense of any sinusoidal signal existing in the circuit, independent of its physical origin. This includes sinusoidal pumps and autonomous oscillations, as well as any parametric or spurious tone that the circuit might generate.

With respect to the strictly periodic case, dealing with a quasi-periodic regime does not introduce any special conceptual difficulty; problems that do arise are essentially of a practical nature and invariably relate to numerical efficiency.

In the time domain, a direct integration can be performed in the usual way, independent of the number of sources acting in the circuit, until steady state is reached. However, in this case the steady state may have quite a long period—theoretically may not be periodic at all—which makes it difficult to determine how long it takes for the transient component to die out. Furthermore some typical multitone circuits, such as mixers with a low IF, may contain large time constants with respect to the RF period, which in turn may considerably slow down the achievement of steady-state conditions. Once again, some improvement may be obtained from shooting methods. For instance, Chua and Ushida [57] describe an algorithm based on a combination of shooting methods and least-squares waveform approximation, yielding both the initial point from which the network starts in steady state, and the Fourier coefficients of the steady state itself. However, the overall job still remains computationally heavy; frequency-domain methods are more appealing because of their ability to directly focus on the steady state.

From the standpoint of harmonic-balance techniques the critical step is the evaluation of the frequency-domain response of the nonlinear subnetwork to a quasi-periodic

input. In the case of commensurate frequencies, one could simply replace the quasi-periodic regime by a strictly periodic one by taking the greatest common divider of the exciting tones as the fundamental, and then proceed in the usual way [58]–[60]. Of course, if the fundamental is too low, the required sampling rate, and the corresponding size of the Fourier transforms, may turn out to be so large as to make this approach totally impractical. An efficient alternative is using a multidimensional grid of sampling points associated with multidimensional Fourier analysis to solve the problem [61]. This method has the advantage of being directly applicable to any combination of exciting frequencies, whether or not they be commensurate, with computational times independent of the actual frequency values. Another possible approach [62] is to carry out the transform by solving a linear system based on a nonuniform sampling scheme, whereby the sampling points are chosen so as to avoid ill-conditioning of the solving system.

These straightforward solution schemes are somewhat time-consuming, but have the advantage of programming simplicity, and provide a quasi-exact reference which can be used to establish the accuracy of approximate solutions.

As a matter of fact, a number of numerical procedures have been developed with the aim of reducing the computational burden of the harmonic-balance treatment of quasi-periodic regimes. For the sake of brevity we shall limit ourselves here to a short mention of some of the best-known and conceptually more relevant ones.

In [56] the response of the nonlinear subnetwork to a multitone excitation is uniformly sampled in the time domain. These samples are approximated in the least-squares sense by a generalized Fourier series of the form (23), thus producing an estimate of the spectral components of the nonlinear response.

In [63]–[65] the nonlinear subnetwork response is sampled at a much lower rate than the Nyquist rate, and Fourier transformed. To eliminate aliasing effects, the process is repeated a number of times with suitably shifted input spectra, and the resulting output spectra are linearly combined.

In [35] the original sparse spectrum (groups of lines separated by large gaps) is mapped onto an auxiliary dense spectrum (little or no gaps) by selecting a suitable set of conventional source frequencies. Calculations are carried out on the auxiliary spectrum, requiring a drastically reduced sampling rate.

In [66] each spectral component of interest is first shifted to dc by performing a frequency shift over the entire spectrum, and is then isolated by passing the shifted signal through a digital bandpass filter of suitable bandwidth.

Finally, a special mention is deserved by the power-series approach [67], [45], [68]. In this case the input and output spectral components are algebraically related by an explicit formula, which was developed by several authors in a number of subsequent steps [69]–[72], so that Fourier transforms are eliminated from the numerical procedure. Computational accuracy then only depends on the reliability of the power-series representation of the nonlinear

subnetwork, and in particular on its convergence properties.

## V. FREQUENCY CONVERSION

An approximate solution has also been developed for the special case of a nonlinear circuit driven by two sinusoidal signals, one being very weak with respect to the other. This is commonly referred to as the mixer case, and is obviously very important from the technical viewpoint, which explains the good deal of attention that has been devoted to this specific subject. For once, there is almost general agreement in the technical literature as to how a mixer analysis problem should be dealt with. The commonly adopted approach relies upon the concept of the conversion matrix of the nonlinear subnetwork [73]–[80]. The basic idea is to consider the weaker, or radio-frequency (RF), signal as a small perturbation of a time-periodic steady-state regime, which may be established either by pumping the circuit with the stronger signal—the local oscillator (LO)—or by self-oscillation. The nonlinear subnetwork equations are then linearized in the neighborhood of the steady-state regime to find the circuit response to the injection of an additional small RF signal. Note the conceptual similarity of this approach to the conventional linearized description of the small-signal operation of a nonlinear device around a fixed bias point. As we shall see this analogy is of considerable help for an intuitive comprehension of a number of related topics, such as stability and noise.

In the mixer case, the periodic time dependence of the unperturbed regime leads to the generation of intermodulation products which in mixer terminology are called sidebands. Due to the assumed smallness of the RF signal, however, the situation is considerably simpler than for a general two-tone excitation, since only first-order products in  $\omega_R$  may be retained. Let the steady-state regime established under LO drive with the RF signal suppressed be denoted by  $\tilde{x}(t)$ . Then the quasi-periodic regime under combined LO and RF excitation is represented to first order by

$$\mathbf{x}(t) = \tilde{\mathbf{x}}(t) + \operatorname{Re} \left[ \sum_k \Delta \mathbf{X}_k \exp \{ j(\omega_R + k\omega_0)t \} \right] \quad (25)$$

where  $\omega_0, \omega_R$  are angular frequencies of the LO and RF signals, and  $\Delta \mathbf{X}_k$  is a vector of spectral components at the  $k$ th sideband. Similar expressions hold for the voltages and currents at the nonlinear subnetwork ports (with  $\Delta \mathbf{X}_k$  replaced by  $\Delta \mathbf{V}_k, \Delta \mathbf{I}_k$ , respectively).

If the nonlinear subnetwork equations (2) are now linearized around  $\tilde{\mathbf{x}}(t)$ , linear relationships are established between the sideband amplitudes  $\Delta \mathbf{X}_k, \Delta \mathbf{V}_k, \Delta \mathbf{I}_k$ . We can express such relationships by the compact matrix notation

$$\begin{aligned} \Delta \mathbf{V} &= \mathbf{P} \Delta \mathbf{X} \\ \Delta \mathbf{I} &= \mathbf{Q} \Delta \mathbf{X} \end{aligned} \quad (26)$$

where  $\Delta \mathbf{X}$  is the vector of all  $\Delta \mathbf{X}_k$ 's, and similar. We call (26) the *conversion equations* of the nonlinear subnetwork. In particular, if  $\mathbf{Q}$  or  $\mathbf{P}$  is nonsingular, we can eliminate

$\Delta X$  between eqs. (26) and write

$$\Delta V = P Q^{-1} \Delta I = Z_c \Delta I \quad (27)$$

or

$$\Delta I = Q P^{-1} \Delta V = Y_c \Delta V \quad (28)$$

where  $Z_c, Y_c$  are the impedance conversion matrix and the admittance conversion matrix of the nonlinear subnetwork, respectively.

The time-domain description (2) of the nonlinear subnetwork lends itself nicely to a straightforward computation of the conversion matrices for a general nonlinear device [80]. In this case the Jacobians (11) must be available, since they are required to carry out the linearization. Making use of the expansion coefficients defined by (11), we introduce the square matrices of size  $n_D$ :

$$\begin{aligned} P_{k,p} &= \sum_{m=0}^n \{j(\omega_R + k\omega_0)\}^m C_{m,p} \\ Q_{k,p} &= \sum_{m=0}^n \{j(\omega_R + k\omega_0)\}^m D_{m,p} \end{aligned} \quad (29)$$

where  $n$  is defined in (2). Then the conversion matrices  $P, Q$  appearing in (26) are defined by [80]

$$\begin{aligned} P &\equiv [P_{k,s-k}] \\ Q &\equiv [Q_{k,s-k}] \end{aligned} \quad (30)$$

where  $s$  acts as the *row* index, and  $k$  as the *column* index, of the generic  $(n_D \times n_D)$  submatrix. If  $N_H$  harmonics are retained to describe the local-oscillator regime, so that  $-N_H \leq k \leq N_H$  as in (4), then the truncated size of the conversion matrices is given by the same number  $N = n_D(2N_H + 1)$  defined by (7).

Note that the Fourier coefficients of the Jacobians used to compute (30) through (29) are the same ones needed to find the gradient of the harmonic-balance error through (12). Thus after performing a harmonic-balance analysis, such coefficients will automatically be available, and the derivation of the conversion matrix will become trivial. This is the reason why most mixer investigators use the harmonic-balance technique to determine the local-oscillator regime. For some simple devices these Fourier coefficients also have an immediate physical meaning: for instance, in the case of a nonlinear current source, they coincide with the Fourier coefficients of the differential conductance [73]. When (2) may be interpreted as the equations of a nonlinear equivalent circuit, it is also possible to combine the conversion matrices of elementary components by circuit-like algebra to find the conversion properties of the entire nonlinear subnetwork [77].

At this stage, mixer analysis has been reduced to a matter of linear circuit algebra. The situation is depicted in Fig. 2. The nonlinear subnetwork is replaced by a linear circuit described in the frequency domain by the conversion equations; each smaller block represents the linear subnetwork at one of the sidebands. Performing the required circuit connections leads to a matrix description of the mixer as the resulting two-port.

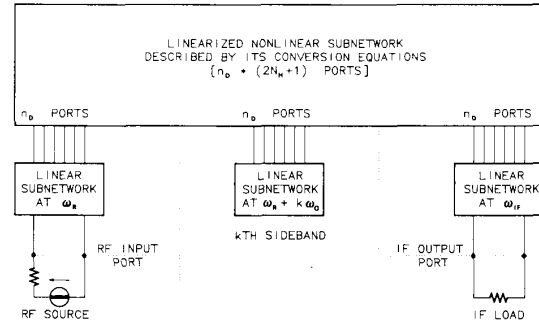


Fig. 2. Linearized equivalent circuit of a microwave mixer.

It is worth mentioning that this linearized behavior must be dealt with some caution. In fact, the two-port mixer matrix just mentioned is not usable for *design* purposes, except, of course, for a hand-driven optimization whereby a circuit parameter is manually changed and the whole analysis procedure is repeated each time. This is easily explained: assume, for instance, that an input matching network is designed on the basis of the linearized matrix description. If this network were connected with the RF port, the whole local oscillator regime would change, and so would the mixer matrix; the designed matching section would thus become meaningless. If we recall the analogy with the small-signal operation of a dc-biased nonlinear device, the same situation would occur if the addition of RF circuitry did result in a change of the bias point. The difference is that the bias circuit can be isolated from the RF by suitable dc-blocking devices, while obviously the local-oscillator regime cannot.

It follows that computer optimization of microwave mixers still remains an open problem: the only viable approach reported in the literature was a direct harmonic-balance optimization implemented on a supercomputer [59], [81].

It should be mentioned here that in the recent technical literature the mixer problem has been treated by several authors [58]–[60], [64], [82] as a conventional nonlinear analysis problem with multiple-frequency excitation (see Section IV). This approach is computationally heavier, but allows nonlinearizable aspects such as conversion-gain compression [59] and intermodulation distortion [82] to be accounted for. With some limitations, intermodulation distortion in diode mixers has also been analyzed by a stepwise procedure based on the conversion-matrix technique [83].

The frequency-conversion analysis outlined above is not only a numerical tool for the simulation and design of microwave mixers. It is also the kernel of a generalized perturbation analysis of periodic steady-state regimes supported by nonlinear microwave circuits. This analysis is compatible with a frequency-domain description of the linear subnetwork, and can thus take advantage of state-of-the-art techniques for passive circuit modeling [84], [85]. As will be shown in the following sections, such advanced and complicated problems as generalized stability and

noise analysis can be treated by the same perturbative approach with suitably chosen boundary conditions. Thus frequency-conversion analysis represents a key step toward the development of a general-purpose nonlinear microwave CAD system that is not confined to the traditional aspects of circuit simulation and optimization.

## VI. STABILITY

If in Fig. 2 we suppress the RF source, the same circuit diagram becomes useful for investigating the stability of the local-oscillator regime. From a more general standpoint, the figure represents the linearized equivalent circuit of the original nonlinear network in the neighborhood of any time-periodic steady-state solution of the network equations. It may thus be used to establish a general-purpose approach to the stability analysis of any such solution which will be developed in the first part of this section. This analysis is restricted to *local* or *conditional* stability [86], in the sense that the results are only valid in the space of *small* perturbations of the steady state. Even if the latter is stable in this respect, a *large* perturbation may force the circuit to abandon it permanently and to jump to a different stable state. This wider viewpoint requires a *global* stability analysis, to be discussed in the second part of this section.

The stability analysis described here does not require any limiting or simplifying assumptions on circuit behavior and is thus considerably more advanced than most previously available solutions of the same problem [87]–[94], many of which it includes as particular cases. Its accuracy is only limited by the high-frequency behavior of the linear and nonlinear subnetwork models [94]. However, since this treatment is based on the same principles leading to mixer analysis via the conversion-matrix concept, its practical validity is indirectly but reliably checked by the large amount of successful mixer work available in the literature [73]–[79].

### A. Local Stability

We first derive a characteristic equation for the natural frequencies of the linearized equivalent circuit shown in Fig. 2. Let a small perturbation of complex frequency  $\sigma + j\omega$  be superimposed to the steady-state solution  $\tilde{x}(t)$ . The resulting electrical regime can be represented to first order by

$$\mathbf{x}(t) = \tilde{\mathbf{x}}(t) + \exp(\sigma t) \operatorname{Re} \left[ \sum_k \Delta X_k \exp \{ j(\omega + k\omega_0)t \} \right] \quad (31)$$

which is identical to (25) except for the amplitude factor. Similar expressions hold for the voltages and currents.  $\sigma + j\omega$  is a natural frequency of the steady state if the spectral components of the perturbation satisfy the linearized network equations. For the nonlinear subnetwork this means that (26) must hold with  $\omega_R$  replaced by  $\omega - j\sigma$ . For the linear subnetwork, which is now source-free, we use the frequency-domain equations (3) with  $\mathbf{D}(\omega) = 0$ .

We can gather all sidebands  $\omega + k\omega_0$  into the compact matrix notation

$$\mathbf{A}_L \Delta V + \mathbf{B}_L \Delta I = 0 \quad (32)$$

where

$$\begin{aligned} \mathbf{A}_L &= \operatorname{diag} [\mathbf{A}(\omega - j\sigma + k\omega_0)] \\ \mathbf{B}_L &= \operatorname{diag} [\mathbf{B}(\omega - j\sigma + k\omega_0)]. \end{aligned} \quad (33)$$

Combining (26) with (33) yields the desired eigenvalue equation:

$$(\mathbf{A}_L \mathbf{P} + \mathbf{B}_L \mathbf{Q}) \Delta X = 0 \quad (34)$$

so that the characteristic equation for the natural frequencies is

$$\det(\mathbf{A}_L \mathbf{P} + \mathbf{B}_L \mathbf{Q}) \equiv \Delta(\sigma + j\omega) = 0. \quad (35)$$

The above procedure can be considered the generalization of a result first discovered by Mees [95], [96]. The formulation adopted is convenient from the mathematical viewpoint, since the determinant (35) has no singularities except at infinity, so that pole-zero cancellations cannot occur. For the sake of physical intuition, however, it is better to rewrite (35) in terms of admittance or impedance matrices. Making use of (27) and (28) we get

$$\begin{aligned} \det(\mathbf{Z}_c + \mathbf{Z}_L) &= 0 \\ \det(\mathbf{Y}_c + \mathbf{Y}_L) &= 0 \end{aligned} \quad (36)$$

where

$$\begin{aligned} \mathbf{Z}_L &= \operatorname{diag} [\mathbf{Z}(\omega - j\sigma + k\omega_0)] \\ \mathbf{Y}_L &= \operatorname{diag} [\mathbf{Y}(\omega - j\sigma + k\omega_0)] \end{aligned} \quad (37)$$

and  $\mathbf{Z}(\omega), \mathbf{Y}(\omega)$  are the conventional impedance and admittance matrix of the linear subnetwork. The eigenvalue equation is thus seen to be formally identical, and conceptually similar, to the one used to find the natural frequencies of a linear network. With respect to the latter case, the conventional device impedance or admittance matrix is replaced by the conversion matrix, while the single-frequency impedance or admittance of the linear subnetwork is replaced by the diagonal sum of all sideband impedances or admittances.

From the computational viewpoint it is virtually impossible to actually find all of the natural frequencies. Thus some indirect way of establishing the nature of the solutions has to be found. One possible approach is to produce a Nyquist stability plot [94]. In the present case, this turns out to be a much easier job than one might suspect, because of some known properties of the determinant. First of all,  $\Delta(\sigma + j\omega)$  is a periodic function of  $\omega$ , so that [94]

$$\Delta[\sigma + j(\omega + h\omega_0)] = (-1)^{nn_D h} \Delta(\sigma + j\omega) \quad (38)$$

where  $h$  is an integer. To remove the singularity of  $\Delta$  at infinity ( $\omega \rightarrow \infty, \sigma > 0$ ), we can thus replace  $\Delta$  by the complex function, having the same finite zeros,

$$F_\Delta(\sigma + j\omega) = \exp \left[ -\frac{nn_D \pi}{\omega_0} (\sigma + j\omega) \right] \Delta(\sigma + j\omega) \quad (39)$$

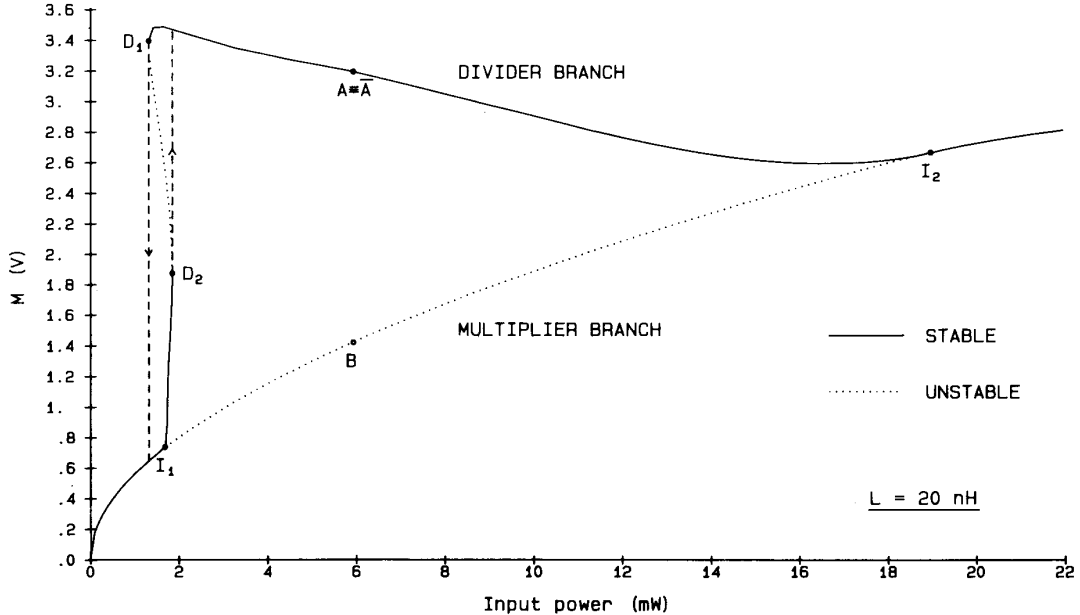


Fig. 3. Bifurcation diagram of the active frequency divider shown in Fig. 1.

which is periodic in  $\omega$  with period  $\omega_0$ . From Nyquist's equation [97], the number of natural frequencies lying in the region  $[0 \leq \omega < \omega_0, \sigma > 0]$  is then given by the number of clockwise encirclements of the origin made by  $F_\Delta(j\omega)$  as  $\omega$  is swept from 0 to  $\omega_0$ . It is assumed that the steady state considered is not a bifurcation point (see Section VI-B), so that  $F_\Delta(j\omega) \neq 0$ . Finally note that [94]

$$F_\Delta(\sigma - j\omega) = F_\Delta^*(\sigma + j\omega) \quad (40)$$

so that only the range  $[0, \omega_0/2]$  need be investigated.

Of course in practice the user does not have to actually draw the Nyquist plot and count the encirclements: all this can be effectively done by the computer, and user interaction is reduced to a printed line on output reporting the total number of unstable natural frequencies. Furthermore, since the calculation is highly repetitive and easily vectorizable, it can be performed most efficiently on a supercomputer, typically in a fraction of a second in most practical cases. Thus it is actually possible to complement a general-purpose analysis and optimization program by an algorithm for local stability analysis in a way completely transparent to the user.

#### B. Global Stability

We first derive a global stability picture for a simple specific circuit by performing a large number of local stability analyses. Then we develop a systematic approach to global stability based on bifurcation theory, and show that in the particular case under examination the two sets of results strictly agree.

Let us consider once again the regenerative frequency divider introduced in Section III. Fig. 3 shows a bifurcation diagram for this circuit, which is drawn in terms of

the quantity

$$M = \left( \sum_{k=1}^{N_H} \|X_k\|^2 \right)^{1/2} \quad (41)$$

versus available input power. The state variables are chosen as the FET gate and drain voltages (Fig. 1).

To find this plot, the divider was first optimized for a 0-dB gain at an input power of 6 mW at 9.4 GHz, which yielded point  $A$ . This point is obviously associated with another steady state, which we name  $\bar{A}$ , having exactly the same harmonics except for a sign reversal of the odd ones. Finally, a third operating point, named  $B$ , was found at the same power level by a harmonic-balance analysis of the circuit with a zero starting point. The curves were then generated by a continuation method (e.g., [33], [35]), and the stability of a large number of points was checked by the Nyquist approach. The results of this analysis are reported in Fig. 3. Note that between points  $I_1$  and  $I_2$  three solution branches exist. Two of them are superimposed in the figure, and correspond to the usual bistable divider operation with a  $180^\circ$  phase shift between the two otherwise identical stable states. The third one is indicated as "multiplier branch" in the figure because of the total absence of any odd harmonics in the steady state. This can be expected to be unstable on a physical ground, since the pumped nonlinear device must produce a negative resistance, and thus unstable eigenvalues, for the onset of frequency division to take place.

This kind of analysis may be produced in a much more systematic way making use of the principles of bifurcation theory [86]. For a parameterized nonlinear system, bifurcations are defined as the states corresponding to those parameter values for which system stability undergoes an

abrupt qualitative change; that is, the real part of one (at least) natural frequency changes sign. For a circuit depending on a free parameter  $\rho$ , the existence of a bifurcation at  $\rho = \rho_B$  requires that (5) and (35) be simultaneously satisfied with  $\sigma = 0$ , so that the mathematical conditions defining a bifurcation are

$$\begin{aligned} E(X, \rho_B) &= 0 \\ \Delta(j\omega, X, \rho_B) &= 0 \end{aligned} \quad (42)$$

$$\frac{d\sigma}{d\rho}(\rho_B) \neq 0. \quad (43)$$

The topological as well as the stability-exchange properties of bifurcations in nonlinear systems have been studied very extensively under very broad assumptions which certainly warrant the application of the results to microwave circuits [86]. A simplified classification of the fundamental types of bifurcations (which are essentially the interesting ones for microwave applications) is given below [98].

The bifurcations of periodic solutions of period  $T_0$  are considered first. We denote a periodic steady state by  ${}_k S^m$ , where  $k$  is the number of unstable natural frequencies and  $m$  indicates a period  $mT_0$  (1 understood). Then the following fundamental types of bifurcations are possible [99]:

1) *D-Type (Double-Point Bifurcation)*: A simple real natural frequency crosses the origin at  $\rho = \rho_B$ , so that equations (42) are satisfied with  $\omega = 0$ . The exchange of stability is defined by

$${}_k S + {}_{k \pm 1} S \leftrightharpoons {}_{k \pm 1} S + {}_k S \quad (44)$$

where the states appearing first (second) on both sides of the arrows correspond to each other.

*Special Case of D-Type (Regular Turning Point)*: This is the same as 1), but the creation or annihilation of two periodic states takes place at  $\rho = \rho_B$ . The exchange of stability is defined by

$$\phi \leftrightharpoons {}_{k \pm 1} S + {}_k S \quad (45)$$

where  $\phi$  denotes the absence of solutions.

2) *I-Type (Period-Doubling Bifurcation)*: Two simple complex-conjugate natural frequencies of the form  $\sigma \pm j\omega_0/2$  cross the imaginary axis at  $\rho = \rho_B$ , so that (42) are satisfied with  $\omega = \pm\omega_0/2$ . The exchange of stability is defined by

$${}_k S \leftrightharpoons {}_{k \pm 1} S + 2 {}_k S^2. \quad (46)$$

Note that  $\sigma \pm j\omega_0/2$  is in fact the same solution of the characteristic equation (35) because of the periodicity of  $\Delta$ . This explains the subscript  $k \pm 1$  in the first term on the right-hand side of (46).

3) *Hopf-Type (Spurious-Exciting Bifurcation)*: Two simple complex-conjugate natural frequencies cross the imaginary axis at  $\rho = \rho_B$ , so that (42) are satisfied with  $0 < |\omega| < \omega_0/2$ . The exchange of stability is defined by

$${}_k S \leftrightharpoons {}_{k \pm 2} S + {}_k (\text{CLOSED CURVE}) \quad (47)$$

where the closed curve represents a quasi-periodic regime which is stable for  $k = 0$  and unstable otherwise.

Because of (40),  $\Delta(0)$  and  $\Delta(j\omega_0/2)$  are real quantities. This means that (42) is a system of  $N+1$  real equations in  $N+1$  real unknowns  $X$ ,  $\rho_B$  for *D*- and *I*-type bifurcations, and is a system of  $N+2$  real equations in  $N+2$  real unknowns  $X$ ,  $\rho_B$ ,  $\omega$  in the case of Hopf bifurcations ( $N$  given by (7)). Thus the system is always well conditioned from a mathematical viewpoint. This also explains why 1)-3) represent the *fundamental* bifurcations: the existence of such bifurcations is mathematically possible in generic situations. On the other hand, more complex kinds of bifurcations requiring additional constraints to be imposed on the same variables appearing in (42) (e.g.,  $\omega = \omega_0/4$  for a period-quadrupling bifurcation) will only exist under exceptional circumstances.

The condition (43) (often referred to as the condition for *strict* loss of stability) must be checked at any solution of (42) to ensure that the solution itself actually represents a bifurcation. It is virtually impossible to do this directly, because the computation of  $d\sigma/d\rho$  requires a knowledge of the third-order partial derivatives of the circuit equations [86], [100]. Fortunately, the Nyquist analysis described in Section VI-A allows (43) to be checked by elementary methods. In fact, all we need do is to show that the Nyquist plot actually crosses the origin at  $\rho = \rho_B$ , i.e., lies on opposite sides of the origin at  $\rho = \rho_B \pm \delta\rho$  ( $\delta\rho \ll \rho_B$ ) in the neighborhood of  $\pm\omega$ . In particular, this implies that the real quantities  $\Delta[0, X(\rho), \rho]$  and  $\Delta[j\omega_0/2, X(\rho), \rho]$  change sign at  $\rho = \rho_B$  in the cases of *D*- and *I*-type bifurcations, respectively.

The preceding argument also indicates the most convenient way of solving the system (42): its first equation is first solved for  $X(\rho)$  by a continuation method; then  $\Delta(0) = 0$  and  $\Delta(j\omega_0/2) = 0$  are solved in the one-dimensional manifold  $X(\rho)$ , and  $\Delta(j\omega) = 0$  is solved in the two-dimensional manifold  $[\omega, X(\rho)]$ . The procedure is then repeated for the bifurcating branches. Since the stability of the circuit does not change, by definition, along a branch not containing bifurcations, a global stability picture for the circuit being considered is readily obtained in this way. Note that this implies that the stability of an *infinite* number of possible states becomes known by a *finite* number of operations.

We now go back to the regenerative frequency divider shown in Fig. 1 and apply the above considerations to this circuit. In the present case, the parameter is chosen as the available power of the pump, i.e.,  $\rho = P_{\text{IN}}(\text{mW})$ . We are interested in the range  $0 \leq \rho \leq 22$ .

The “multiplier branch” (Fig. 3) is first determined by a continuation method starting from  $\rho = 0$ . A local stability analysis of the bias point chosen ( $V_{gs0} = -1.9$  V,  $V_{ds0} = 6$  V) reveals that the circuit is dc stable; thus the multiplier branch is stable in the neighborhood of the origin. Two solutions of the system (42) are found on the multiplier branch within the range of interest: two *I*-type bifurcations (points  $I_1, I_2$ ) at  $\rho = \rho_1 \approx 1.7$  and  $\rho = \rho_2 \approx 18.8$ , respectively. The two-parameter bifurcation analysis reported below (see Fig. 4) shows that  $I_1, I_2$  belong to the same eigenvalue  $\sigma \pm j\omega_0/2$ . Thus the multiplier branch is

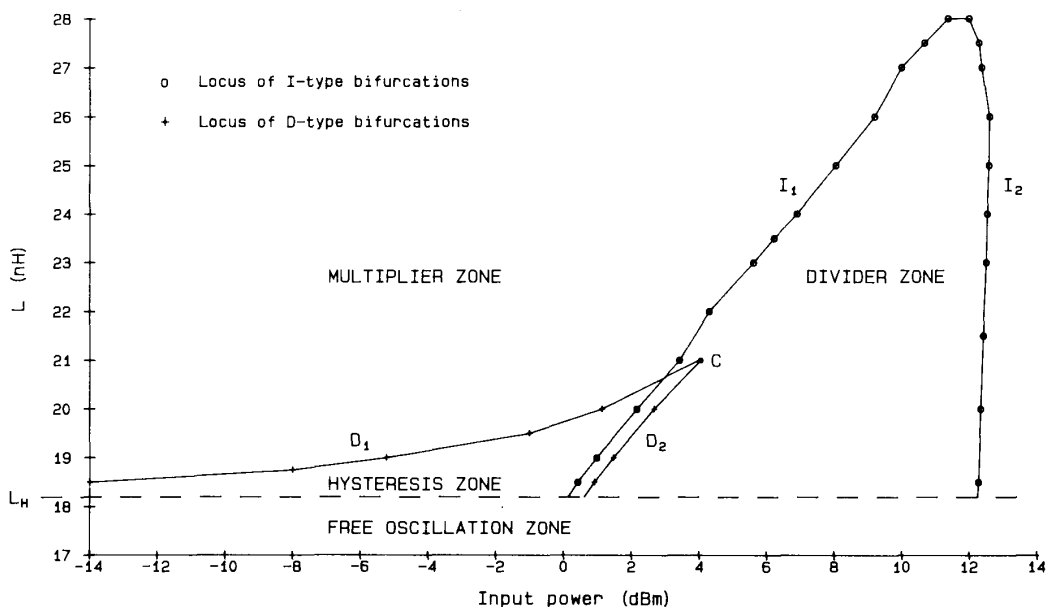


Fig. 4. Bifurcation analysis of the active frequency divider in a two-dimensional parameter space.

stable for  $\rho < \rho_1$  and  $\rho > \rho_2$  and unstable elsewhere. Starting at  $\rho = \rho_1$ , the "divider branch" is then determined by a continuation method. This branch starts at  $I_1$  and terminates at  $I_2$ . The bifurcation at  $I_1$  is *supercritical*, i.e., is described by (46) with the arrow pointing right and  $k = 0$ . Thus the divider branch is stable in the vicinity of the bifurcation. Two solutions of the system (42) are found on the divider branch within the range of interest: two *D*-type bifurcations corresponding to the regular turning points  $D_2, D_1$  (Fig. 3). Because of (45), the divider branch becomes unstable beyond  $D_2$ . Once again, the two-dimensional bifurcation analysis reported below (Fig. 4) shows that  $D_1, D_2$  belong to the same real eigenvalue. Thus the divider branch is stable beyond  $D_1$ , and a narrow hysteresis cycle appears around the threshold. Also, the nominal operating point  $A$  is found to be stable. Finally, frequency division ceases at point  $I_2$ , representing an *I*-type bifurcation of the *subcritical* kind (i.e., described by (46) with the arrow pointing left and  $k = 0$ ). Note that each point of the divider branch is actually representative of two states, differing only in the sign of the odd harmonics, and thus associated with the same value of  $M$ .

A deeper insight into the global stability picture for the frequency divider is provided by a bifurcation analysis in a two-dimensional parameter space. The second parameter is chosen as the inductance  $L$  of the feedback branch, since feedback is expected to have a critical influence on circuit performance. The results are reported in Fig. 4.

On the  $L$  axis ( $P_{IN} = 0$ ) a Hopf bifurcation of the bias point is encountered at  $L = L_H \approx 18.2$  nH (Fig. 4). For  $L \leq L_H$  the circuit behaves as a free-running oscillator with a fundamental around 4.7 GHz, and is thus useless as a frequency divider. In the region above  $L_H$  the circuit is

dc-stable, and its qualitative behavior is always of the kind depicted in Fig. 3. The loci of the four relevant bifurcations  $I_1, I_2, D_1, D_2$  are shown in the figure. The continuity of the two curves shows that  $I_1, I_2$  are generated by the sign reversal of the real part of the same natural frequency, and so are  $D_1, D_2$ . Further note that the turning-point curve exhibits the classic pattern of the so-called "cusp catastrophe" [4], the cusp occurring at point  $C$ .

The overall behavior of the frequency divider is clearly apparent at a glance from Fig. 4. Frequency division will take place when the selected combination of inductance and drive power falls within the "divider zone." For any inductance value, the left-hand border of this region represents the divider threshold. A hysteresis cycle may exist around threshold, depending on the selected inductance value. Above the cusp point ( $L \geq 21$  nH, approximately) hysteresis is eliminated, but threshold becomes relatively high (around 4 dBm). On the other hand, decreasing the inductance will lower the threshold, but at the same time a hysteresis cycle of growing width will appear. Furthermore, the circuit will become noisier, since the conditions for oscillation are approached.

As a final point, we shall briefly discuss the bifurcations of static solutions of the circuit equations ( $X_k = 0$  for  $k \neq 0$ ). In this case the fundamental bifurcations are the *D*- and the Hopf-type. For microwave applications, the latter plays an essential role in oscillator design and parasitic bias-circuit oscillations control in general microwave subsystems. The former may be of interest in relation to the design of dc-stable bias networks.

The conditions defining a bifurcation of a static solution are obviously much simpler than (42). If  $X_0$  is the dc (and the only nonzero) component of the state vector at the

bifurcation, we must have

$$\begin{aligned} \mathbf{E}_0(\mathbf{X}_0, \rho_B) &= 0 \\ \det[\mathbf{1}_{n_D} - \mathbf{S}(\omega, \rho_B)\mathbf{S}_D(\omega, \mathbf{X}_0, \rho_B)] &= 0 \end{aligned} \quad (48)$$

$$\frac{d\sigma}{d\rho}(\rho_B) \neq 0 \quad (49)$$

where  $\mathbf{S}$  is the conventional scattering matrix of the linear subnetwork (which may depend on the parameter  $\rho$ ), and  $\mathbf{S}_D$  is the small-signal scattering matrix of the nonlinear subnetwork describing its linearized behavior around the bias point defined by  $\mathbf{X}_0$ .

The exchange of stability at the bifurcation is discussed in detail in [98]. As a general rule, in the case of a simple real eigenvalue (*D*-type) or of two simple complex-conjugate eigenvalues (Hopf-type) crossing the imaginary axis at  $\rho = \rho_B$ , supercritical bifurcated states are stable, while subcritical ones are unstable [86].

For a *D*-type bifurcation ( $\omega = 0$ ), (48) is a system of  $n_D + 1$  real equations in  $n_D + 1$  real unknowns  $\mathbf{X}_0, \rho_B$ . In the Hopf case, it is a system of  $n_D + 2$  real equations in  $n_D + 2$  real unknowns  $\mathbf{X}_0, \rho_B, \omega$ . Thus the system is generally solvable from the mathematical viewpoint. The solution is now simplified by the fact that the second of eqs. (48) simply states that one of the eigenvalues (in a conventional sense) of the matrix  $\mathbf{SS}_D$  must be equal to 1 at the bifurcation. Thus a convenient way of solving (48) is now as follows: i) the first of (48) is solved for  $\mathbf{X}_0(\rho)$  by a continuation method; ii) to find *D*-type bifurcations, the one-dimensional manifold  $\mathbf{X}_0(\rho)$  is searched for the points  $\rho_B$  at which one eigenvalue of  $\mathbf{SS}_D$  becomes unity; iii) to find Hopf-type bifurcations the two-dimensional manifold  $[\omega, \mathbf{X}_0(\rho)]$  is searched for those points  $(\omega, \rho_B)$  at which one eigenvalue of  $\mathbf{SS}_D$  becomes unity. To verify (49) we only have to check that the magnitude of the above-mentioned eigenvalue is  $< 1$  at  $\rho_B - \delta\rho$  and  $> 1$  at  $\rho_B + \delta\rho$  ( $\delta\rho \ll \rho_B$ ), or conversely.

### C. Stability Analysis in the Time Domain

In principle, a similar stability analysis can also be carried out by time-domain techniques.

Let us assume, for instance, that the circuit is described by the set of evolution equations (1). Static (dc) solutions may be obtained by setting  $dx_1/dt = du/dt = 0$  in (1) and then solving the resulting system of nonlinear algebraic equations. The original system is then linearized in the neighborhood of any dc solution to find the corresponding natural frequencies. The latter are given by the eigenvalues of the Jacobian of the right-hand side of (1) with respect to the state variables, evaluated in equilibrium conditions. Periodic steady-state solutions  $\tilde{x}(t)$  must first be determined by the techniques described in Section II-A. The system (1) is then linearized in the neighborhood of  $\tilde{x}(t)$  and the evolution of a small perturbation  $\Delta x(t)$  is studied by Floquet analysis [86]. This means that by further

numerical integration one has to derive the *monodromy matrix* defining the change of the perturbation across one period  $T_0$  of the steady-state:

$$\Delta x(t + T_0) = \Phi(T_0) \Delta x(t). \quad (50)$$

The eigenvalues  $\lambda$  of  $\Phi(T_0)$  then yield the natural frequencies through the relationship

$$\lambda = \exp\{(\sigma + j\omega)T_0\}. \quad (51)$$

While the above procedure represents the conceptual basis for all mathematical treatments of stability, it is very difficult to implement numerically when the size of the system (1) is large (as is the case for practical microwave circuits), mainly because of the lengthy numerical integrations involved.

For this reason a true stability analysis is often replaced by a *transient* analysis [101], that is, a full numerical integration of the evolution equations from circuit turn-on up to the achievement of a steady state. It is implied that *all* natural frequencies will be excited during the transient, so that the effects of unstable ones will show up in the final waveforms. While this may be sufficient for many practical purposes, a global stability picture of the kind described in the preceding sections cannot be obtained in this way.

## VII. NOISE

In Section V we derived a generalized solution of the frequency-conversion (mixer) problem by injecting a small RF deterministic signal into a nonlinear network supporting a periodic steady-state regime, and by analyzing the resulting perturbation. When the RF source is replaced by a set of random noise generators as the perturbing mechanism, it is quite reasonable to expect that the same arguments will lead to a noise analysis of the steady state. Of course in this case the problem is much more complicated, since the free sources can only be described in a statistical sense. If several noise generators exist, they may not be statistically independent, and their correlation must be accounted for in evaluating the noise power delivered to a prescribed load. Further correlations are established among the noise sidebands because of the intermodulation of noise waveforms with the periodic steady state. All such effects are included in the general noise analysis to be presented in this section.

Because of its practical importance, a good deal of attention is paid to the noise problem in the technical literature. Several authors treat the subject for specific subsystems and with the aid of drastic simplifying assumptions, often aimed at the development of closed-form expressions highlighting some of its basic aspects [90], [92], [102]–[109]. Both frequency-domain [110], [111] and time-domain techniques [112] have been proposed to model the near-carrier noise in FET oscillators. Probably the most advanced treatment is given by Kerr in his noise analysis of diode mixers [74], [75], which makes use of a classic result established by Dragone [113] to correctly represent

the noise-sidebands correlation in the pumped diodes. The approach described here can be considered as an extension of Kerr's work to include generalized circuit topologies and multiport noisy nonlinear devices. As usual, the results are suitable for computer implementation in a general-purpose CAD environment.

Let us consider a stable steady-state solution  $\tilde{x}(t)$  of the circuit equations, time-periodic of period  $T_0 = 2\pi/\omega_0$ , and let a random perturbation  $\delta x(t)$  be superimposed on it. We assume that the perturbation is Fourier-transformable and write

$$\begin{aligned}\delta x(t) &= \int_{-\infty}^{\infty} F_x(\omega) \exp(j\omega t) d\omega \\ &= \int_0^{\omega_0} \sum_k F_x(\omega + k\omega_0) \exp\{j(\omega + k\omega_0)t\} d\omega \quad (52)\end{aligned}$$

where  $F_x(\omega)$  is a vector of Fourier transforms (divided by  $2\pi$ ). All vectors appearing in (52) have the same size  $n_D$ , equal to the number of ports of the nonlinear (or linear) subnetwork.

In the following, our interest will mainly be focused on *spot* noise calculations, so that we shall consider noise perturbations of the form

$$\delta x(t) = \sum_k \delta X_k(\omega) \exp\{j(\omega + k\omega_0)t\} \quad (0 < \omega < \omega_0) \quad (53)$$

where, according to (52)

$$\delta X_k(\omega) = F_x(\omega + k\omega_0) d\omega. \quad (54)$$

$\delta X_k(\omega)$  may be interpreted as a vector of complex amplitudes of "pseudosinusoidal" noise components at frequency  $\omega + k\omega_0$  (i.e., at the  $k$ th sideband associated with  $\omega$ ). With the formulation adopted, the squared magnitude of the  $i$ th element of  $\delta X_k(\omega)$  ( $1 \leq i \leq n_D$ ) represents the RMS value of those components of the noise waveform  $\delta x_i(t)$  whose spectrum lies in a narrow band  $d\omega$  in the neighborhood of  $\omega + k\omega_0$ . Thus if a spectral density  $G_{xi}(\omega)$  can be associated with  $\delta x_i(t)$ , we have

$$|\delta X_{ki}(\omega)|^2 = G_{xi}(\omega + k\omega_0) d\omega. \quad (55)$$

To develop our noise analysis, we are going to replace the nonlinear network under consideration by the equivalent circuit shown in Fig. 5. This transformation requires some comments.

As usual, the original circuit is first subdivided into a linear and a nonlinear subnetwork. The vector of noise voltages at the connecting ports is denoted by  $\delta v(t)$ . The linear subnetwork is replaced by its Norton equivalent, consisting of a noise-free network with a noise current source connected across each port. These will be referred to as the "linear" noise sources and their set will be indicated by  $j_L(t)$  (see Fig. 5). The linear noise sources are correlated, so that their statistical properties are described in terms of an  $(n_D \times n_D)$  spot correlation matrix  $\underline{\mathcal{C}}_L(\omega)$ . If we adopt the representation (53), that is,

$$j_L(t) = \sum_k J_{Lk}(\omega) \exp\{j(\omega + k\omega_0)t\} \quad (56)$$

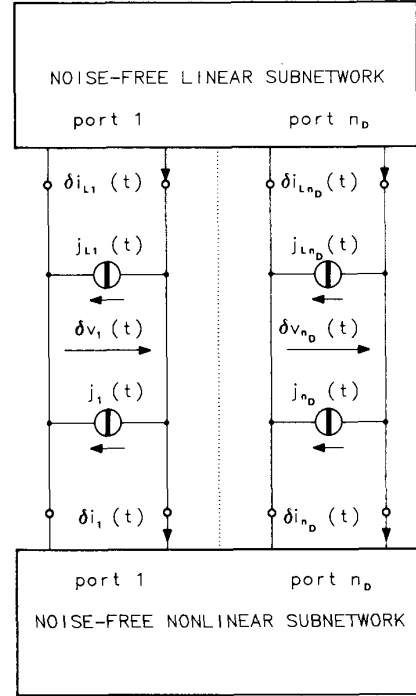


Fig. 5. Equivalent representation of a noisy nonlinear network.

then the correlation properties of the sidebands are expressed by

$$\langle J_{Lp}(\omega) J_{Lq}^*(\omega) \rangle = \delta_p^q \underline{\mathcal{C}}_L(\omega + p\omega_0) \quad (57)$$

where  $\delta$  is Kronecker's symbol,  $\langle \rangle$  indicates the statistical mean, and  $*$  the Hermitian conjugate. An important point is that a general computer algorithm, allowing  $\underline{\mathcal{C}}_L(\omega)$  to be derived for a completely arbitrary configuration of the linear subnetwork, is available in the technical literature [114].

In Fig. 5 the noisy nonlinear subnetwork is dealt with in a similar way, i.e., is replaced by a noise-free nonlinear multiport with a noise current source connected across each port. Such sources account for the noise generated inside the nonlinear subnetwork and their properties are affected by the steady-state regime supported by the circuit, as described below. They will be referred to as the "nonlinear" noise sources, and their set will be denoted by  $j(t)$  (see Fig. 5).

Note that the representation adopted for the nonlinear subnetwork does not have the meaning of a Norton equivalent circuit. In fact, the Norton transformation is based on the superposition principle, and its applicability is strictly confined to linear circuits. To produce the topology shown in Fig. 5, we simply open an additional external port of the nonlinear subnetwork at the terminals of each noise source which is not naturally connected across a port. For each fictitious port thus created, we must also add an open-circuited port to the linear subnetwork and a new state variable in the equations (2). Thus a noise analysis, although possible in general, may force us to

work with a number of ports  $n_D$  larger than required by a conventional nonlinear analysis not including noise.

We next derive the correlation properties of the nonlinear noise sources. Let us first focus our attention on the bias point of the nonlinear subnetwork, which is defined by the subset  $X_0$  of the state vector  $X$ . If the nonlinear subnetwork were operated under dc conditions at the bias point  $X_0$ , its noise behavior would be described by a set of noise sources, namely  $j_{dc}(X_0, t)$ , depending on  $X_0$  in a deterministic way. The statistical properties of  $j_{dc}$  can be derived in the usual way from the physical properties of the nonlinear subnetwork; for the most common microwave devices they are thoroughly described in the technical literature [115]. In particular, we will regard as known the spot correlation matrix of  $j_{dc}$ , namely  $\mathcal{C}_{dc}(X_0, \omega)$ .

The dynamic case can now be studied by a quasi-static assumption. Following [113], we think of noise as arising from the superposition of statistically independent random disturbances whose duration is much smaller than  $T_0$ . The statistical properties are determined by the probability distribution of such elementary events, whose magnitude is proportional to a deterministic function of  $X_0$ . The periodic steady state may thus be treated as a time-dependent bias point: in this case the magnitude of the probability distribution is expressed by the same function with  $X_0$  replaced by  $\tilde{x}(t)$ , and becomes a periodic function of time. We thus write

$$j(t) = \mathbf{h}(t) j_{dc}(X_0, t) \quad (58)$$

where  $\mathbf{h}(t)$  is diagonal of size  $n_D$ , is time-periodic of period  $T_0$ , and has nonnegative elements. To evaluate  $\mathbf{h}(t)$ , we consider the  $i$ th element of  $j_{dc}$  ( $1 \leq i \leq n_D$ ), and denote by  $G_{dc,i}(X_0, \omega)$  its spectral density. The corresponding (normalized) available noise power is given by

$$N_{dc,i} = \int_B G_{dc,i}(X_0, \omega) d\omega \quad (59)$$

where  $B$  is the noise bandwidth of interest. In the dynamic case, this power will be modulated by a periodic function of time, which can be identified as  $h_i^2(t)$  according to (58). Using the quasi-static assumption we thus obtain from (59)

$$\begin{aligned} N_i(t) &= h_i^2(t) N_{dc,i} \\ &= \int_B G_{dc,i}\{\tilde{x}(t), \omega\} d\omega \end{aligned} \quad (60)$$

and finally

$$h_i(t) = \left[ \frac{\int_B G_{dc,i}\{\tilde{x}(t), \omega\} d\omega}{\int_B G_{dc,i}(X_0, \omega) d\omega} \right]^{1/2} \quad 1 \leq i \leq n_D. \quad (61)$$

Thus  $\mathbf{h}(t)$  can be immediately derived once the steady state  $\tilde{x}(t)$  and the noise properties of the dc-biased nonlinear subnetwork are known.

Since  $\mathbf{h}(t)$  is real and time-periodic, we may write

$$\mathbf{h}(t) = \sum_p \mathbf{H}_p \exp(jp\omega_0 t) \quad (62)$$

where  $\mathbf{H}_p$  is diagonal of size  $n_D$ , and  $\mathbf{H}_{-p} = \mathbf{H}_p^*$ .

Let us represent the static and dynamic noise current waveforms by expansions similar to (56) and denote by  $\mathbf{J}_{dc,k}(X_0, \omega)$  and  $\mathbf{J}_k(\omega)$  their pseudosinusoidal component amplitudes, respectively. Introducing such expansions and (62) into (58) yields

$$\mathbf{J}_p(\omega) = \sum_k \mathbf{H}_{p-k} \mathbf{J}_{dc,k}(X_0, \omega). \quad (63)$$

Since the correlation properties of  $\mathbf{J}_{dc}$  may be expressed as in (57) (with  $\mathcal{C}_L$  replaced by  $\mathcal{C}_{dc}$ ), from (63) we obtain directly

$$\langle \mathbf{J}_p(\omega) \mathbf{J}_q^*(\omega) \rangle = \sum_k \mathbf{H}_{p-k} \mathcal{C}_{dc}(X_0, \omega + k\omega_0) \mathbf{H}_{k-q}. \quad (64)$$

Equation (64) shows that different sidebands of the nonlinear noise sources are in general correlated because of the modulation of the dc noise waveforms operated by the periodic steady state. It is easy to check that the result derived by Dragone [113] and used by Kerr [74], [75] can be reobtained from (64) in the case of a set of uncorrelated sources of white noise ( $\mathcal{C}_{dc}$  diagonal and independent of  $\omega$ ).

At this stage the noise analysis can be developed in a straightforward way. To make the equations formally simple, we first introduce for each noise waveform of interest the vector of the pseudosinusoidal component amplitudes at all sidebands: for instance, for the random perturbation  $\delta x(t)$  we define

$$\delta \mathbf{X}(\omega) \equiv [\delta X_k(\omega)] \quad (65)$$

and so forth. Such vectors satisfy a set of equations that are formally identical to (26) and (32), that is,

$$\begin{aligned} \delta V(\omega) &= \mathbf{P} \delta \mathbf{X}(\omega) \\ \delta I(\omega) &= \mathbf{Q} \delta \mathbf{X}(\omega) \\ \mathbf{A}_L \delta V(\omega) + \mathbf{B}_L \delta I_L(\omega) &= 0 \end{aligned} \quad (66)$$

where the currents at the linear subnetwork ports have been denoted by the subscript  $L$  (see Fig. 5). From the figure we also obtain

$$\delta I_L(\omega) = \delta I(\omega) + \mathbf{J}_L(\omega) + \mathbf{J}(\omega). \quad (67)$$

Combining (66) and (67) yields

$$\delta V(\omega) = -\mathbf{P}(\mathbf{A}_L \mathbf{P} + \mathbf{B}_L \mathbf{Q})^{-1} \mathbf{B}_L \{ \mathbf{J}_L(\omega) + \mathbf{J}(\omega) \}. \quad (68)$$

We can select the  $k$ th sideband by writing

$$\delta V_k(\omega) = \mathbf{U}_k \delta V(\omega) \quad (69)$$

where

$$\mathbf{U}_k \equiv [\cdots \mathbf{0} \cdots \mathbf{1}_{n_D} \cdots \mathbf{0} \cdots] \quad (70)$$

and  $\mathbf{1}_{n_D}$  is an identity matrix of size  $n_D$ . Because of (35), the matrix  $(\mathbf{A}_L \mathbf{P} + \mathbf{B}_L \mathbf{Q})$  is nonsingular, and thus (68) is meaningful at any  $\omega$  between 0 and  $\omega_0$ , if the steady state

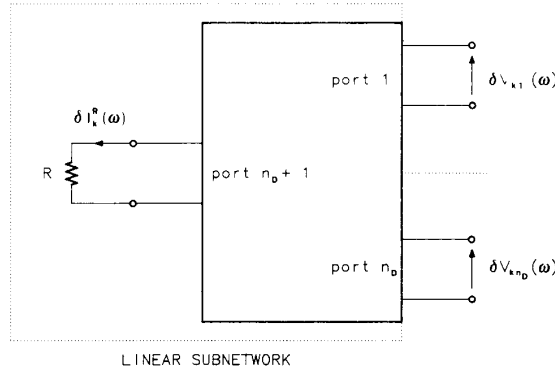


Fig. 6. Identification of a load within the linear subnetwork.

is asymptotically stable, i.e., all its natural frequencies have a negative real part.

To complete the noise analysis, we arbitrarily select a resistor within the linear subnetwork, which is assigned the meaning of load, and compute the spectral distribution of the noise power *actually delivered* to this load. For this purpose we rearrange the linear subnetwork in the way shown in Fig. 6, and carry out a conventional linear analysis of the  $(n_D + 1)$ -port network thus obtained at  $\omega + k\omega_0$ . From the admittance matrix of the  $(n_D + 1)$ -port, we can readily derive a  $(1 \times n_D)$  transadmittance matrix  $Y_R(\omega)$  such that

$$\delta I_k^R(\omega) = Y_R(\omega + k\omega_0) \delta V_k(\omega) \quad (71)$$

where  $\delta I_k^R(\omega)$  is the complex amplitude of the pseudo-sinusoidal noise current component through  $R$  at  $\omega + k\omega_0$ . Making use of (69) and (68), we get

$$\delta I_k^R(\omega) = T_k \{ J_L(\omega) + J(\omega) \}, \quad (72)$$

where

$$T_k = -Y_R(\omega + k\omega_0) U_k P (A_L P + B_L Q)^{-1} B_L. \quad (73)$$

Since the linear and nonlinear noise sources are not correlated, their effects may be superimposed in power. Thus the noise power delivered to  $R$  within a narrow frequency band  $d\omega$  in the neighborhood of  $\omega + k\omega_0$  is

$$\begin{aligned} dN_k(\omega) &= R \langle |\delta I_k^R(\omega)|^2 \rangle \\ &= R T_k \langle J_L(\omega) J_L^*(\omega) \rangle T_k^* \\ &\quad + R T_k \langle J(\omega) J^*(\omega) \rangle T_k^*. \end{aligned} \quad (74)$$

If we now partition  $T_k$  into  $(1 \times n_D)$  submatrices, namely

$$T_k \equiv [T_{kp}] \quad (75)$$

and recall (57) and (64), we get the final result

$$\begin{aligned} dN_k(\omega) &= R \sum_p T_{kp} \mathcal{G}_L(\omega + p\omega_0) T_{kp}^* \\ &\quad + R \sum_{p,q} T_{kp} \left\{ \sum_s H_{p-s} \mathcal{G}_{DC}(X_0, \omega + s\omega_0) H_{s-q} \right\} T_{kq}^*. \end{aligned} \quad (76)$$

By means of (76), noise in a nonlinear network is essentially described as a frequency conversion effect, with each  $T_{kp}$  playing the role of a sideband-to-sideband conversion matrix. In particular, the quantity

$$\begin{aligned} dN_k^0(\omega) &= R T_{k0} \mathcal{G}_L(\omega) T_{k0}^* \\ &\quad + R \sum_{p,q} T_{kp} H_p \mathcal{G}_{DC}(X_0, \omega) H_q^* T_{kq}^* \end{aligned} \quad (77)$$

represents the contribution due to the up-conversion of baseband noise to the  $k$ th sideband. If the usual truncation is adopted, all summation indexes in (76) and (77) range from  $-N_H$  to  $N_H$ .

Besides the noise power described by (76), having a continuous spectral distribution, a finite power is obviously delivered to the load at each harmonic of the steady state. This can be expressed as

$$S(k\omega_0) = \frac{1}{2} R |Y_R(k\omega_0) \Phi_k(X)|^2 \quad (78)$$

where  $X$  is the state vector, and  $\Phi_k$  is the  $k$ th harmonic of the first of (2) computed in steady-state conditions. Equation (78) represents a set of discrete spectral lines that are superimposed to the continuous spectrum (76).

### VIII. IMPACT OF SUPERCOMPUTERS

It has now become evident from the preceding discussion that nonlinear analysis and design problems concerning realistic microwave circuits may be large-size ones from the numerical standpoint. Many kinds of passive components require the use of sophisticated modeling techniques, while the nonlinear equivalent circuits of even the simplest microwave devices often contains several nonlinear elements such as resistors or dependent sources. Basic operations such as analysis and optimization require expensive search algorithms involving repeated multi-frequency analyses of the linear subnetwork. The number of unknowns may be quite large, especially for broad-band operation, not to mention the case of multitone excitation such as in mixer or intermodulation problems. Stability and noise analyses require large-order matrices to be repeatedly evaluated and inverted. In order to implement all this, from the viewpoint of both software development and systematic use, it is rather natural to resort to the highest available computational power, namely, supercomputers.

For the time being, let us make use of a simple performance-oriented definition of a supercomputer, i.e., something that is roughly two orders of magnitude faster than a VAX and has several millions 64-bits words of central semiconductor memory. There are many reasons why such a machine can be attractive for nonlinear microwave CAD purposes, and some of them are conceptually more relevant than mere computational speedup. Of course, the latter is important by itself: some advanced nonlinear applications may require such a long CPU time as to make the use of a medium-size mainframe definitely impractical.

There is, however, much more than that. The computer-aided solution of any problem of applied science always

requires some amount of analytical preprocessing. There is always a tradeoff between mathematical and numerical work, and the use of sophisticated analytic and programming techniques is often convenient in order to alleviate the computational burden committed to the machine. On supercomputers, the opposite is often true: in fact, not only are they fast, but the simpler program architecture, the faster they perform, as we shall discuss later. Thus it may be convenient to waive a consistent part of the programmer's task and to rely upon the number-crunching capabilities of the computer. Simple, straightforward solution approaches which would be out of the question on medium-size scalar machines may now become the most natural way to solve the problem. An example concerning nonlinear microwave circuits under multiple-frequency excitation is reported in [59].

The availability of virtually unlimited memory resources is another important point. Once again, the classic tradeoff between memory occupation and computational speed may be pushed all the way in favour of numerical efficiency. To do the same on smaller-size machines one must often resort to virtual memory, which can slow down computation in a significant way.

#### A. Vector Processors

The increased computational power of supercomputers relies upon two fundamental mechanisms: technological advance and architectural evolution. The former is transparent to the user, and will not be considered here, but the latter is not, in the sense that codes should usually be matched to computer architecture in order to achieve maximum efficiency. In turn, architectural evolution with respect to the classic Von Neumann structure is essentially based on one of the fundamental concepts of modern computer science, namely, parallel processing.

As a matter of fact, most present-day supercomputers belong to the special class of vector processors [116], [117]. Vector processors are really available commercially and are relatively widespread; they feature the highest available computational power and are easily accessible to any user for general-purpose scientific calculations. In such machines, parallel processing is implemented by a number of basic mechanisms, the most important of which are listed below:

- pipelining of vector operations;
- chaining of vector operations;
- parallel execution of independent operations (arithmetic, logical, address calculations, ...) on independent functional units;
- parallel execution of vector and scalar operations;
- multitasking.

Pipelining is the fundamental aspect, and is schematically illustrated in Fig. 7 [118], [119]. Let us consider a binary operation of the form

$$C(I) = A(I) \text{ OP } B(I) \quad (79)$$

where  $\text{OP}$  is any arithmetic or logical operator and  $I$  is an

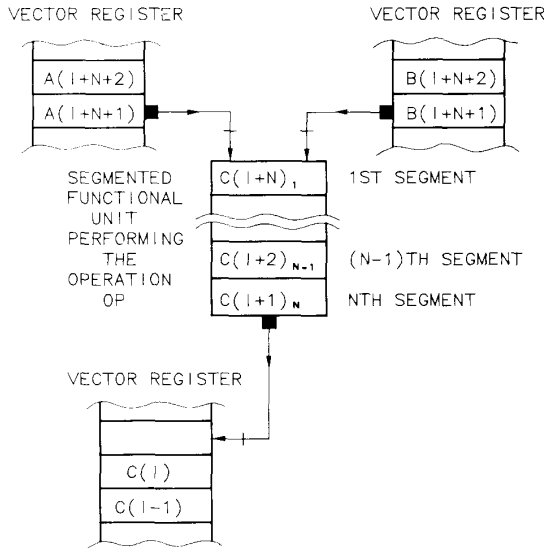


Fig. 7. Schematic illustration of the pipeline concept.  $C(J)_k$  denotes the  $k$ th step of the computation of  $A(J) \text{ OP } B(J)$  in the segmented functional unit.

integer index. This operation is actually executed through a number of elementary steps, each requiring one clock period, such as sign control, exponent fitting, addition of mantissas, and normalization, for a floating-point addition. The functional unit is thus subdivided into a corresponding number of cascaded subunits or segments, each performing one of the elementary steps.

Now assume that the code is carrying out a sequence of identical operations for increasing values of  $I$ , namely a vector operation, so that operands are continuously fed to the functional unit at a rate of a couple for each clock period. Once the entire process has been initialized, that is, after the vector startup time has elapsed, results will also be produced at the same rate. Thus the vector processor will execute binary vector operations at a peak speed, measured in floating-point operations per second, or flops, equal to the inverse of the clock period.

However, pipelining is not restricted to the binary case illustrated in Fig. 7: in fact, more complex vector operations can be executed in parallel in the pipeline sense (one result per clock period) by an additional mechanism, named chaining [117]. The concept is very simple: as soon as a result becomes available in a vector register (strictly speaking, one cycle later), it can be fed to the input of a different functional unit to serve as an operand for the subsequent operation. In this way the vector hardware may be configured as an extended functional unit with several inputs, where a multiple-operand arithmetic or logical operation can be pipelined.

All this is obviously handled by the compiler and is transparent to the user, except for one aspect: the calculations to be performed by the program should be organized into the largest possible groups of consecutive operations of the same kind, that is, into vector operations of the

maximum possible length. This is what we mean by *vectorizing* a program.

The other mechanisms mentioned above are in fact something different, in that they implement a more conventional concept of parallelism, namely, different functional units simultaneously execute independent operations on different operands. Multitasking is similar except that parallelism is exploited here at the highest level: if the system is a multiprocessor, the user's program can be organized into sections to be run concurrently on different CPU's. Organizing the tasks and synchronizing them when several ones merge again into a single instruction stream is up to the user, and can be done at the FORTRAN programming level by suitable calls to specialized system subroutines.

Note that the above discussion is somewhat Cray-oriented since this is the system family the authors are most familiar with; however, the principles are substantially valid for many different kinds of vector processors.

The same discussion makes it clear that program vectorization is the most important action to be taken in order to effectively exploit the computational power of a vector supercomputer. The same code on the same machine can run in a CPU time ranging from, say, 1 to 10 in relative terms depending on its degree of vectorization. This has a direct impact on computer costs, too: in fact, the user will pay exactly the same amount for one CPU second regardless of whether his calculations are vectorized or fully scalar. This means that any speedup obtained by vectorization will result in a cost reduction by exactly the same amount. An important related point is that vectorizing invariably means making a program simpler and better structured, which is clearly shown by the fact that vectorized programs are usually more efficient from the scalar viewpoint, too [122], [123]. This happens because vectorizing leads to the elimination of a number of non-productive but time-consuming procedures such as *if* statements and subroutine calls. Of course this does not imply that vectorization is good for scalar machines, since it always results in a large increase of memory requirements. In fact, space has to be provided to store the entire vector operands, which must be physically available, while in the scalar approach subsequent elements may overwrite the same memory locations, since results are produced sequentially rather than in parallel.

#### B. Supercomputers in Microwave CAD

Going back to our main subject, it is quite obvious that a nonlinear microwave CAD program is a natural candidate for an efficient vectorization. For instance, a circuit optimization is usually carried out by some sort of iterative method, and is thus a highly repetitive job, which will spend most of the CPU time in executing exactly the same set of operations over and over again. Thus in principle vectorizing just becomes matter of organizing such operations in a convenient order.

Let us focus our attention on a relatively expensive numerical procedure such as the optimization of a nonlin-

TABLE II  
PERFORMANCE OF A TYPICAL VECTOR PROCESSOR (CRAY X-MP)

1) FFT ( $N_s$ = NUMBER OF SAMPLING POINTS)		
	$N_s = 32$	$N_s = 1024$
VECTOR SPEEDUP	7.3	14.7
COMBINED SPEEDUP WITH RESPECT TO THE CDC 7600	19.3	39.0
2) SAMPLING OF NONLINEAR RESPONSE		
	$N_s = 32$	$N_s = 1024$
VECTOR SPEEDUP	6.5	11.9
COMBINED SPEEDUP WITH RESPECT TO THE CDC 7600	18.9	34.7
3) MULTIFREQUENCY LINEAR SUBNETWORK ANALYSIS ( $N_f$ = NUMBER OF FREQUENCIES)		
	$N_f = 7$	$N_f = 49$
VECTOR SPEEDUP	2.9	5.9
COMBINED SPEEDUP WITH RESPECT TO THE CDC 7600	14.6	29.7

ear circuit by the harmonic-balance approach. Three mechanisms are essentially responsible for the computer time requirement of this kind of job, namely, sampling the time-domain response of the nonlinear subnetwork, Fourier transforming it, and analyzing the linear subnetwork at all the design frequencies and their harmonics. The relative importance of these aspects is strongly job-dependent; however, they are usually responsible for more than 90 percent of the overall time, so this is where the vectorization effort has to be spent.

Typical speedups measured on a Cray X-MP system are reported in Table II. Of course the FFT represents the easiest and most rewarding job since fully vectorized and very efficient subroutines performing this algorithm are available in all supercomputer libraries.

As for the nonlinear response, vectorization here is up to the user, but is still easy and may be carried out by direct application of elementary principles. The scalar approach would be to code the nonlinear subnetwork equations in a subroutine yielding the response at a given time, and then to repeatedly call it at all sampling instants. In a vector logic one has to move the iteration inside the subroutine, so that the calculation of the entire response becomes a unique vector operation; in other words all sampling points are processed in parallel in the pipeline sense.

The approach to the linear subnetwork analysis is conceptually similar: a sequence of single-frequency analyses is changed into a single multifrequency analysis; that is, any aspect of network performance is treated simultaneously at all frequencies of interest. In this case, to enhance the degree of vectorization and thus to improve the overall performance, some further actions can be taken, such as the parallel computation of all physically similar circuit components, and the parallel execution of topologically similar component connections. These ideas have been discussed in detail in the recent technical literature [123].

The results shown in Table II include a comparison with the performance of an equivalent scalar code on a classic scalar mainframe such as the Cyber 76. Very similar results are obtained with modern scalar systems such as the VAX 8800. The figures clearly show that supercomputers can indeed be used to carry out large applications with fast job turnaround and good cost-to-performance ratio and have the potential to bridge the gap between linear and nonlinear microwave CAD techniques.

## REFERENCES

- [1] "Nonlinear analysis and design of microwave circuits", in *Proc. 15th European Microwave Conf.*, Tutorial Session no. 2 (Paris), Sept. 1985, pp. 1087-1124.
- [2] C. A. Desoer, Ed., Special Issue on Nonlinear Circuits, *IEEE Trans. Circuit Theory*, vol. CT-19, Nov. 1972.
- [3] R. W. Lin, Ed., Special Issue on Nonlinear Circuits and Systems, *IEEE Trans. Circuits Syst.*, vol. CAS-27, Nov. 1980.
- [4] L. O. Chua, Ed., Special Issue on Nonlinear Phenomena, Modeling, and Mathematics, *IEEE Trans. Circuits Syst.*, vol. CAS-30, Aug.-Sept. 1983.
- [5] E. S. Kuh, Ed., Centennial Issue, *IEEE Trans. Circuits Syst.*, vol. CAS-31, Jan. 1984.
- [6] D. O. Pederson, "A historical review of circuit simulation," *IEEE Trans. Circuits Syst.*, vol. CAS-31, pp. 103-111, Jan. 1984.
- [7] V. K. Tripathi and J. B. Rettig, "A SPICE model for multiple coupled microstrips and other transmission lines," in *1985 IEEE MTT-S Int. Microwave Symp. Dig.* (St. Louis), Sept. 1985, pp. 703-706.
- [8] J. E. Schutt-Aine and R. Mittra, "Analysis of pulse propagation in coupled transmission lines," *IEEE Trans. Circuits Syst.*, vol. CAS-32, pp. 1214-1219, Dec. 1985.
- [9] F. Romeo and M. Santomauro, "Time-domain simulation of n-coupled transmission lines," *IEEE Trans. Microwave Theory Tech.*, vol. MTT-35, pp. 131-137, Feb. 1987.
- [10] S. E. Sussman-Fort, S. Narasimhan, and K. Mayaram, "A complete GaAs MESFET computer model for SPICE," *IEEE Trans. Microwave Theory Tech.*, vol. MTT-32, pp. 471-473, Apr. 1984.
- [11] A. K. Jastrzebski and M. I. Sobhy, "Analysis of microwave circuits using state-space approach," in *Proc. 1984 IEEE Int. Symp. Circuits Syst.* (Montreal), May 1984, pp. 1119-1122.
- [12] J. M. Golio, P. A. Blakey, and R. O. Grondin, "A general CAD tool for large-signal GaAs MESFET circuit design," in *1985 IEEE MTT-S Int. Microwave Symp. Dig.* (St. Louis), June 1985, pp. 417-420.
- [13] M. I. Sobhy and A. K. Jastrzebski, "Direct integration methods of non-linear microwave circuits," in *Proc. 15th European Microwave Conf.* (Paris), Sept. 1985, pp. 1110-1118.
- [14] C. W. Gear, "Simultaneous numerical solution of differential-algebraic equations," *IEEE Trans. Circuit Theory*, vol. CT-18, pp. 89-95, Jan. 1971.
- [15] P. M. Russo, "On the time-domain analysis of linear time-invariant networks with large time-constant spreads by digital computers," *IEEE Trans. Circuit Theory*, vol. CT-18, pp. 194-197, Jan. 1971.
- [16] R. L. Veghte and C. A. Balanis, "Dispersion of transient signals in microstrip transmission lines," *IEEE Trans. Microwave Theory Tech.*, vol. MTT-34, pp. 1427-1436, Dec. 1986.
- [17] J. F. Whitaker et al., "Pulse dispersion and shaping in microstrip lines," *IEEE Trans. Microwave Theory Tech.*, vol. MTT-35, pp. 41-47, Jan. 1987.
- [18] L. W. Nagel, "SPICE2: A computer program to simulate semiconductor circuits," Electronic Research Laboratory, University of California-Berkeley, Memo ERL-M520, 1975.
- [19] T. Brazil et al., "Large-signal FET simulation using time domain and harmonic-balance methods," *Proc. Inst. Elec. Eng.*, pt. H, vol. 133, pp. 363-367, Oct. 1986.
- [20] S. W. Director, "A method for quick determination of the periodic steady-state in nonlinear networks," in *Proc. 9th Allerton Conf. Circuit Syst. Theory*, (University of Illinois, Urbana-Champaign), Oct. 1971, pp. 131-139.
- [21] T. J. Aprille Jr. and T. N. Trick, "Steady-state analysis of nonlinear circuits with periodic inputs," *Proc. IEEE*, vol. 60, pp. 108-114, Jan. 1972.
- [22] T. J. Aprille Jr. and T. N. Trick, "A computer algorithm to determine the steady-state response of nonlinear oscillators," *IEEE Trans. Circuit Theory*, vol. CT-19, pp. 354-360, July 1972.
- [23] F. R. Colon and T. N. Trick, "Fast periodic steady-state analysis for large-signal electronic circuits," *IEEE J. Solid-State Circuits*, vol. SC-8, pp. 260-269, Aug. 1973.
- [24] S. Skelboe, "Computation of the periodic steady-state response of nonlinear networks by extrapolation methods," *IEEE Trans. Circuits Syst.*, vol. CAS-27, pp. 161-175, Mar. 1980.
- [25] M. S. Nakhla and J. Vlach, "A piecewise harmonic-balance technique for determination of periodic response of nonlinear systems," *IEEE Trans. Circuits Syst.*, vol. CAS-23, pp. 85-91, Feb. 1976.
- [26] J. C. Lindenlaub, "An approach for finding the sinusoidal steady state response of nonlinear systems," in *Proc. 7th Allerton Conf. Circuit Syst. Theory* (University of Illinois, Chicago), 1969.
- [27] K. S. Kundert and A. Sangiovanni-Vincentelli, "Simulation of nonlinear circuits in the frequency domain," *IEEE Trans. Computer-Aided Design*, vol. CAD-5, pp. 521-535, Oct. 1986.
- [28] D. M. Himmelblau, *Applied Nonlinear Programming*. New York: McGraw-Hill, 1972.
- [29] M. J. D. Powell, "Minimization of functions of several variables," in *Numerical Analysis: An Introduction*, J. Walsh, Ed., Washington, D.C.: Thompson, 1967.
- [30] R. Fletcher, "A new approach to variable metric algorithms," *Computer J.*, vol. 13, pp. 317-322, Aug. 1970.
- [31] H. Wacker, *Continuation Methods*. New York: Academic Press, 1978.
- [32] F. Filicori, V. A. Monaco, and C. Naldi, "Analysis and optimization of non-linear circuits with periodic excitation," in *Proc. SPACECAD '79* (Bologna), Sept. 1979, pp. 171-176.
- [33] F. Filicori, V. A. Monaco, and C. Naldi, "Simulation and design of microwave Class-C amplifiers through harmonic analysis," *IEEE Trans. Microwave Theory Tech.*, vol. MTT-27, pp. 1043-1051, Dec. 1979.
- [34] C. Naldi and F. Filicori, "Computer-aided design of GaAs MESFET power amplifiers," in *Proc. 12th European Microwave Conf.* (Helsinki), Sept. 1982, pp. 435-440.
- [35] D. Hente and R. H. Jansen, "Frequency-domain continuation method for the analysis and stability investigation of nonlinear microwave circuits," *Proc. Inst. Elec. Eng.*, pt. H, vol. 133, pp. 351-362, Oct. 1986.
- [36] L. O. Chua and A. Ushida, "A switching-parameter algorithm for finding multiple solutions of nonlinear resistive circuits," *Int. J. Circuit Theory Appl.*, vol. 4, pp. 215-239, 1976.
- [37] V. Rizzoli et al., "User-oriented software package for the analysis and optimization of nonlinear microwave circuits," *Proc. Inst. Elec. Eng.*, pt. H, vol. 133, pp. 385-391, Oct. 1986.
- [38] F. B. Hildebrand, *Introduction to Numerical Analysis*. New York: McGraw-Hill, 1967.
- [39] A. R. Kerr, "A technique for determining the local oscillator waveforms in a microwave mixer," *IEEE Trans. Microwave Theory Tech.*, vol. MTT-23, pp. 828-831, Oct. 1975.
- [40] R. G. Hicks and P. J. Khan, "Numerical technique for determining pumped nonlinear device waveforms," *Electron. Lett.*, vol. 16, pp. 375-376, May 1980.
- [41] R. G. Hicks and P. J. Khan, "Numerical analysis of nonlinear solid-state device excitation in microwave circuits," *IEEE Trans. Microwave Theory Tech.*, vol. MTT-30, pp. 251-259, Mar. 1982.
- [42] C. Camacho-Péñalosa, "Numerical steady-state analysis of nonlinear microwave circuits with periodic excitation," *IEEE Trans. Microwave Theory Tech.*, vol. MTT-31, pp. 724-730, Sept. 1983.
- [43] F. Filicori and C. Naldi, "An algorithm for the periodic or quasi-periodic steady-state analysis of non-linear circuits," in *Proc. 1983 IEEE Int. Symp. Circuits Syst.* (Newport Beach), May 1983, pp. 366-369.
- [44] D. Hwang and T. Itoh, "Large-signal modeling and analysis of GaAs MESFET," in *Proc. 16th European Microwave Conf.* (Dublin), Sept. 1986, pp. 189-194.
- [45] G. W. Rhyne and M. B. Steer, "A new frequency-domain approach to the analysis of nonlinear microwave circuits," in *1985 IEEE MTT-S Int. Microwave Symp. Dig.* (St. Louis), June 1985, pp. 401-404.
- [46] G. L. Heiter, "Characterization of nonlinearities in microwave devices and systems," *IEEE Trans. Microwave Theory Tech.*, vol. MTT-21, pp. 797-805, Dec. 1973.
- [47] R. S. Tucker, "Third-order intermodulation distortion and gain compression of GaAs FET's," *IEEE Trans. Microwave Theory Tech.*, vol. MTT-27, pp. 400-408, May 1979.

- [48] F. Filicori, C. Naldi, and M. R. Scalas, "Non-linear circuit analysis through periodic spline approximation," *Electron. Lett.*, vol. 15, pp. 597–599, Sept. 1979.
- [49] F. Filicori, M. R. Scalas, and C. Naldi, "Periodic steady-state analysis of non-linear circuits using spline functions," in *Proc. SPACECAD '79* (Bologna), Sept. 1979, pp. 189–193.
- [50] S. W. Director and K. Wayne Current, "Optimization of forced nonlinear periodic circuits," *IEEE Trans. Circuits Syst.*, vol. CAS-23, pp. 329–335, June 1976.
- [51] A. Lipparini, E. Marazzi, and V. Rizzoli, "A new approach to the computer-aided design of nonlinear networks and its application to microwave parametric frequency dividers," *IEEE Trans. Microwave Theory Tech.*, vol. MTT-30, pp. 1050–1058, July 1982.
- [52] V. Rizzoli, A. Lipparini, and E. Marazzi, "A general-purpose program for nonlinear microwave circuit design," *IEEE Trans. Microwave Theory Tech.*, vol. MTT-31, pp. 762–770, Sept. 1983.
- [53] A. Lipparini, E. Marazzi, and V. Rizzoli, "Computer-aided design of microwave parametric frequency dividers," in *1981 IEEE MTT-S Int. Microwave Symp. Dig.* (Los Angeles), June 1981, pp. 229–231.
- [54] V. Rizzoli and A. Lipparini, "A computer-aided approach to the nonlinear design of microwave transistor oscillators," in *1982 IEEE MTT-S Int. Microwave Symp. Dig.* (Dallas), June 1982, pp. 453–455.
- [55] C. Rauscher, "Regenerative frequency division with a GaAs FET," *IEEE Trans. Microwave Theory Tech.*, vol. MTT-32, pp. 1461–1468, Nov. 1984.
- [56] A. Ushida and L. O. Chua, "Frequency-domain analysis of nonlinear circuits driven by multi-tone signals," *IEEE Trans. Circuits Syst.*, vol. CAS-31, pp. 766–779, Sept. 1984.
- [57] L. O. Chua and A. Ushida, "Algorithms for computing almost-periodic steady-state response of nonlinear systems to multiple input frequencies," *IEEE Trans. Circuits Syst.*, vol. CAS-28, pp. 953–971, Oct. 1981.
- [58] M. A. Smith et al., "RF nonlinear device characterization yields improved modeling accuracy," in *1986 IEEE MTT-S Int. Microwave Symp. Dig.* (Baltimore), June 1986, pp. 381–384.
- [59] V. Rizzoli, C. Cecchetti, and A. Neri, "Supercomputer-aided generalized mixer analysis and optimization," in *Proc. 16th European Microwave Conf.* (Dublin), Sept. 1986, pp. 692–697.
- [60] W. R. Curtice, "Nonlinear analysis of GaAs MESFET amplifiers, mixers, and distributed amplifiers using the harmonic balance technique," *IEEE Trans. Microwave Theory Tech.*, vol. MTT-35, pp. 441–447, Apr. 1987.
- [61] V. Rizzoli, C. Cecchetti, and A. Lipparini, "A general-purpose program for the analysis of nonlinear microwave circuits under multitone excitation by multidimensional Fourier transform," in *Proc. 17th European Microwave Conf.* (Rome), Sept. 1987, pp. 635–640.
- [62] G. B. Sorkin, K. S. Kundert, and A. Sangiovanni-Vincentelli, "An almost-periodic Fourier transform for use with harmonic balance," in *1987 IEEE MTT-S Int. Microwave Symp. Dig.* (Las Vegas), June 1987, pp. 717–720.
- [63] R. J. Gilmore and F. J. Rosenbaum, "Modeling of nonlinear distortion in GaAs MESFETS," in *1984 IEEE MTT-S Int. Microwave Symp. Dig.* (San Francisco), June 1984, pp. 430–431.
- [64] J. Dreifuss, A. Madjar, and A. Bar-Lev, "A full large-signal analysis of active microwave mixers," in *Proc. 16th European Microwave Conf.* (Dublin), Sept. 1986, pp. 687–691.
- [65] R. Gilmore, "Nonlinear circuit design using the modified harmonic-balance algorithm," *IEEE Trans. Microwave Theory Tech.*, vol. MTT-34, pp. 1294–1307, Dec. 1986.
- [66] M. Gayral et al., "The spectral balance: A general method for analysis of nonlinear microwave circuits driven by non-harmonically related generators," in *1987 IEEE MTT-S Int. Microwave Symp. Dig.* (Las Vegas), June 1987, pp. 119–121.
- [67] J. J. Bussgang, L. Ehrman, and J. W. Graham, "Analysis of nonlinear systems with multiple inputs," *Proc. IEEE*, vol. 62, pp. 1088–1119, Aug. 1974.
- [68] G. W. Rhyne and M. B. Steer, "Simulation of intermodulation distortion in MESFET circuits with arbitrary frequency separation of tones," in *1986 IEEE MTT-S Int. Microwave Symp. Dig.* (Baltimore), June 1986, pp. 547–550.
- [69] R. G. Sea, "An algebraic formula for amplitudes of intermodulation products involving an arbitrary number of frequencies," *Proc. IEEE*, vol. 56, pp. 1388–1389, Aug. 1968.
- [70] R. G. Sea and A. G. Vacroux, "On the computation of intermodulation products for a power series nonlinearity," *Proc. IEEE*, vol. 57, pp. 337–338, Mar. 1969.
- [71] G. B. Price and P. J. Khan, "Large-signal analysis of semiconductor circuits with multifrequency excitation," *Proc. IEEE*, vol. 67, pp. 177–178, Jan. 1979.
- [72] M. B. Steer and P. J. Khan, "An algebraic formula for the output of a system with large-signal, multifrequency excitation," *Proc. IEEE*, vol. 71, pp. 177–179, Jan. 1983.
- [73] S. Egami, "Nonlinear, linear analysis and computer-aided design of resistive mixers," *IEEE Trans. Microwave Theory Tech.*, vol. MTT-22, pp. 270–275, Mar. 1974.
- [74] D. N. Held and A. R. Kerr, "Conversion loss and noise of microwave and millimeter-wave mixers: Part 1—Theory," *IEEE Trans. Microwave Theory Tech.*, vol. MTT-26, pp. 49–55, Feb. 1978.
- [75] A. R. Kerr, "Noise and loss in balanced and subharmonically pumped mixers: Part 1—Theory," *IEEE Trans. Microwave Theory Tech.*, vol. MTT-27, pp. 938–943, Dec. 1979.
- [76] M. T. Faber and W. K. Gwarek, "Nonlinear-linear analysis of microwave mixers with any number of diodes," *IEEE Trans. Microwave Theory Tech.*, vol. MTT-28, pp. 1174–1181, Nov. 1980.
- [77] S. A. Maas, "Theory and analysis and GaAs MESFET mixers," *IEEE Trans. Microwave Theory Tech.*, vol. MTT-32, pp. 1402–1406, Oct. 1984.
- [78] J. Dreifuss, A. Madjar, and A. Bar-Lev, "A novel method for the analysis of microwave two-port active mixers," *IEEE Trans. Microwave Theory Tech.*, vol. MTT-33, pp. 1241–1244, Nov. 1985.
- [79] J. Dreifuss et al., "Application of the harmonic-balance method to analysis of MESFET oscillators and dual-gate MESFET mixers," in *Proc. 15th European Microwave Conf.* (Paris), Sept. 1985, pp. 521–526.
- [80] V. Rizzoli, C. Cecchetti, and A. Lipparini, "Frequency conversion in general nonlinear multiport devices," in *1986 IEEE MTT-S Int. Microwave Symp. Dig.* (Baltimore), June 1986, pp. 483–486.
- [81] V. Rizzoli et al., "Optimization of nonlinear microwave circuits by a harmonic-balance technique," in *Dig. IEE Colloquium CAD Microwave Circuits* (London), Nov. 1985, pp. 13/1–13/5.
- [82] V. Rizzoli and C. Cecchetti, "Analysis of frequency-conversion effects in nonlinear microwave circuits," in *Proc. 1987 Microwave Symp./Brazil* (Rio de Janeiro), July 1987, pp. 1147–1154.
- [83] S. A. Maas, "Two-tone intermodulation in diode mixers," *IEEE Trans. Microwave Theory Tech.*, vol. MTT-35, pp. 307–314, Mar. 1987.
- [84] J. R. Mosig, "Accurate numerical techniques for characterization of microstrip structures and discontinuities," presented at the Workshop on Present Trends in Microwave CAD, Baltimore, June 5, 1986.
- [85] Y. L. Chow et al., "A modified moment method for the computation of complex MMIC circuits," in *Proc. 16th European Microwave Conf.* (Dublin), Sept. 1986, pp. 625–630.
- [86] G. Ioos and D. D. Joseph, *Elementary Stability and Bifurcation Theory*. New York: Springer-Verlag, 1980.
- [87] K. Kurokawa, "Some basic characteristics of broadband negative-resistance oscillator circuits," *Bell Syst. Tech. J.*, vol. 48, pp. 1937–1955, July–Aug. 1969.
- [88] C. A. Brackett, "Characterization of second-harmonic effects in IMPATT diodes," *Bell Syst. Tech. J.*, vol. 49, pp. 1777–1810, Oct. 1970.
- [89] G. H. B. Hansson and K. J. Lundström, "Stability criteria for phase-locked oscillators," *IEEE Trans. Microwave Theory Tech.*, vol. MTT-20, pp. 641–645, Oct. 1972.
- [90] M. E. Hines, "Large-signal noise, frequency conversion and parametric instabilities in IMPATT diode networks," *Proc. IEEE*, vol. 60, pp. 1534–1548, Dec. 1972.
- [91] J. Gonda and W. E. Schroeder, "IMPATT diode circuit design for parametric stability," *IEEE Trans. Microwave Theory Tech.*, vol. MTT-23, pp. 343–352, May 1977.
- [92] R. Knöchel, "Unified large-signal stability and noise theory for synchronized oscillators," in *Proc. Inst. Elec. Eng.*, pt. H, vol. 128, pp. 137–145, June 1981.
- [93] E. F. Calandra and A. M. Sommariva, "Stability analysis of injection locked oscillators in their fundamental mode of operation," *IEEE Trans. Microwave Theory Tech.*, vol. MTT-29, pp. 1137–1144, Nov. 1981.
- [94] V. Rizzoli and A. Lipparini, "General stability analysis of periodic steady-state regimes in nonlinear microwave circuits," *IEEE Trans. Microwave Theory Tech.*, vol. MTT-33, pp. 30–37, Jan. 1985.

- [95] A. I. Mees, "Limit cycle stability," *Journal I.M.A.*, vol. 11, pp. 281-295, 1973.
- [96] D. J. Allwright, "Harmonic balance and the Hopf bifurcation," *Math. Proc. Camb. Phil. Soc.*, vol. 82, pp. 453-467, 1977.
- [97] J. J. Di Stefano, A. R. Stublerud, and I. J. Williams, *Feedback and Control Systems*. Los Angeles: McGraw-Hill, 1967.
- [98] V. Rizzoli and A. Neri, "Global stability analysis of microwave circuits by a frequency-domain approach," in *1987 IEEE MTT-S Int. Microwave Symp. Dig.* (Las Vegas), June 1987, pp. 689-692.
- [99] H. Kawakami, "Bifurcation of periodic responses in forced dynamic nonlinear circuits: Computation of bifurcation values of the system parameters," *IEEE Trans. Circuits Syst.*, vol. CAS-31, pp. 248-260, Mar. 1984.
- [100] A. I. Mees and L. O. Chua, "The Hopf bifurcation theorem and its applications to nonlinear oscillations in circuits and systems," *IEEE Trans. Circuits Syst.*, vol. CAS-26, pp. 235-254, Apr. 1979.
- [101] M. I. Sobhy *et al.*, "The design of microwave monolithic voltage-controlled oscillators," in *Proc. 15th European Microwave Conf.* (Paris), Sept. 1985, pp. 925-930.
- [102] K. Kurokawa, "Noise in synchronized oscillators," *IEEE Trans. Microwave Theory Tech.*, vol. MTT-16, pp. 234-240, Apr. 1968.
- [103] R. D. Kuvärs, "Nonlinear noise theory for IMPATT diodes," *IEEE Trans. Electron Devices*, vol. ED-23, pp. 395-411, 1976.
- [104] K. F. Schunemann and K. Behm, "Nonlinear noise theory for synchronized oscillators," *IEEE Trans. Microwave Theory Tech.*, vol. MTT-27, pp. 452-458, May 1979.
- [105] R. A. Puel and J. Curtis, "Near-carrier noise in FET oscillators," in *1983 IEEE MTT-S Int. Microwave Symp. Dig.* (Boston), June 1983, pp. 282-284.
- [106] B. T. Debney and J. S. Joshi, "A theory of noise in GaAs FET microwave oscillators and its experimental verification," *IEEE Trans. Electron Devices*, vol. ED-30, pp. 769-776, July 1983.
- [107] G. K. Tie and C. S. Aitchinson, "Noise figure and associated conversion gain of a microwave MESFET gate mixer," in *Proc. 13th European Microwave Conf.* (Nürnberg), Sept. 1983, pp. 579-584.
- [108] H. Rohdin, C. Yi, and C. Stolte, "A study of the relation between device low-frequency noise and oscillator phase noise for GaAs MESFETs," in *1984 IEEE MTT-S Int. Microwave Symp. Dig.* (San Francisco), June 1984, pp. 267-269.
- [109] B. Villeneuve *et al.*, "RF spectrum of thermal noise and frequency stability of a microwave cavity-oscillator," *IEEE Trans. Microwave Theory Tech.*, vol. MTT-32, pp. 1565-1572, Dec. 1984.
- [110] H. J. Siveris and B. Schiek, "Analysis of noise upconversion in microwave FET oscillators," *IEEE Trans. Microwave Theory Tech.*, vol. MTT-33, pp. 233-242, Mar. 1985.
- [111] H. J. Siveris and B. Schiek, "A GaAs FET oscillator noise model with a periodically driven noise source," in *Proc. 16th European Microwave Conf.* (Dublin), Sept. 1986, pp. 681-686.
- [112] J. M. Bunting, M. J. Howes, and J. R. Richardson, "Large-signal time-domain modelling of noise in the design of MESFET oscillators," in *Proc. 16th European Microwave Conf.* (Dublin), Sept. 1986, pp. 201-206.
- [113] C. Dragone, "Analysis of thermal and shot noise in pumped resistive diodes," *Bell. Syst. Tech. J.*, vol. 47, pp. 1883-1902, Nov. 1968.
- [114] V. Rizzoli and A. Lipparini, "Computer-aided noise analysis of linear multiport networks of arbitrary topology," *IEEE Trans. Microwave Theory Tech.*, vol. MTT-33, pp. 1507-1512, Dec. 1985.
- [115] H. Fukui, Ed., *Low-Noise Microwave Transistors & Amplifiers*. New York: IEEE Press, 1981.
- [116] K. Hwang, Ed., *Supercomputers: Design and Applications*. Silver Spring, MD: IEEE Computer Society Press, 1984.
- [117] J. T. Devreese and P. Van Camp, Eds., *Supercomputers in Theoretical and Experimental Science*. New York: Plenum Press, 1985.
- [118] K. Hwang *et al.*, "Vector computer architecture and processing techniques," *Advances in Comput.*, vol. 20, pp. 115-197.
- [119] R. W. Hockney and C. R. Jesshope, *Parallel Computers*. Bristol: Adam Hilger Ltd., 1981.
- [120] L. Nelson and P. Rigsbee, "Multitasking at Cray," *CRAY CHANNELS*, vol. 7, pp. 12-15, Summer 1985.
- [121] M. Booth and K. Misegades, "Microtasking: A new way to harness multiprocessors," *CRAY CHANNELS*, vol. 8, pp. 24-27, Summer 1986.
- [122] V. Rizzoli and M. Ferlito, "Vector processing concepts in microwave circuit design," in *Proc. 14th European Microwave Conf.* (Liège), Sept. 1984, pp. 847-852.
- [123] V. Rizzoli, M. Ferlito, and A. Neri, "Vectorized program architectures for supercomputer-aided circuit design," *IEEE Trans. Microwave Theory Tech.*, vol. MTT-34, pp. 135-141, Jan. 1986.

†

**Vittorio Rizzoli** (M'79) was born in Bologna, Italy, in 1949. He graduated from the School of Engineering, University of Bologna, in July 1971.



From 1971 to 1973, he was with the Centro Onde Millimetriche of Fondazione Ugo Bordoni, Pontecchio Marconi, Italy, where he was involved in research on millimeter-waveguide communication systems. In 1973, he was with the Hewlett-Packard Company, Palo Alto, CA, working in the areas of MIC and microwave power devices. From 1974 to 1979, he was an Associate Professor at the University of Bologna, teaching a course on microwave integrated circuits. In 1980, he joined the University of Bologna as a full Professor of Electromagnetic Fields and Circuits. His current research interests are in the fields of MIC and MMIC, with special emphasis on nonlinear circuits. He is also heading a research project aimed at the development of vectorized software for microwave circuit design applications.

‡

**Andrea Neri** was born in Bologna, Italy, in 1957. He graduated in electronic engineering from the University of Bologna in July 1981.



In 1983 and 1984, he obtained research grants issued by Fondazione G. Marconi, Pontecchio Marconi, Italy, and Selenia S.p.A., Rome, Italy, to work on dielectric resonators and their applications in MIC. In 1985, he joined Fondazione U. Bordoni, Rome, Italy, where he is currently involved in research on nonlinear microwave circuit design. His main fields of interest are the characterization of microwave components by means of electromagnetic methods and the application of supercomputers in MIC and MMIC design.

# The Basic Concept

As the non-linear elements are still modeled in time domain, the circuit first must be separated into a linear and a non-linear part. The internal impedances  $Z_i$  of the voltage sources are put into the linear part as well. Figure 7.1 illustrates the concept. Let us define the following symbols:

- M = number of (independent) voltage sources
- N = number of connections between linear and non-linear subcircuit
- K = number of calculated harmonics
- L = number of nodes in linear subcircuit

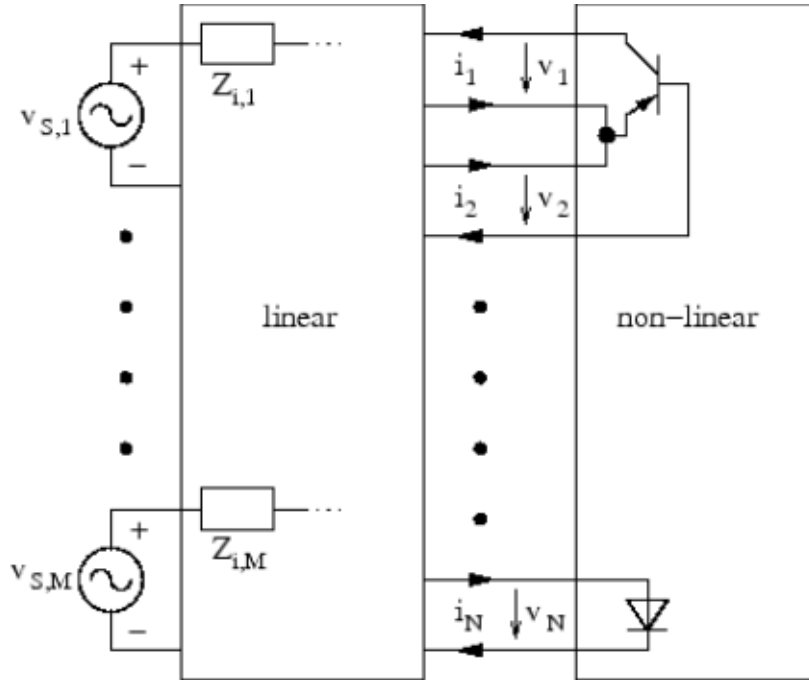


**Figure 7.1:** circuit partitioning in harmonic balance

The linear circuit is modeled by two transadmittance matrices: The first one  $\bar{Y}$  relates the source voltages  $v_{S,1} \dots v_{S,M}$  to the interconnection currents  $i_1 \dots i_N$  and the second one  $\hat{Y}$  relates the interconnection voltages  $v_1 \dots v_N$  to the interconnection currents  $i_1 \dots i_N$ . Taking both, we can express the current flowing through the interconnections between linear and non-linear subcircuit:

$$\mathbf{I} = \bar{Y}_{N \times M} \cdot \mathbf{V}_S + \hat{Y}_{N \times N} \cdot \mathbf{V} = \mathbf{I}_S + \hat{Y} \cdot \mathbf{V} \quad (7.1)$$

Because  $\mathbf{V}_S$  is known and constant, the first term can already be computed to give  $\mathbf{I}_S$ . Taking the whole linear network as one block is called the "piecewise" harmonic balance technique.

The non-linear circuit is modeled by its current function  $i(t) = f_g(v_1, \dots, v_P)$  and by the charge of its capacitances  $q(t) = f_q(v_1, \dots, v_Q)$ . These functions must be Fourier-transformed to give the frequency-domain vectors  $\mathbf{Q}$  and  $\mathbf{I}_G$ , respectively.

A simulation result is found if the currents through the interconnections are the same for the linear and the non-linear subcircuit. This principle actually gave the harmonic balance simulation its name, because through the interconnections the currents of the linear and non-linear subcircuits have to be *balanced* at every *harmonic* frequency. To be precise the described method is called Kirchhoff's current law harmonic balance (KCL-HB). Theoretically, it would also be possible to use an algorithm that tries to balance the voltages at the subcircuit interconnections. But then the Z matrix (linear subcircuit) and current-dependend voltage laws (non-linear subcircuit) have to be used. That doesn't fit the need (see other simulation types).

So, the non-linear equation system that needs to be solved writes:

$$\mathbf{F}(\mathbf{V}) = \underbrace{(\mathbf{I}_S) + (\hat{\mathbf{Y}}) \cdot (\mathbf{V})}_{\text{linear}} + \underbrace{j \cdot \boldsymbol{\Omega} \cdot \mathbf{Q} + \mathbf{I}_G}_{\text{non-linear}} = \mathbf{0} \quad (7.2)$$

where matrix  $\boldsymbol{\Omega}$  contains the angular frequencies on the first main diagonal and zeros anywhere else,  $\mathbf{0}$  is the zero vector.

After each iteration step, the inverse Fourier transformation must be applied to the voltage vector  $\mathbf{V}$ . Then the time domain voltages  $v_{0,1} \dots v_{K,N}$  are put into  $i(t) = f_g(v_1, \dots, v_P)$  and  $q(t) = f_q(v_1, \dots, v_Q)$  again. Now, a Fourier transformation gives the vectors  $\mathbf{Q}$  and  $\mathbf{I}_G$  for the next iteration step. After repeating this several times, a simulation result has hopefully be found.

Having found this result means having got the voltages  $v_1 \dots v_N$  at the interconnections of the two subcircuits. With these values the voltages at all nodes can be calculated: Forget about the non-linear subcircuit, put current sources at the former interconnections (using the calculated values) and perform a normal AC simulation. After that the simulation is complete.

A short note to the construction of the quantities: One big difference between the HB and the conventional simulation types like a DC or an AC simulation is the structure of the matrices and vectors. A vector used in a conventional simulation contains one value for each node. In an HB simulation there are many harmonics and thus, a vector contains  $K$  values for each node. This means that within a matrix, there is a  $K \times K$  diagonal submatrix for each node. Using this structure, all equations can be written in the usual way, i.e. without paying attention to the special matrix and vector structure. In a computer program, however, a special matrix class is needed in order to not waste memory for the off-diagonal zeros.

[Next: Going through each Step](#) [Up: Harmonic Balance Analysis](#) [Previous: Harmonic Balance Analysis](#)

This document was generated by Stefan Jahn on 2007-12-30 using [latex2html](#).

# Harmonic Balance Simulation on ADS

## ***General Description of Harmonic Balance in Agilent ADS<sup>1</sup>***

Harmonic balance is a frequency-domain analysis technique for simulating nonlinear circuits and systems. It is well-suited for simulating analog RF and microwave circuits, since these are most naturally handled in the frequency domain. Circuits that are best analyzed using HB under large signal conditions are:

- ❖ power amplifiers
- ❖ frequency multipliers
- ❖ mixers
- ❖ oscillators
- ❖ modulators

Harmonic Balance Simulation calculates the magnitude and phase of voltages or currents in a potentially nonlinear circuit. Use this technique to:

- ❖ Compute quantities such as P1dB, third-order intercept (TOI) points, total harmonic distortion (THD), and intermodulation distortion components
- ❖ Perform power amplifier load-pull contour analyses
- ❖ Perform nonlinear noise analysis
- ❖ Simulate oscillator harmonics, phase noise, and amplitude limits

In contrast, S-parameter or AC simulation modes do not provide any information on nonlinearities of circuits. Transient analysis, in the case where there are harmonics and or closely-spaced frequencies, is very time and memory consuming since the minimum time step must be compatible with the highest frequency present while the simulation must be run for long enough to observe one full period of the lowest frequency present.

Harmonic balance simulation makes possible the simulation of circuits with multiple input frequencies. This includes intermodulation frequencies, harmonics, and frequency conversion between harmonics. Not only can the circuit itself produce harmonics, but each signal source (stimulus) can also produce harmonics or small-signal sidebands. The stimulus can consist of up to twelve nonharmonically related sources. The total number of frequencies in the system is limited only by such practical considerations as memory, swap space, and simulation speed.

## ***The Simulation Process<sup>1</sup> (FYI – skip to next section if you want to get started now)***

The harmonic balance method is iterative. It is based on the assumption that for a given sinusoidal excitation there exists a steady-state solution that can be approximated to satisfactory accuracy by means of a finite Fourier series. Consequently, the circuit node

---

<sup>1</sup> From Agilent ADS Circuit Simulation Manual, Chap. 7, Harmonic Balance.

voltages take on a set of amplitudes and phases for all frequency components. The currents flowing from nodes into linear elements, including all distributed elements, are calculated by means of a straightforward frequency-domain linear analysis. Currents from nodes into nonlinear elements are calculated in the time-domain. Generalized Fourier analysis is used to transform from the time-domain to the frequency-domain.

A frequency-domain representation of all currents flowing away from all nodes is available. According to Kirchoff's Current Law (KCL), these currents should sum to zero at all nodes. The probability of obtaining this result on the first iteration is extremely small.

Therefore, an error function is formulated by calculating the sum of currents at all nodes. This error function is a measure of the amount by which KCL is violated and is used to adjust the voltage amplitudes and phases. If the method converges (that is, if the error function is driven to a given small value), then the resulting voltage amplitudes and phases approximate the steady-state solution.

- Designers are usually most interested in a system's steady-state behavior. Many high-frequency circuits contain long time constants that require conventional transient methods to integrate over many periods of the lowest-frequency sinusoid to reach steady state. Harmonic balance, on the other hand, captures the steady-state spectral response directly.
- The applied voltage sources are typically multitone sinusoids that may have very narrowly or very widely spaced frequencies. It is not uncommon for the highest frequency present in the response to be many orders of magnitude greater than the lowest frequency. Transient analysis would require an integration over an enormous number of periods of the highest-frequency sinusoid. The time involved in carrying out the integration is prohibitive in many practical cases.
- At high frequencies, many linear models are best represented in the frequency domain. Simulating such elements in the time domain by means of convolution can result in problems related to accuracy, causality, or stability.

## **Harmonic Balance Setup**

The HB method depends on calculating currents and voltages at many harmonically related frequencies for each fundamental signal under consideration. Since we are interested in the steady state solution of a nonlinear problem, we must allow the HB simulator to use enough harmonics so that a Fourier series constructed from these harmonic amplitudes and phases can reproduce a reasonable replica of the time domain solution.

Figure 1 illustrates a very basic HB simulation setup. The Harmonic Balance controller specifies several key simulation parameters. In the example below, one fundamental frequency,  $\text{Freq}[1]=450 \text{ MHz}$ , is specified as an input. The index [1] shows that only one fundamental frequency is being considered. Order[1] specifies the number of harmonic frequencies to be calculated (15) for the first (and only) frequency in this case. One of

the most common errors in HB simulation setup is to use too low of an order. You can determine what order is optimum if you first simulate your circuit with a small order then increase the order in steps of 1 or 2 harmonics. When the solution stops changing within a significant bound, you have reached the optimum order. Using too high of an order is wasteful of memory, file size and simulation time, so it is not efficient to just clobber the problem with a very high order. Some user discretion is advised.

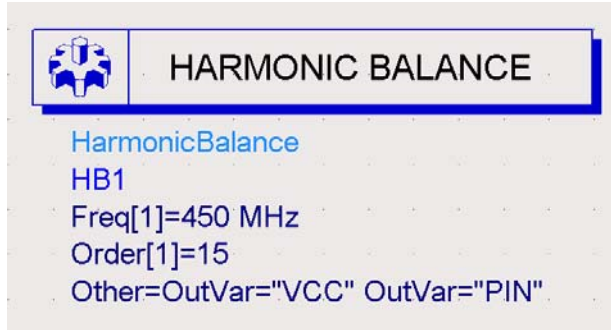


Figure 1. Example of the HB controller used for a very simple single tone (frequency) simulation.

Other=OutVar is used to pass parameters from the schematic to the display panel. Calculated node voltages are automatically transferred, but the input parameters used for independent voltage, current or power sources are not (unless they are being swept by a sweep controller setting). Then they become a parameter that is automatically passed to the display.).

The fundamental frequency of the input source must be the same as specified on the controller. The *Sources-Freq Domain* palette includes many sources suitable for use with HB. The single tone source *P\_1Tone* is illustrated below. This source provides a single frequency sinusoid at a specified available power. Here we see that the internal source resistance (50 ohms) is included. The available source power is provided as PIN (in dBm, which will be converted to Watts by the dbmtow function) and degrees of phase.



Figure 2. Single frequency source. Frequency, source impedance, and available power must be specified.

You could also have selected a voltage source,  $V\_ITone$ , or for multiple frequency simulations, there are  $V\_nTone$  and  $P\_nTone$  sources. These are often used for intermodulation distortion simulations. Voltage or current sources require an external source resistance or impedance whereas the power sources include an internal source resistance or impedance,  $Z$ .

Nodes must be labeled in the harmonic balance simulation in order to transfer their voltages to the display. If currents are to be used in calculations as well, a current probe must be inserted from the *Probe Components* menu. An example of a PA output network is shown in the next figure. Nodes Vce and Vload are labeled using the Insert pulldown menu: *Insert > Wire/Pin Label*. This opens a text box where you can enter the node name you want.  $I_{ce}$  and  $I_{load}$  were measured with the current probes as shown.

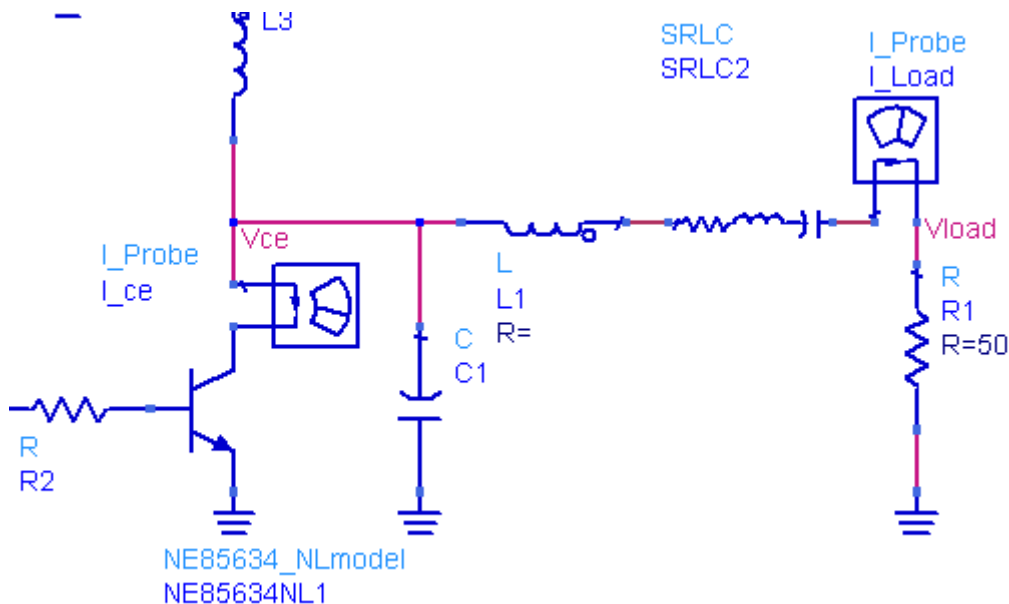


Figure 3. PA output circuit showing node voltage and current labels and probes.

## ***Displaying results***

The output voltages and currents calculated by the HB analysis will contain many frequency components. You can display all of them in a spectral display by just plotting the voltage or current on an X-Y plot. Markers can be used to read out the spectral line amplitudes or powers.

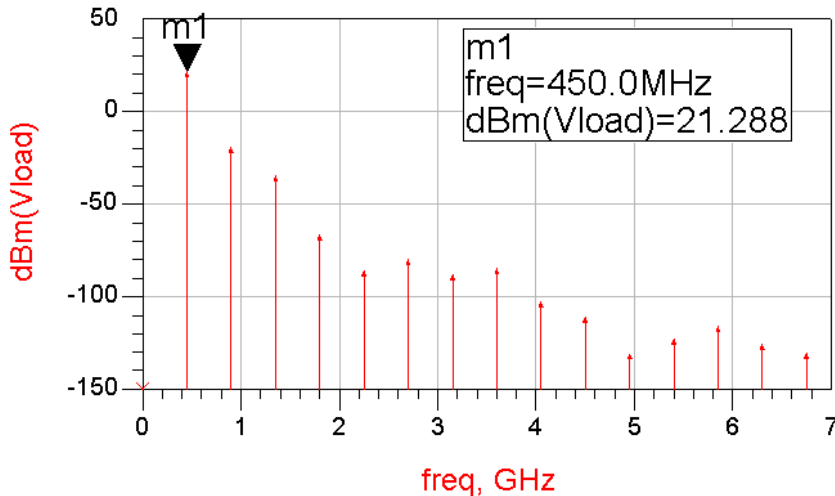


Figure 4. Spectrum in dBm is plotted for Vload. You can see the 15 harmonics.

Often you will want to plot power in dBm. If your load impedance is real, you can use the dbm function in an equation. If the load has a complex impedance, then use the definition for sinusoidal power.

$$P_{out\_dBm} = 10 * \log(0.5 * real(Vload * conj(I\_load.i))) + 30$$

This will give you the power in dBm in all cases. This is the preferred method. Note that calculated quantities much below – 100 dBm are probably not very reliable due to the limited precision of the device models

To perform calculations of power and efficiency, you will want to be able to select specific frequency components. The harmonic index (harmindex) can be used to do this. If you plot your output variable in a table format, you will see a list of frequencies.

freq	Pout	Pout_dBm
0.0000 Hz	0.0000	<invalid>
450.0MHz	134.5m	21.29
900.0MHz	11.47u	-19.41
1.350GHz	336.8n	-34.73
1.800GHz	219.8p	-66.58
2.250GHz	2.250p	-86.48
2.700GHz	9.389p	-80.27
3.150GHz	1.465p	-88.34

Figure 5. Table showing the value of Pout and Pout\_dBm at several harmonic frequencies. The frequencies are printed in order and can be designated by an index, ranging from 0 for DC to Order – 1 for the highest harmonic frequency.

The first frequency in the table is DC and has index 0. Fundamental is index 1. So, to select the voltage at the fundamental frequency, for example, you could write Vload[1] or to select power, Pout[1] or Pout\_dBm[1] in this example. The second harmonic would be

$\text{Pout}[2]$ . Of course, we do not need to draw a table to use the index. For example, the DC component of the power supply voltage can be extracted by using the 0 index:  $\text{VCC}[0]$ . Then, if the supply voltage and current were measured and passed to the output display, you could calculate DC input power by

$$\text{Eqn P\_DC} = \text{real}(\text{VCC}[0] * \text{I\_DC.i}[0])$$

To display the results of equations such as this, you use the table or rectangular plot features in the display panel. The data set must be changed to Equations as shown in order to find the result of the calculations.

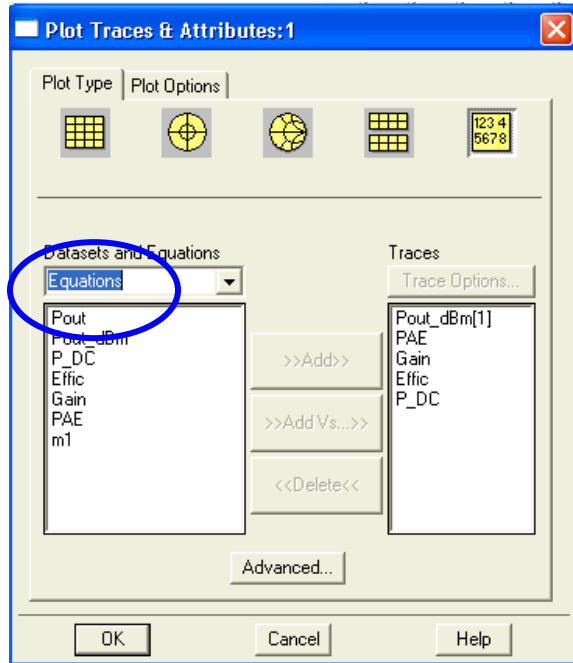


Figure 6. To plot the results of an equation in the data display, select Equations in the data set

If you want to see the time domain version of a voltage or current, the display can perform the inverse Fourier transform while plotting. Select the Time domain signal option.

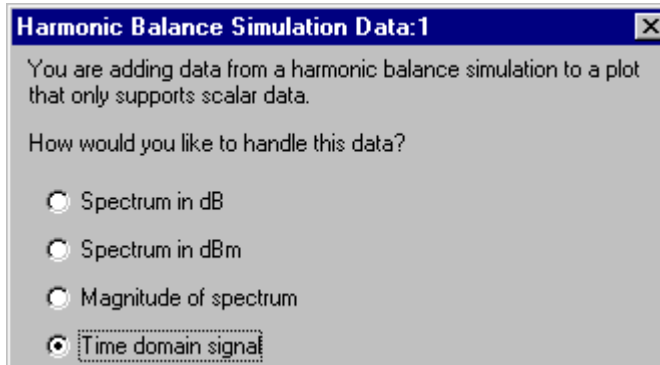


Figure 7. When plotting HB data, you must convert it to a scalar quantity (dB, dBm, or magnitude). Notice that a time domain conversion can also be performed by an FFT if requested.

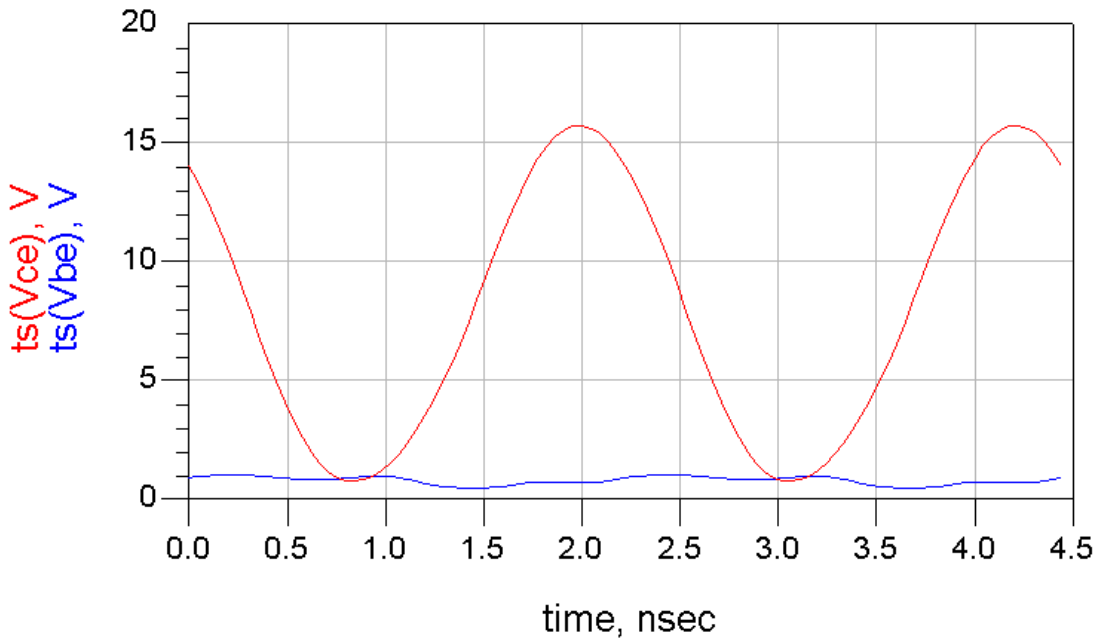


Figure 8. Example of a time domain plot from a HB simulation.

Once the simulation has been run, the data is available on the display panel. You can use equations to calculate power, gain, and power added efficiency. Note the use of the indices once again.

$$\begin{array}{lll} \text{Eqn } P_{\text{out}}=0.5*\text{real}(V_{\text{load}}*\text{conj}(I_{\text{Load}}.i)) & \text{Eqn } P_{\text{out\_dBm}}=10*\log(P_{\text{out}})+30 & \text{Eqn } P_{\text{DC}}=\text{real}(V_{\text{CC}}[0]*I_{\text{DC}}.i[0]) \\ \text{Eqn } \text{Gain}=P_{\text{out\_dBm}}[1]-\text{PIN} & \text{Eqn } \text{PAE}=(P_{\text{out}}[1]-\text{dbmton}(P_{\text{IN}}))/P_{\text{DC}} & \text{Eqn } \text{Effic}=\text{mag}(P_{\text{out}}[1])/P_{\text{DC}} \end{array}$$

### **Parameter Sweeps**

It is possible to sweep any of the independent parameters in the HB simulation. To set up the sweep, double click on the Harmonic Balance Controller.

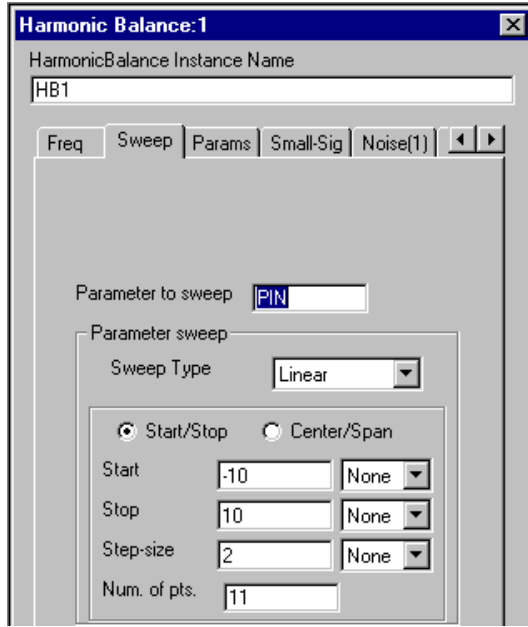


Figure 9. Selecting the Sweep tab allows you to sweep one independent variable.

Click on the Sweep tab. Choose the parameter to be swept, the sweep type (Linear, Log), and the Start, Stop, and Step variables (or number of points instead of step-size). In this example, we are sweeping the input power to the amplifier to determine the gain compression behavior. The more sweep points chosen, the longer the simulation time and the greater the data file size.<sup>2</sup>



Figure 10. A double axis plot of Pout vs Pin and PAE vs. Pin for a power amplifier.

---

<sup>2</sup> If two variables are to be swept, a ParamSweep controller icon from the HB menu must be added to the schematic.

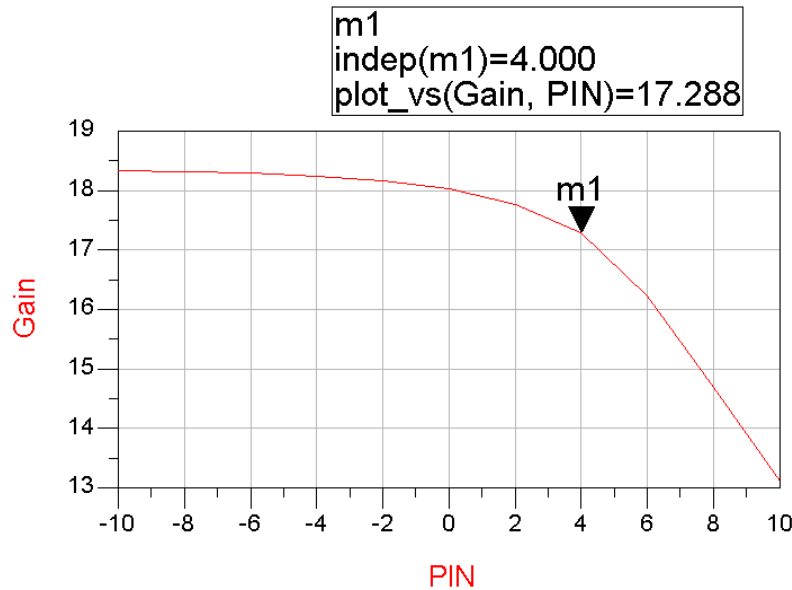


Figure 11. Amplifier gain vs. Pin.

From this plot, we can see that the  $P_{1\text{dB}}$  compression input power is about 4 dBm.

### **Multiple frequency simulations**

Multiple frequencies or “tones” (mainly two-tone) are widely used for evaluation of intermodulation distortion in amplifiers or mixers. In fig. 12, you can see that now two frequencies have been selected, Freq[1] and Freq[2]. Each frequency must also declare an order (number of harmonic frequencies to be considered).

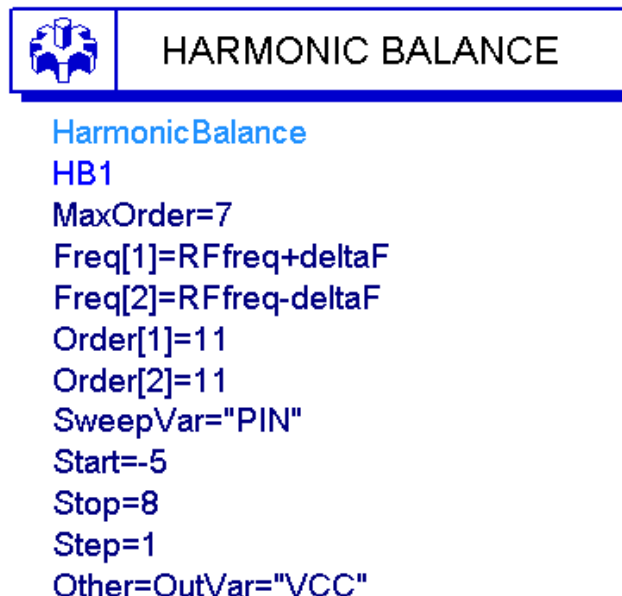


Figure 12. HB controller example for a two-tone PA simulation.

Intermodulation distortion occurs when more than one input frequency is present in the circuit under evaluation. Therefore, additional frequencies need to be specified when setting up for this type of simulation. Two-tone simulations are generally performed with two closely spaced input frequencies. In this example, the two inputs are at 449.8 and 450.2 MHz. The frequency spacing must be small enough that the two tones are well within the signal bandwidth of the circuit under test.

Maximum order corresponds to the highest order mixing product ( $n + m$ ) to be considered ( $n * \text{freq}[1] \pm m * \text{freq}[2]$ ). There will be a frequency component in the output file corresponding to all possible combinations of  $n$  and  $m$  up to the *MaxOrder* limit. The simulation will run faster with lower *MaxOrder* and fewer harmonics of the sources, but may be less accurate. Often accurate IMD simulations will require a large maximum order. In this case, a larger number of spectral products will be summed to estimate the time domain waveform and therefore provide greater accuracy. This will increase the size of the data file and time required for the simulation. Increase the orders and *MaxOrder* in increments of 2 and watch for changes in the IMD output power. When no further significant change is observed, then the order is large enough. If large asymmetry is noted in the intermodulation components, higher orders are indicated.

Sometimes, increasing the *oversampling ratio* for the FFT calculation (use the *Param* menu of the HB controller panel) can reduce errors. This oversampling controls the number of time points taken when converting back from time to frequency domain in the harmonic balance simulation algorithm. A larger number of time samples increases the accuracy of the transform calculation but increases memory requirements and simulation time. Both order and oversampling should be increased until you are convinced that further increases are not worthwhile.

For multiple frequency simulations, the simulation time will be reduced substantially by using the Krylov option which can be selected on the *Display* tab of the HB controller.

The two tone source frequencies are provided with a *P\_nTone* generator from the Sources – Freq Domain menu. The two frequencies are sometimes specified in a *Var* block. The same approach is used to specify frequencies in the HB controller so that the effect caused by changes in *deltaF* could be evaluated by changing only one variable. The available power, *PIN*, is specified in dBm for each source frequency.



Figure 13. Two-tone source example.

## Displaying Results of Multitone Simulations

You can view the result around the fundamental frequencies by disabling the autoscale function in the plot and specifying your own narrow range. The display below shows intermodulation products up to the 7<sup>th</sup> order (MaxOrder specified on the HB controller).

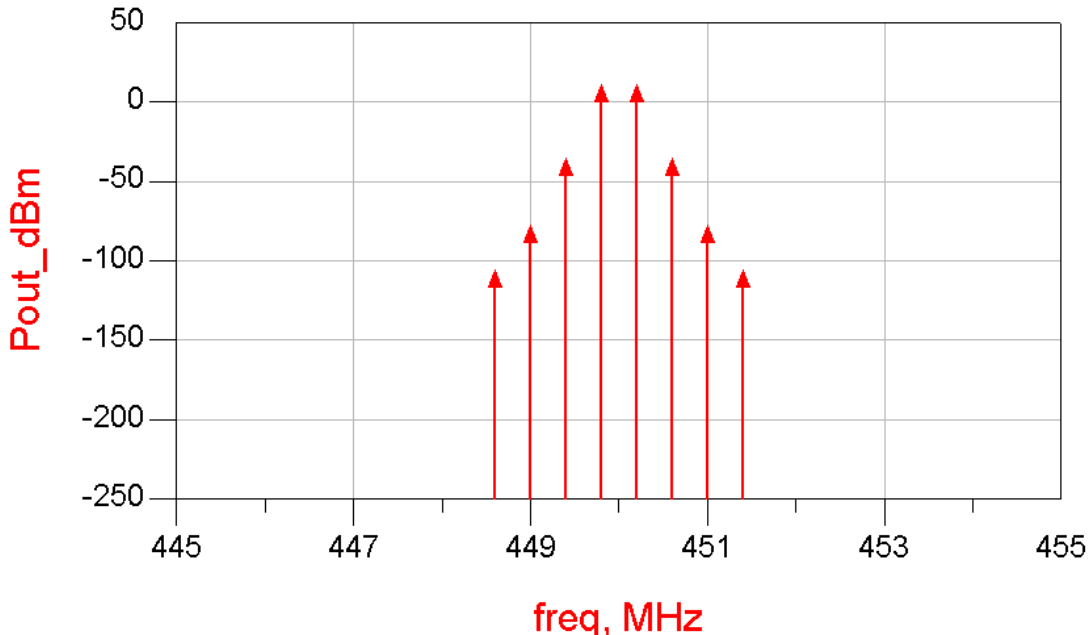


Fig. 14.

We would like to study the output voltage at the fundamental frequencies and the third-order IMD product frequencies. This can be selected from the many frequencies in the output data set by using the *mix* function. The desired frequencies could be selected by:

$$\begin{array}{ll} (\text{RFfreq} + \text{deltaF}) & \text{Vfund1} = \text{mix}(\text{Vload}, \{1,0\}) \\ (\text{RFfreq} - \text{deltaF}) & \text{Vfund2} = \text{mix}(\text{Vload}, \{0,1\}) \\ (2*(\text{RFfreq} + \text{deltaF}) - \text{RFfreq} - \text{deltaF}) & \text{VIM1} = \text{mix}(\text{Vload}, \{2,-1\}) \\ (2*(\text{RFfreq} - \text{deltaF}) - \text{RFfreq} + \text{deltaF}) & \text{VIM2} = \text{mix}(\text{Vload}, \{-1,2\}) \end{array}$$

The respective indices used with the mix function to select this frequency are shown to the right. The indices in the curly brackets are ordered according to the HB fundamental analysis frequencies.

## Mixer Simulations

In the case of a mixer simulation, at least 2 frequencies are always needed: LO and RF. Figure 16 shows an example of the setup used for a two-tone simulation of a mixer. The format is similar to that described above for power amplifier two tone simulations except now 3 frequencies are required. The frequency with the highest power level (in this

example, the LO) is always the first frequency to be designated in the harmonic balance controller. Other inputs follow sequencing from highest to lowest power.

```

SIMULATION CONTROL
HARMONIC BALANCE
HB2
MaxOrder=11
Freq[1]=LOfreq
Freq[2]=RFfreq+Fspacing/2
Freq[3]=RFfreq-Fspacing/2
Order[1]=9
Order[2]=3
Order[3]=3
Oversample[1]=1
Oversample[2]=1
Oversample[3]=1
UseKrylov=yes

```

Increase the LO order and max order until there are no significant changes in the IMD power predictions.  
Oversampling can also be increased as needed.

Figure 16. HB controller example for a mixer simulation.

The harmonic order should be higher for high amplitude signals. For the example above, the LO order is highest because it is intended to switch the mixer. The RF orders can be smaller since they are rarely of high amplitude compared with the LO.

In the case of a mixer simulation, we would like to study the output voltage at the IF frequency. This must be selected from many frequencies in the output data set. A particular frequency is selected by using the *mix* function. In this example, the desired IF frequencies could be:

$\text{LOfreq} - (\text{RFfreq} + \text{Fspacing}/2)$	$\text{VIF} = \text{mix}(\text{Vout}, \{1, -1, 0\})$ .
$\text{LOfreq} - (\text{RFfreq} - \text{Fspacing}/2)$	$\text{VIF} = \text{mix}(\text{Vout}, \{1, 0, -1\})$
$\text{LOfreq} + (\text{RFfreq} + \text{Fspacing}/2)$	$\text{VIF} = \text{mix}(\text{Vout}, \{1, 1, 0\})$
$\text{LOfreq} + (\text{RFfreq} - \text{Fspacing}/2)$	$\text{VIF} = \text{mix}(\text{Vout}, \{1, 0, 1\})$

and the respective indices used with the mix function to select this frequency are shown to the right. The indices in the curly brackets are ordered according to the HB fundamental analysis frequencies. Thus,  $\{1, -1, 0\}$  selects  $1*\text{LOfreq} - 1*\text{RFfreq}[1] + 0*\text{RFfreq}[2]$ .

## ***DesignGuides***

There are so many types of simulations that could be performed on a mixer that it is not reasonable to try to describe them all in this tutorial. Instead, you can use the Mixer DesignGuide, a set of schematic and display templates that can be pulled into your project file. Go to the DesignGuides pulldown menu and select Mixer DesignGuide. Choose a representative sample mixer schematic to modify if you want to create your own mixer circuit. Determine whether your mixer is single ended or differential. The differential circuit templates include baluns; single-ended do not. Choose from a large set of simulation types, some with parameter sweeps, some without.

Refer to the Mixer Design Guide tutorial for more information.

## ***Convergence Woes***

Any user of the harmonic balance simulator will eventually encounter convergence problems. Unfortunately, when this happens, no useful information is provided by the simulator. Problems with convergence generally arise when the circuit under simulation is or becomes highly nonlinear. In the case of mixers, there are inherent nonlinearities that are required for the mixing process, but these are usually not so bad unless you are seriously overdriving one of the inputs. If the simulation fails, check the biasing of the transistors. HB doesn't do well with BJTs driven into their saturation region. If that is not the problem, then try decreasing either LO power or the RF power sweep range. You may be driving the mixer well beyond saturation when using default power levels in mixer DG templates. As a last resort, you can try using the Direct solver rather than Krylov, but this will increase simulation time by a large factor.

## Harmonic Balance Basics

[http://www.ece.uci.edu/eceware/ads\\_docs/cktsimhb/ckhb014.html#1104539](http://www.ece.uci.edu/eceware/ads_docs/cktsimhb/ckhb014.html#1104539)

### The Simulation Process

The harmonic balance method is iterative. It is based on the assumption that for a given sinusoidal excitation there exists a steady-state solution that can be approximated to satisfactory accuracy by means of a finite Fourier series. Consequently, the circuit node voltages take on a set of amplitudes and phases for all frequency components. The currents flowing from nodes into linear elements, including all distributed elements, are calculated by means of a straightforward frequency-domain linear analysis. Currents from nodes into nonlinear elements are calculated in the time-domain. Generalized Fourier analysis is used to transform from the time-domain to the frequency-domain.

The Harmonic Balance solution is approximated by truncated Fourier series and this method is inherently incapable of representing transient behavior. The time-derivative can be computed exactly with boundary conditions,  $v(0)=v(t)$ , automatically satisfied for all iterates. The truncated Fourier approximation + N circuit equations results in a residual function that is minimized.

N x M nonlinear algebraic equations are solved for the Fourier coefficients using Newton's method and the inner linear problem is solved by:

- Direct method (Gaussian elimination) for small problems.
- Krylov-subspace method (e.g. GMRES) for larger problems.

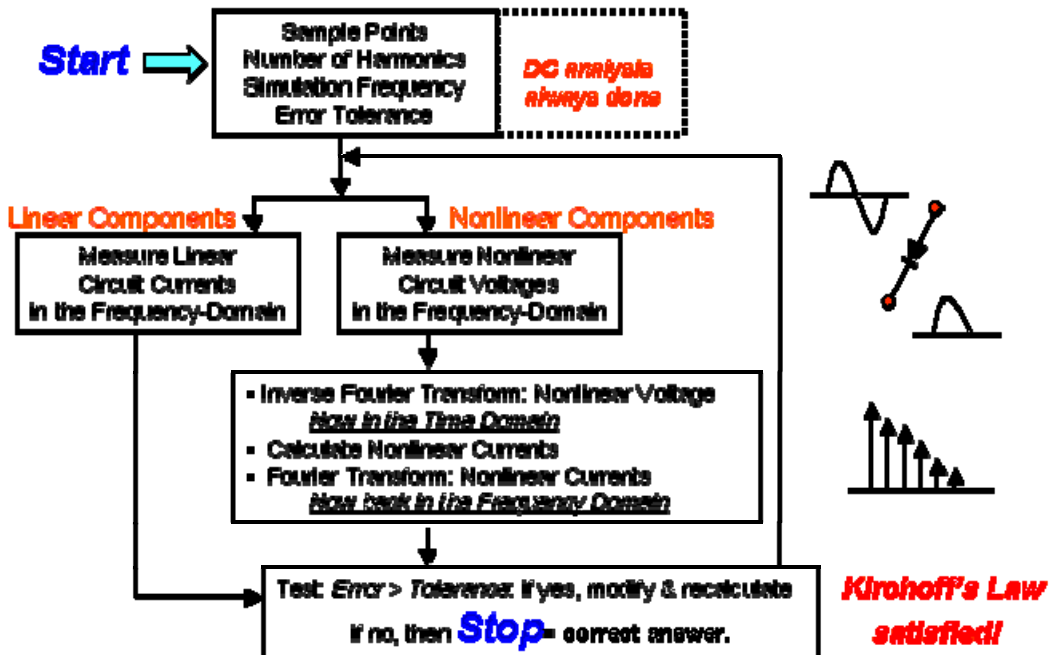
Nonlinear devices (transistors, diodes, etc.) in Harmonic Balance are evaluated (sampled) in the time-domain and converted to frequency-domain via the FFT.

A frequency-domain representation of all currents flowing away from all nodes is available. According to Kirchoff's Current Law (KCL), these currents should sum to zero at all nodes. The probability of obtaining this result on the first iteration is extremely small.

Therefore, an error function is formulated by calculating the sum of currents at all nodes. This error function is a measure of the amount by which KCL is violated and is used to adjust the voltage amplitudes and phases. If the method converges (that is, if the error function is driven to a given small value), then the resulting voltage amplitudes and

phases approximate the steady-state solution. The following flow chart presents a visual representation of the process:

## Harmonic Balance Simulation Flow Chart



### Comparing Harmonic Balance and Time Domain Simulators

In the context of high-frequency circuit and system simulation, harmonic balance has a number of advantages over conventional time-domain transient analysis:

- Designers are usually most interested in a system's steady-state behavior. Many high-frequency circuits contain long time constants that require conventional transient methods to integrate over many periods of the lowest-frequency sinusoid to reach steady state. Harmonic balance, on the other hand, captures the steady-state spectral response directly.
- Harmonic balance is faster at solving typical high-frequency problems that transient analysis can't solve accurately or can only do so at prohibitive costs. The applied voltage sources are typically multitone sinusoids that may have very narrowly or very widely spaced frequencies. It is not uncommon for the highest frequency present in the response to be many orders of magnitude greater than the

lowest frequency. Transient analysis would require an integration over an enormous number of periods of the highest-frequency sinusoid. The time involved in carrying out the integration is prohibitive in many practical cases.

- At high frequencies, many linear models are best represented in the frequency domain. Simulating such elements in the time domain by means of convolution can result in problems related to accuracy, causality, or stability.

### Harmonics and Maximum Order

With multiple sources in a circuit, mixing products will occur. The parameter *Maximum order* (under the *Freq* tab) determines how many mixing products are to be included in the simulation. Consider an example with two sources and three harmonics:

Source	Frequency	Order
Fund 1	5 MHz	3
Fund 2	7 MHz	3

If *Maximum order* is 0 or 1, no mixing products are simulated. The frequency list consists of the fundamental (Fund) frequency and the first, second, and third harmonics of each source, as follows:

Frequency	Combination
0 Hz	DC term
5 MHz	Fund 1
7 MHz	Fund 2
10 MHz	Second harmonic of Fund 1
14 MHz	Second harmonic of Fund 2
15 MHz	Third harmonic of Fund 1
21 MHz	Third harmonic of Fund 2

If *Maximum order* is 2, the sum and difference frequencies of the two fundamentals are added to the list:

Frequency	Combination
2 MHz	Fund 2 - Fund 1
12 MHz	Fund 2 + Fund 1

If *Maximum order* is 3, the second harmonic of one source can mix with the fundamental of the other. These frequencies are also added to the list:

Frequency	Combination
3 MHz	Second harmonic of Fund 1 - Fund 2
9 MHz	Second harmonic of Fund 2 - Fund 1
17 MHz	Second harmonic of Fund 1 + Fund 2
19 MHz	Second harmonic of Fund 2 + Fund 1

## Selecting a Solver

Many harmonic balance simulators rely on the Newton-Raphson technique to solve the nonlinear systems of algebraic equations that arise in large-signal frequency-domain circuit simulation problems. Each iteration of Newton-Raphson requires an inversion of the Jacobian matrix associated with the nonlinear system of equations. When the matrix is factored by direct methods, memory requirements climb as  $O(H^2)$ , where  $H$  is the number of harmonics. Thus, the factorization of a Jacobian at  $H=500$  will require 2500 times as much RAM as one at  $H=10$ .

An alternate approach to solving the linear system of equations associated with the Jacobian is to use a Krylov subspace iterative method such as GMRES (generalized minimum residual). This method does not require the explicit storage of the Jacobian matrix  $J$ , but rather only the ability to carry out matrix-vector products of the form  $J \square V$ , where  $V$  is an arbitrary vector. But the information needed to carry out such an operation can be stored in  $O(H)$  memory, not in  $O(H^2)$ , in the context of harmonic balance. Thus,

Krylov subspace solvers offer substantial savings in memory requirements for large harmonic-balance problems. Similar arguments show that even larger increases in computational speed can be obtained.

---

**Note** For circuits involving large numbers of frequencies, consider using the Circuit Envelope simulator.

---

Use the following guidelines when selecting a solver:

- Direct Solver

The *Direct Solver* option is recommended for the majority of small problems. A small problem can be roughly described as one where the circuit contains relatively few nonlinear components, there are one or two fundamental frequencies, relatively few harmonics, etc. In general, in such cases the Direct Solver is not only faster, but also exhibits superior convergence.

- Krylov Solver

The *Krylov Solver* option should be used when solving *large problems*. A large problem can roughly be described as one where memory usage exceeds 100 MB or the memory capacity of the computer (whichever occurs first). A problem may be *large* because of a large number of nonlinear components, a large number of harmonics required for simulation, or both. Krylov is less robust than the Direct Solver method because it uses iterative algorithms to solve the matrix equations. Krylov uses iteration for both the linear and nonlinear steps.

- Auto Select

Selecting this option allows the simulator to choose which solver to use. The simulator analyzes factors such as circuit or spectral complexity and compares memory requirements for each solver against the available computer memory. Based on this analysis it selects either direct solver or Krylov solver in a manner transparent to the user. Furthermore, if the Krylov solver is chosen by the simulator, several options for that solver are also automatically set.

Simulation time may *not* be a good indicator for the choice. Some problems are *small*, but still take a long time to simulate because parameters are being swept over many steps; such a problem should really be viewed as a sequence of small problems, and thus Krylov is not necessarily applicable. When a parameter is swept, if it takes X seconds to compute a single solution using the Krylov solver, it will probably take approximately 10X seconds to compute 10 solutions. On the other hand, if it takes Y seconds to compute a single solution using the direct solver, it will probably take far less than 10Y seconds to compute 10 swept steps of the analysis.

For system-level applications (behavioral mixers, amplifiers, etc.), the Krylov solver should be the preferred method of solution, as it is very robust in this area. For some transistor-level circuits, the Krylov solver may experience convergence difficulties at high input power levels. If this occurs, an analysis using the direct solver or the Envelope simulator should be attempted.

To select a specific solver:

1. Select the **Solver** tab in the Harmonic Balance controller dialog box.
2. Select the desired solver option. In general, we recommend that you accept the defaults and click **OK** to close the dialog box (or select another tab to set additional simulation specifications, as needed).



Contents lists available at SciVerse ScienceDirect

## International Journal of Electronics and Communications (AEÜ)

journal homepage: [www.elsevier.de/aeue](http://www.elsevier.de/aeue)

## Improved harmonic balance implementation of Floquet analysis for nonlinear circuit simulation

Fabio L. Traversa<sup>a</sup>, Fabrizio Bonani<sup>b,\*</sup><sup>a</sup> Departament d'Enginyeria Electrònica, Universitat Autònoma de Barcelona, Bellaterra 08193, Spain<sup>b</sup> Dipartimento di Elettronica, Politecnico di Torino, Corso Duca degli Abruzzi 24, Torino 10129, Italy

## ARTICLE INFO

## Article history:

Received 20 March 2011

Received in revised form 8 July 2011

Accepted 6 September 2011

## Keywords:

Circuit simulation

Floquet theory

Frequency domain analysis

Harmonic balance

## ABSTRACT

We present a novel algorithm for the efficient numerical computation of the Floquet quantities (eigenvalues, direct and adjoint eigenvectors) relevant to the assessment of the stability and noise properties of nonlinear forced and autonomous circuits. The approach is entirely developed in the frequency domain by means of the application of the Harmonic Balance technique, thus avoiding lengthy time-frequency transformations which might also impair the accuracy of the calculated quantities. An improvement in the computation time around one order of magnitude is observed.

© 2011 Elsevier GmbH. All rights reserved.

## 1. Introduction

Floquet analysis, although a classical topic in the mathematical literature [1,2], is the object of a renewed interest in the circuit simulation community because of the central role played in two important areas of nonlinear circuit performance assessment: the rigorous study of phase and amplitude noise in oscillators [3–8], and the appraisal of the stability of the time-periodic working point solution of a nonlinear circuit, either driven or autonomous [1,2,9–13].

Floquet theorem was originally derived with reference to Ordinary Differential Equations (ODEs) [1], and recently has been extended to the case of index-1 Differential Algebraic Equations (DAEs) [14]. This step has significant practical importance, since DAE is the general form of the describing equations obtained from the application of nodal analysis to a nonlinear circuit made of lumped components [15]. In general, the circuit nodal equations can be cast in the form

$$\begin{bmatrix} \mathbf{L}_1 \frac{d\mathbf{x}}{dt} \\ \frac{d}{dt}\mathbf{f}(\mathbf{x}(t)) \end{bmatrix} = \begin{bmatrix} \mathbf{L}_2 \mathbf{x} \\ \mathbf{g}(\mathbf{x}(t), t) \end{bmatrix} + \begin{bmatrix} \mathbf{c}(t) \\ \mathbf{d}(t) \end{bmatrix} \quad (1)$$

where  $\mathbf{x}(t) \in \mathbb{R}^n$  is the unknown vector,  $\mathbf{L}_1, \mathbf{L}_2 \in \mathbb{R}^{m \times n}$  with  $m \leq n$  are constant matrices describing the linear part of the circuit,  $\mathbf{c}(t) \in \mathbb{R}^m$  and  $\mathbf{f}, \mathbf{g}, \mathbf{d} \in \mathbb{R}^{n-m}$ . The nonlinear functions  $\mathbf{f}, \mathbf{g}$  are due to the

nonlinear elements in the circuit. The forcing terms in (1) (if any) are time-periodic functions of period  $T$ , and a non-trivial  $T$ -periodic solution (limit cycle)  $\mathbf{x}_S(t)$  is assumed to exist.<sup>1</sup>

Floquet theorem [14] applies to the linearization of (1) around  $\mathbf{x}_S(t)$ , i.e. it is a tool to characterize the effect of a small-change perturbation applied to the circuit limit cycle (see [11], and references therein). The main result is that the stability of  $\mathbf{x}_S(t)$  is dependent on a set of  $n$  (complex) numbers  $\lambda_k$  ( $k = 1, \dots, n$ ) called the *Floquet multipliers* (FMs) of  $\mathbf{x}_S(t)$ : if all of them (or, for oscillators, all but one which is exactly equal to 1) are placed strictly inside the unit circle of the complex plane, the limit cycle is asymptotically stable; on the other hand, if at least one of them has magnitude larger than one, the solution is unstable. The computation of the FMs provides therefore an assessment of the stability of the circuit working point. On the other hand, each FM is also associated to a (*direct*) *Floquet eigenvector*  $\mathbf{u}_k(t)$  ( $k = 1, \dots, n$ ) which, together with the (*adjoint*) *Floquet eigenvectors*  $\mathbf{v}_k(t)$  ( $k = 1, \dots, n$ ) associated to the adjoint linearized system<sup>2</sup>, are the basic ingredients required to perform oscillator noise analysis [3,7,8].

The calculation of the Floquet multipliers and eigenvectors can be performed either in the time or in the frequency domain. The problem has been traditionally tackled for ODEs in the time domain [9,11,16,17], devising numerical approaches with various degrees of efficiency and accuracy. On the other hand for many applications spectral techniques, such as the harmonic balance (HB) method,

<sup>\*</sup> Corresponding author.E-mail address: [fabrizio.bonani@polito.it](mailto:fabrizio.bonani@polito.it) (F. Bonani).<sup>1</sup> The same hypothesis holds for the case of autonomous circuits, for which of course no source term is present.<sup>2</sup> Both the direct and adjoint linearized systems share the same FMs [1,14].

provide significant advantages for the determination of the circuit limit cycle [15,18,19]. A general purpose, frequency-domain algorithm based on the HB approach for the determination of the direct and adjoint Floquet quantities was proposed in [10] and [20], respectively. In both cases, a generalized eigenvalue problem has to be solved, thus requiring a numerical procedure whose computational burden is  $O(N^3)$  where  $N$  is the matrices size. Notice that for HB,  $N = n(2N_H + 1)$  where  $N_H$  is the number of harmonics included in the simulation besides DC. In this contribution, we propose a numerical approach applicable to both the direct and adjoint problem which, making use of fast matrix manipulation completely taking place in the frequency domain, allows for a significant advantage with respect to previous algorithms by reducing the computational complexity to  $O(N^2)$ . The algorithm ultimately corresponds to a general methodology for constructing a linear ODE fully equivalent to the linearized DAE, thus extending the applicability of the approach in [9,16,17].

## 2. Fundamentals

We provide here the fundamentals required to effectively present the numerical procedure we developed. Linearization of (1) around the limit cycle  $\mathbf{x}_S(t)$  leads to a Linear Periodic Time Varying (LPTV) system of the form

$$\frac{d}{dt}[\mathbf{C}(t)\mathbf{z}] = \mathbf{A}(t)\mathbf{z}(t) \quad (2)$$

where  $\mathbf{C}, \mathbf{A} \in \mathbb{R}^{n \times n}$  are  $T$ -periodic matrices (since they correspond to the Jacobian of the full system calculated into  $\mathbf{x}_S(t)$ ) and  $\mathbf{z}(t) \in \mathbb{R}^n$  represents the perturbation of the limit cycle. In many cases, matrix  $\mathbf{C}(t)$  is not full rank although we assume that the rank  $\rho \leq n$  is independent of time (index-1 DAE) [14]: this has important consequences on the calculation of the Floquet quantities, as we will see shortly.

According to the generalization of Floquet theorem to DAEs [14], (2) is solved by  $\rho$  independent functions taking the form  $\mathbf{z}(t) = \exp(\mu_k t)\mathbf{u}_k(t)$  ( $k = 1, \dots, \rho$ ), where  $\mu_1, \dots, \mu_\rho$  are the *Floquet exponents* (FEs) of (2) (and  $\lambda_k = \exp(\mu_k T)$  are the corresponding *Floquet multipliers*),  $\mathbf{u}_k(t)$  is  $T$ -periodic and is called the *direct Floquet eigenvector* associated to  $\mu_k$ . Notice that  $\rho < n$  corresponds to the appearance of  $n - \rho$  FEs equal to  $-\infty$ .

On the other hand, the *adjoint* system to (2) reads [14]

$$\mathbf{C}^T(t) \frac{d\mathbf{w}}{dt} = -\mathbf{A}^T(t)\mathbf{w}(t) \quad (3)$$

and is solved by a linear combination of the  $\rho$  independent functions  $\mathbf{w}(t) = \exp(-\mu_k t)\mathbf{v}_k(t)$ , where  $\mathbf{v}_k(t)$  is again  $T$ -periodic and is called the *adjoint Floquet eigenvector* associated to  $\mu_k$ .

### 2.1. The HB technique

The HB technique is based on representing each scalar time periodic function  $\alpha(t)$  through the (truncated) Fourier series

$$\alpha(t) = \tilde{\alpha}_{0,c} + \sum_{h=1}^{N_H} [\tilde{\alpha}_{h,c} \cos(h\omega_0 t) + \tilde{\alpha}_{h,s} \sin(h\omega_0 t)] \quad (4)$$

where  $\tilde{\alpha}_{0,c}$  represents the DC component of  $\alpha(t)$ . The harmonic components are collected into a vector of size  $2N_H + 1$   $\tilde{\alpha} = [\tilde{\alpha}_{0,c}, \tilde{\alpha}_{1,c}, \tilde{\alpha}_{1,s}, \dots, \tilde{\alpha}_{N_H,c}, \tilde{\alpha}_{N_H,s}]^T$ , and put in one-to-one correspondence with a set of  $2N_H + 1$  time samples (distributed into the interval  $[0, T]$ ) of  $\alpha(t)$ , collected into vector  $\hat{\alpha} = [\alpha(t_1), \alpha(t_2), \dots, \alpha(t_{2N_H+1})]^T$ . The relationship between  $\hat{\alpha}$  and  $\tilde{\alpha}$  is provided by an invertible linear operator  $\Gamma^{-1}$  corresponding to the discrete Fourier transform (DFT) [15]

$$\hat{\alpha} = \Gamma^{-1}\tilde{\alpha} \Leftrightarrow \tilde{\alpha} = \Gamma\hat{\alpha}. \quad (5)$$

Notice that the matrix representation is used for formal derivation only: in the actual implementation the more efficient DFT algorithm [15] is used.

Denoting as  $\dot{\alpha}(t)$  the first derivative of  $\alpha(t)$ , trivial calculations yield the Fourier representation of the derivative as a function of the Fourier components of the original function

$$\tilde{\dot{\alpha}} = \Gamma\hat{\dot{\alpha}} = \Omega\tilde{\alpha}, \quad (6)$$

where  $\Omega \in \mathbb{R}^{(2N_H+1) \times (2N_H+1)}$  is a tridiagonal constant matrix proportional to  $\omega_0$  (see [10,15] for the explicit representation).

In case of an  $n$  size vector  $\alpha(t)$ , (5) and (6) are easily generalized by considering a vector of time-sample vectors and frequency components, defined by expanding each element  $\alpha_j(t)$  ( $j = 1, \dots, n$ ) into the time sample  $\hat{\alpha}_j$  and similarly for the harmonic components. One finds

$$\hat{\alpha} = \Gamma_n^{-1}\tilde{\alpha} \quad \tilde{\dot{\alpha}} = \Omega_n\tilde{\alpha}, \quad (7)$$

where  $\Gamma_n^{-1}$  and  $\Omega_n$  are block diagonal matrices built replicating  $n$  times the fundamental operators  $\Gamma^{-1}$  and  $\Omega$ , respectively.

More attention is required to derive the HB representation of  $\beta(t) = \Xi(t)\alpha(t)$  and of its time derivative, where  $\Xi(t)$  is a  $T$ -periodic matrix and  $\alpha(t)$  a  $T$ -periodic vector. Denoting as  $\tilde{\Xi}$  the  $n \times n$  block diagonal matrix built expanding each element  $\xi_{h,k}(t)$  of  $\Xi(t)$  as a  $(2N_H + 1) \times (2N_H + 1)$  diagonal matrix formed by the time samples  $\hat{\xi}_{h,k}$ , we have

$$\tilde{\beta} = \tilde{\Xi}\tilde{\alpha} \quad \tilde{\dot{\beta}} = \Omega_n\tilde{\beta} = \Omega_n\tilde{\Xi}\tilde{\alpha} \quad (8)$$

where  $\tilde{\Xi} = \Gamma_n\tilde{\Xi}\Gamma_n^{-1}$ . The transformation leading to  $\tilde{\Xi}$  results into the sum of a Toeplitz and of a Hankel matrix (see [21] for details), whose building blocks are the Fourier coefficients of the elements of  $\Xi(t)$ : in other words,  $\tilde{\Xi}$  can be easily assembled after evaluating (through DFT) the Fourier coefficients of the elements of  $\Xi(t)$ .

## 3. Previous work

Substituting  $\mathbf{z}(t) = \exp(\mu_k t)\mathbf{u}_k(t)$  into (2) and  $\mathbf{w}(t) = \exp(-\mu_k t)\mathbf{v}_k(t)$  into (3), the Floquet direct and adjoint eigenproblems are made explicit in the time domain [10,20]

$$\mu_k \mathbf{C}(t) \mathbf{u}_k(t) = \mathbf{A}(t) \mathbf{u}_k(t) - \frac{d}{dt}[\mathbf{C}(t) \mathbf{u}_k(t)] \quad (9)$$

$$\mu_k \mathbf{C}^T(t) \mathbf{v}_k(t) = \mathbf{A}^T(t) \mathbf{v}_k(t) + \mathbf{C}^T(t) \frac{d\mathbf{v}_k(t)}{dt}. \quad (10)$$

After time-sampling, the use of (6) and (8) allows to convert (9) and (10) in the spectral domain

$$\mu_k \tilde{\mathbf{C}} \tilde{\mathbf{u}}_k = [\tilde{\mathbf{A}} - \Omega_n \tilde{\mathbf{C}}] \tilde{\mathbf{u}}_k \quad (11)$$

$$\mu_k \tilde{\mathbf{C}}^T \tilde{\mathbf{v}}_k = [\tilde{\mathbf{A}}^T + \tilde{\mathbf{C}}^T \Omega_n] \tilde{\mathbf{v}}_k. \quad (12)$$

Notice that  $\tilde{\mathbf{C}}^T = \Gamma_n \tilde{\mathbf{C}}^T \Gamma_n^{-1}$  is not simply the transpose of  $\tilde{\mathbf{C}}$  (the same holds for  $\tilde{\mathbf{A}}^T$ ). Nevertheless, since  $\tilde{\mathbf{C}}$  is made of diagonal blocks (deriving from the time-sampling of the elements of  $\mathbf{C}(t)$ ),  $\tilde{\mathbf{C}}^T$  can easily be built from the components of  $\tilde{\mathbf{C}}$  avoiding any further calculation [20]. In summary, the Floquet quantities can be calculated as the solution of the generalized eigenvalue problems in (11) and (12), whose matrices correspond to the Jacobians of the HB problem defining the limit cycle, and therefore are available as a byproduct of the Newton iterations normally exploited for the determination of  $\mathbf{x}_S(t)$ .

The solution of the generalized eigenproblems (11) and (12) yields  $n(2N_H + 1)$  FEs (and the corresponding direct and adjoint eigenvectors). In an ideal system, i.e. if the number of harmonics is large enough, the FEs should be positioned in the complex plane

along vertical lines, i.e. they should be ordered in  $n$  groups sharing the same real part, and with imaginary parts whose distance is an integer multiple of  $\omega_0$  [1]. Because of the truncation error corresponding to the finite value of  $N_H$ , the FE distributions deviate from the ideal case for large values of the imaginary part. As a general rule, therefore, a wise choice for the better representative FE value appears to concentrate on the eigenvalues whose imaginary part is closer to the real axis [10]. Actually, a more detailed analysis suggests to slightly modify this choice: since all the FE having the same real part differ in the imaginary part of  $h\omega_0$  for some integer  $h \in \mathbb{Z}$ , the corresponding frequency domain eigenvectors are (if infinite harmonics are considered) shifted copies one of the other, where the shift takes place in the harmonic index. Therefore, we expect that the more precise eigenvector representation is that whose harmonics run from  $-N_H$  to  $N_H$  (in exponential notation), since all other representatives associated to the same FE are based on frequency components approximated in circulant form (see [22] and (18) below). In other words, since the available FEs are all the possible combinations  $\mu_k + h\omega_0$  with  $k = 1, \dots, n$  and  $h = -N_H, \dots, N_H$ , we look for the  $n$  values having  $h = 0$ , which in turn correspond to those eigenvectors characterized by those harmonic components whose order is symmetrical around DC.

#### 4. The novel approach

The main disadvantage of (11) and (12) is the numerical complexity of the generalized eigenvalue determination, which is  $O(N^3)$  [23] (the QZ algorithm is considered here), where  $N = n(2N_H + 1)$ . Since, even for comparatively small circuits, the number of harmonics  $N_H$  might become large to accurately describe the nonlinear behaviour, the numerical burden rapidly becomes significant.

The idea behind the approach we propose is quite simple: the generalized eigenvalue problems are transformed into standard eigenvalue systems

$$\mu_k \tilde{\mathbf{u}}_k = \tilde{\mathbf{C}}^{-1} [\tilde{\mathbf{A}} - \Omega_n \tilde{\mathbf{C}}] \tilde{\mathbf{u}}_k \quad (13)$$

$$\mu_k \tilde{\mathbf{v}}_k = \tilde{\mathbf{C}}_T^{-1} [\tilde{\mathbf{A}}_T + \tilde{\mathbf{C}}_T \Omega_n] \tilde{\mathbf{v}}_k, \quad (14)$$

where a direct inspection of the blocks forming  $\tilde{\mathbf{C}}_T$  (see [20] for details) shows that  $\tilde{\mathbf{C}}_T^{-1}$  is easily obtained by a proper rearrangement of the blocks constituting  $\tilde{\mathbf{C}}^{-1}$ .

The main advantage of (13) and (14) is of course based on the fact that the direct eigenvalue problem is  $O(N^2)$  [23]. The advantage, however, strictly depends on the computation of the system matrix  $\tilde{\mathbf{C}}^{-1} [\tilde{\mathbf{A}} - \Omega_n \tilde{\mathbf{C}}]$ . Using the Gaussian elimination implemented in the LAPACK package [25], we found that this step is in our problems anyway numerically convenient, thus making the transformation advantageous from a numerical standpoint. Fig. 1 shows a comparison in the computation time between the generalized eigenvalue problem (11) and the approach in (13) for the circuit example in Section 5 as a function of the number of harmonics  $N_H$  (notice that the total size  $N$  linearly depends on  $N_H$ ). The results clearly show that, despite the matrix inversion step, the new approach is  $O(N^2)$  with respect to the cubic dependence of the generalized eigenvalue problem.

On the other hand, a major difficulty is due to the fact that applying to a nonlinear circuit the nodal analysis and linearizing the corresponding DAE around the periodic working point, in general matrix  $\mathbf{C}(t)$  is not full rank, thus making  $\tilde{\mathbf{C}}$  not invertible. This problem, however, can be easily circumvented exploiting a trick proposed in [11]: let us consider (11) (the treatment of (12)

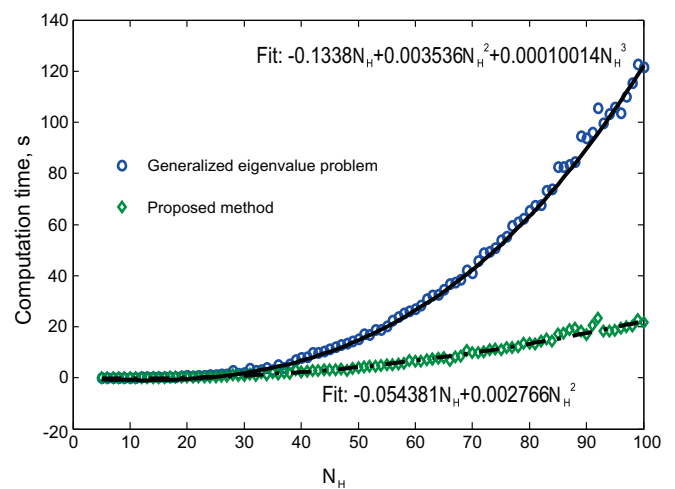


Fig. 1. Computation time (on an Intel Centrino Core2 Duo 2.53 GHz PC running Windows 7 64 bit, MATLAB [24] implementation) of (11) and (13) as a function of  $N_H$  for the example in Section 5. A polynomial best fit is also shown in the two cases.

is fully analogous) and build the modified generalized eigenvalue problem

$$\mu_{k'} [\tilde{\mathbf{C}} + \epsilon (\tilde{\mathbf{A}} - \Omega_n \tilde{\mathbf{C}})] \tilde{\mathbf{u}}_k = [\tilde{\mathbf{A}} - \Omega_n \tilde{\mathbf{C}}] \tilde{\mathbf{u}}_k \quad (15)$$

where  $\epsilon$  is a properly chosen real number making  $\tilde{\mathbf{C}} + \epsilon(\tilde{\mathbf{A}} - \Omega_n \tilde{\mathbf{C}})$  invertible: in our experience, a very good choice is  $\epsilon = \|\tilde{\mathbf{C}}\|_\infty / \|\tilde{\mathbf{A}} - \Omega_n \tilde{\mathbf{C}}\|_\infty$ . Simple calculations allow to verify that the relationship between the solutions of (11) and (15) is

$$\tilde{\mathbf{u}}_k = \tilde{\mathbf{u}}_{k'} \quad \mu_k = \frac{1}{1/\mu_{k'} - \epsilon} \quad (16)$$

#### 4.1. Problem size minimization

Although the approach in (15) is effective in coping with the  $\tilde{\mathbf{C}}$  invertibility issue, the numerical efficiency of the Floquet quantities determination still is significantly dependent on the size  $N = n(2N_H + 1)$  of  $\mathbf{C}(t)$ . This section introduces a numerical approach entirely based on the HB domain matrices, i.e. avoiding any time-consuming and accuracy-reducing time-frequency conversion, to minimize the size  $n$ . Although the algorithm is not in general able to produce a reduced system matrix which is invertible (and, therefore, (15) still needs to be used), the numerical advantage becomes however the more significant the larger is the value of  $N_H$ .

Linearization of (1) around  $\mathbf{x}_S(t)$  yields

$$\begin{bmatrix} \mathbf{L}_1 \frac{dz}{dt} \\ \frac{d}{dt} (\mathbf{J}_f(t)z) \end{bmatrix} = \begin{bmatrix} \mathbf{L}_2 z \\ \mathbf{J}_g(t)z \end{bmatrix} \quad (17)$$

where  $T$ -periodic matrices  $\mathbf{J}_f(t)$  and  $\mathbf{J}_g(t)$  are the Jacobians of the nonlinear functions  $f$  and  $g$  calculated in  $\mathbf{x}_S(t)$ . We assume that  $\mathbf{L}_1$  is full rank: in case of a rank deficient matrix, a reduction procedure such as that proposed below for  $\tilde{\mathbf{J}}_{g,z}$  can easily be implemented. Notice that since  $\mathbf{L}_1$  describes the linear part of the circuit, the reduction can take place at the beginning of the simulation, irrespective of the input tone, and is not plagued by the problems related to the time dependency of the kernel of  $\mathbf{J}_f(t)$ . We consider explicitly the direct eigenvalue problem only, since the extension to the adjoint system is trivial.

For the sake of simplicity we introduce the discussion assuming a Fourier expansion of the  $T$ -periodic matrices in exponential form, although the actual implementation is performed in trigonometric

form at the cost of a much more complex notation. This means that  $\tilde{\mathbf{J}}_f$  can be written as a block Toeplitz matrix

$$\tilde{\mathbf{J}}_f = \begin{bmatrix} \tilde{\mathbf{J}}_{f0} & \cdots & \tilde{\mathbf{J}}_{f2N_H} \\ \vdots & \ddots & \vdots \\ \tilde{\mathbf{J}}_{f-2N_H} & \cdots & \tilde{\mathbf{J}}_{f0} \end{bmatrix} \quad (18)$$

where  $\tilde{\mathbf{J}}_{fh}$  ( $h = -N_H, \dots, N_H$ ) is the  $n \times n$  complex matrix collecting the  $h$ -th Fourier coefficient of the elements of  $\mathbf{J}_f(t)$  calculated by the HB solution, and the other terms (i.e.  $N_H + 1 \leq |h| \leq 2N_H$ ) are approximated according to the block circulant structure in [22]. Furthermore, the time derivative operator  $\Omega$  is a complex, diagonal matrix of size  $2N_H + 1$ .

The first step is the application of the null space decomposition (NSD) algorithm presented in Appendix A.1.1 to  $\mathbf{J}_f(t)$ , identifying a unitary matrix  $\mathbf{H}$  able to single out the kernel of  $\mathbf{J}_f(t)$ . Notice that, although the rank of  $\mathbf{J}_f(t)$  is assumed constant, the kernel (i.e. the rows of the unitary matrix identifying the kernel of the matrix) is in general time varying: in order to be able to allow for an algorithm completely in the HB domain, we need a constant matrix  $\mathbf{H}$  and therefore we have devised the algorithm in Appendix A.2 to determine a constant matrix  $\mathbf{Z}_\perp$  extracting the constant part of the nullspace of  $\mathbf{J}_f(t)$ . Since the total NSD transformation is unitary, its rows must span the entire  $\mathbb{R}^{n-m}$ . Therefore we can easily build a constant unitary matrix  $\mathbf{H}$  such that

$$\mathbf{H}\mathbf{J}_f(t) = \begin{bmatrix} \mathbf{K} \\ \mathbf{Z}_\perp \end{bmatrix} \mathbf{J}_f(t) = \begin{bmatrix} \mathbf{J}_{f,nz}(t) \\ \mathbf{0}_{(n-m-\rho_\perp) \times n} \end{bmatrix} \quad (19)$$

where  $\mathbf{K} \in \mathbb{R}^{\rho_\perp \times n}$  and  $\mathbf{Z}_\perp \in \mathbb{R}^{(n-m-\rho_\perp) \times n}$  are pseudo-unitary matrices,  $\rho_\perp$  is the size of the time-invariant part of the kernel of  $\mathbf{J}_f(t)$ , and  $\mathbf{0}_{p \times q}$  is the zero matrix of size  $p \times q$ .  $\mathbf{K}$  is assembled choosing, through a standard orthonormalization procedure,  $\rho_\perp$  normalized vectors which, together with the rows of  $\mathbf{Z}_\perp$ , span  $\mathbb{R}^{n-m}$ . Since  $\mathbf{Z}_\perp$  contains only the time invariant part of the nullspace of  $\mathbf{J}_f(t)$ ,  $\mathbf{J}_{f,nz}(t)$  is not guaranteed to be invertible (unless  $\rho_\perp = \rho$ ), thus leading to a noninvertible reduced system matrix that needs to be regularized as in (15).

Since  $\mathbf{H}$  is independent of  $t$  (as well as  $\mathbf{L}_1$  and  $\mathbf{L}_2$ ), the frequency transformed version  $\tilde{\mathbf{H}} \in \mathbb{R}^{(n-m)(2N_H+1) \times (2N_H+1)}$  is block diagonal, and therefore commutes with the (block diagonal) time derivative operator  $\Omega_{n-m}$ . Using the Floquet ansatz  $\mathbf{z}(t) = \exp(\mu_k t)\tilde{\mathbf{u}}_k(t)$ , in frequency domain (17) becomes

$$(\mu_k \mathbf{I}_{n(2N_H+1)} + \Omega_n) \begin{bmatrix} \tilde{\mathbf{L}}_1 \\ \tilde{\mathbf{H}}\tilde{\mathbf{J}}_f \end{bmatrix} \tilde{\mathbf{u}}_k = \begin{bmatrix} \tilde{\mathbf{L}}_2 \\ \tilde{\mathbf{H}}\tilde{\mathbf{J}}_g \end{bmatrix} \tilde{\mathbf{u}}_k \quad (20)$$

where  $\mathbf{I}_{n(2N_H+1)}$  is the identity matrix of size  $n(2N_H+1)$ , and

$$\tilde{\mathbf{H}}\tilde{\mathbf{J}}_f = \begin{bmatrix} \tilde{\mathbf{J}}_{f,nz} \\ \mathbf{0}_{(n-m-\rho_\perp)(2N_H+1) \times n(2N_H+1)} \end{bmatrix} \quad (21)$$

and  $\tilde{\mathbf{J}}_{f,nz}$  has size  $\rho_\perp(2N_H+1) \times n(2N_H+1)$ . We now focus on the last  $(n-m-\rho_\perp)(2N_H+1)$  rows of  $\tilde{\mathbf{H}}\tilde{\mathbf{J}}_g$ , denoted as  $\tilde{\mathbf{J}}_{g,z}$ :

$$\tilde{\mathbf{H}}\tilde{\mathbf{J}}_g = \begin{bmatrix} \tilde{\mathbf{J}}_{g,nz} \\ \tilde{\mathbf{J}}_{g,z} \end{bmatrix} \quad (22)$$

Because of (21)

$$\tilde{\mathbf{J}}_{g,z}\tilde{\mathbf{u}}_k = \mathbf{0}, \quad (23)$$

therefore the size of (20) can be reduced eliminating  $(n-m-\rho_\perp)(2N_H+1)$  real equations. Notice that for (20) to be consistent,  $\tilde{\mathbf{J}}_{g,z}$  should be full rank.

In order to make use of the rectangular linear system (23), we should be able to extract an invertible submatrix of  $\tilde{\mathbf{J}}_{g,z}$ , e.g. by applying the reduced row echelon form (RREF) algorithm in Appendix A.1.2. A direct application of RREF would however be numerically very intensive, because of the size of  $\tilde{\mathbf{J}}_{g,z}$ , especially if a large  $N_H$  is used. We propose here a heuristical approach, which in our experience has been proven to be very effective: consider the real and positive  $(n-m-\rho_\perp) \times n$  matrix  $\tilde{\mathbf{J}}_{g,e}$  obtained by summing on the harmonic index the square magnitude of the elements of  $\tilde{\mathbf{J}}_{g,z}$ , which can be easily and quickly assembled. Because of Parseval identity, this corresponds to the collection of the energy of each element of  $\mathbf{Z}_\perp \mathbf{J}_g(t)$ . The RREF algorithm is then applied to  $\tilde{\mathbf{J}}_{g,e}$ , obtaining the pivoting set  $j_{\tilde{\mathbf{J}}_{g,e}}$  and its complement  $\bar{j}_{\tilde{\mathbf{J}}_{g,e}}$  leading to the partition (and pivoting) of  $\tilde{\mathbf{J}}_{g,z}$  into

$$[\tilde{\mathbf{J}}_{g,z1} \quad \tilde{\mathbf{J}}_{g,z2}] \quad (24)$$

where  $\tilde{\mathbf{J}}_{g,z1} = \tilde{\mathbf{J}}_{g,z}(:, \bar{j}_{\tilde{\mathbf{J}}_{g,e}})((n-m-\rho_\perp)(2N_H+1) \times (m+\rho_\perp)(2N_H+1))$ , i.e. the collection of columns of  $\tilde{\mathbf{J}}_{g,z}$  corresponding to the set  $\bar{j}_{\tilde{\mathbf{J}}_{g,e}}$  where the choice of the columns should be intended implemented as applied to the harmonic blocks ordered as in (18). Matrix  $\tilde{\mathbf{J}}_{g,z2} = \tilde{\mathbf{J}}_{g,z}(:, j_{\tilde{\mathbf{J}}_{g,e}})((m+\rho_\perp)(2N_H+1) \times (m+\rho_\perp)(2N_H+1))$  is, if the pivoting vector is well chosen, invertible. Therefore, the quality of the pivoting vector is verified by checking the condition number of  $\tilde{\mathbf{J}}_{g,z2}$ .

Applying the pivoting operation also to the unknown vector

$$\tilde{\mathbf{u}}_k \rightarrow \begin{bmatrix} \tilde{\mathbf{u}}_{k,1} \\ \tilde{\mathbf{u}}_{k,2} \end{bmatrix} = \begin{bmatrix} \tilde{\mathbf{u}}_k(\bar{j}_{\tilde{\mathbf{J}}_{g,e}}) \\ \tilde{\mathbf{u}}_k(j_{\tilde{\mathbf{J}}_{g,e}}) \end{bmatrix}, \quad (25)$$

from (23) follows

$$\tilde{\mathbf{u}}_{k,2} = -\tilde{\mathbf{J}}_{g,z2}^{-1} \tilde{\mathbf{J}}_{g,z1} \tilde{\mathbf{u}}_{k,1}, \quad (26)$$

i.e. the number of real unknowns is reduced to  $(m+\rho_\perp)(2N_H+1)$ , the size of  $\tilde{\mathbf{u}}_{k,1}$ . Making use of (26) into (20), a system like (11) of size  $(m+\rho_\perp)(2N_H+1)$  is obtained, where

$$\tilde{\mathbf{C}} = \begin{bmatrix} \tilde{\mathbf{L}}_{1,1} - \tilde{\mathbf{L}}_{1,2} \tilde{\mathbf{J}}_{g,z2}^{-1} \tilde{\mathbf{J}}_{g,z1} \\ \tilde{\mathbf{J}}_{f,nz1} - \tilde{\mathbf{J}}_{f,nz2} \tilde{\mathbf{J}}_{g,z2}^{-1} \tilde{\mathbf{J}}_{g,z1} \end{bmatrix} \quad (27)$$

$$\tilde{\mathbf{A}} = \begin{bmatrix} \tilde{\mathbf{L}}_{2,1} - \tilde{\mathbf{L}}_{2,2} \tilde{\mathbf{J}}_{g,z2}^{-1} \tilde{\mathbf{J}}_{g,z1} \\ \tilde{\mathbf{J}}_{g,nz1} - \tilde{\mathbf{J}}_{g,nz2} \tilde{\mathbf{J}}_{g,z2}^{-1} \tilde{\mathbf{J}}_{g,z1} \end{bmatrix} \quad (28)$$

and the unknown vector is  $\tilde{\mathbf{u}}_{k,1}$ . In the previous equations, matrices  $\tilde{\mathbf{L}}_{1,q}$ ,  $\tilde{\mathbf{L}}_{2,q}$ ,  $\tilde{\mathbf{J}}_{g,nzq}$  and  $\tilde{\mathbf{J}}_{f,nzq}$  ( $q = 1, 2$ ) are defined through the application of the pivoting set to the corresponding original matrices. Notice that if  $\rho_\perp$  is equal to the rank of  $\mathbf{J}_f(t)$ , i.e. if the kernel of  $\mathbf{J}_f(t)$  is independent of time, the matrix defined in (27) is full rank.

#### 4.2. Summary of the algorithm

For the sake of clarity, we summarize here the steps of the proposed algorithm, pointing out the sequence of actions to be implemented:

1. assemble the full circuit equations according to the generalized nodal approach;
2. minimize matrix  $\mathbf{L}_1$  representing the linear part of the circuit making it full rank. This step is to be performed once (since matrix is constant) by applying the RREF algorithm;
3. determine the circuit time-periodic working point  $\mathbf{x}_S(t)$  by means of the HB technique;
4. minimize the size of the  $\mathbf{J}_f(t)$  Jacobian exploiting the algorithm in Section 4.1;

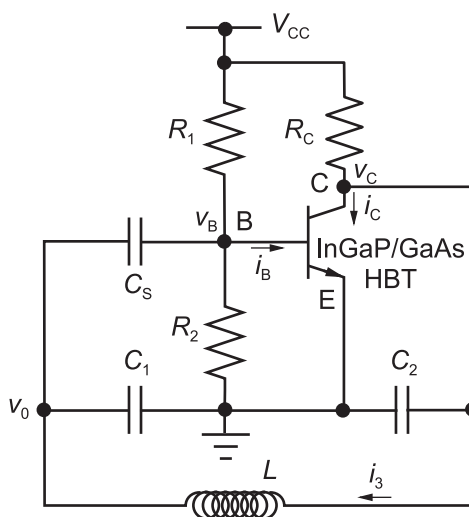


**Fig. 2.** Circuit of the Colpitts oscillator.

5. if the kernel of  $J_f(t)$  is not full rank, apply (15) checking the condition number of the obtained modified matrix;
6. calculate the Floquet quantities exploiting (13) and (14).

## 5. Example

As an example of application we consider the Colpitts oscillator in Fig. 2. The transistor is the InGaP/GaAs HBT described by the Gummell Poon model in [26], including device nonlinear capacitances and parasitic effects. The circuit parameters are:  $V_{CC} = 6\text{ V}$ ,  $R_1 = 10\text{ k}\Omega$ ,  $R_2 = 4.2\text{ k}\Omega$ ,  $R_C = 300\text{ }\Omega$ ,  $C_1 = 5\text{ pF}$ ,  $C_2 = 5\text{ pF}$ ,  $C_S = 1\text{ }\mu\text{F}$  and  $L = 10\text{ nH}$ . As shown in [8], the oscillation frequency obtained through a HB simulation with  $N_H = 300$  is 0.994 GHz.

After the reduction of the linear part of the circuit system matrix, the number of unknowns is  $n = 9$ , leading to a size of the HB Floquet problem equal to  $n(2N_H + 1) = 5409$ . Applying the NSD to  $J_f(t)$ , the nullspace is found to have size 4 (which means that the LPTV system has 4 FEs equal to  $-\infty$ ). Two of the elements of the orthonormal base of the kernel of  $J_f(t)$  are constant, while for the other two a

**Table 1**

Comparison between the generalized eigenvalue and the simple eigenvalue methodologies. MATLAB [24] implementation on an Intel Centrino Core2 Duo 2.53 GHz PC running Windows 7 64 bit.

	Previous method	This work
Time	1816 s	148 s
$\mu_1$	-473760.9482	-473761.6942
$\mu_2$	-1158.8725	-1158.8808
$\mu_3$	-2237488716.6516	-2237491363.8365
$\mu_4$	-3222824027.1933	-3222819597.1577
$\mu_5$	+3124059245.1654j	+3124060182.7958j
	$-4.36927537 \times 10^{12}$	$-4.37020515 \times 10^{12}$

time dependent rotation is observed, as shown in Fig. 3: this means that  $\rho_\perp = 2$ . Therefore, the application of the reduction procedure described in Section 4.1 leads to the problem size  $7(2N_H + 1) = 4207$ , i.e. a 22% reduction.

The results of the application of the previous method, based on the solution of a generalized eigenvalue problem, and of the algorithm proposed in this work are summarized in Table 1, where the Floquet eigenvalues are compared. Notice that the table lists 5 FEs only, since the partial reduction of the system due to the nonconstant nullspace still leaves 2 FEs equal to  $-\infty$ . The first eigenvalue  $\mu_1$  is associated to the tangent vector to the oscillator solution, and in principle should be zero. As well known in the literature [27], the numerical accuracy of its determination is very poor: as usual, the proper eigenvalue is chosen by looking for the direct eigenvector that better approximates the orthogonality condition with the corresponding adjoint eigenvector  $v_1(t) = \dot{x}_S(t)$  [20]. Applying the same error estimation procedure in [20], the other FEs result well approximated up to the fifth digit. The complex FE  $\mu_4$  appears without the corresponding complex conjugate value because the imaginary part is equal to  $\omega_0/2$ , and therefore is mapped onto a real FM.

The computation time for the generalized eigenvalue problem is measured on the full system (i.e. no reduction of the system size is performed), while for the present approach the entire computation is taken into account (i.e. both the system reduction and the determination of the FEs). Comparing the results of the two methods, the accuracy of the new approach appears excellent, whereas the computation time is improved by one order of magnitude.

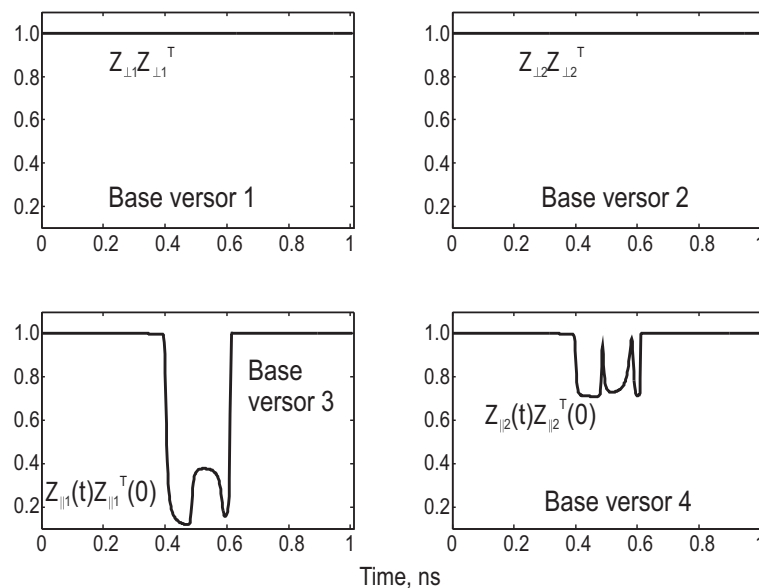


**Fig. 3.** Time-dependence (over one period) of the orthonormal base elements  $Z_{ij}(t)$  and  $Z_{jj}(t)$  (the  $j$ -th row of the corresponding matrix in (A.5)) projected along the corresponding value for  $t = 0$  for the nullspace of  $J_f(t)$  as found by the NSD algorithm.

## 6. Conclusion

We have presented an algorithm for the computation of all the Floquet quantities relevant for important assessments of the operation of nonlinear circuits working in time-periodic conditions. The method can be applied to both forced and autonomous systems, and is entirely based on the HB technique. In particular, all the matrix transformations are entirely taking place in the spectral domain, thus avoiding time intensive DFT operations which, on the other hand, may also imply a degradation of the numerical accuracy.

The application of the algorithm shows that an important improvement of the computation time of one order of magnitude with respect to previous approaches is observed, without any significant reduction in the precision of the calculated Floquet quantities.

## Appendix A.

### A.1. Matrix manipulation tools

We briefly describe in this section the relevant properties of two matrix manipulation tools that we use in the implementation of Floquet analysis, the *null space decomposition* (NSD) and the *reduced row echelon form* (RREF) [28,29]. To fix the ideas, let us consider a matrix  $\mathbf{M} \in \mathbb{R}^{m \times n}$  ( $m \leq n$ ) of rank  $\rho \leq m$ .

#### A.1.1. Null space decomposition

We consider here a matrix linear transformation that allows to identify the kernel of  $\mathbf{M}$ . A unitary matrix  $\mathbf{H} \in \mathbb{R}^{m \times m}$  exists (i.e.  $\mathbf{HH}^T = \mathbf{H}^T \mathbf{H} = \mathbf{I}_m$  where  $\mathbf{I}_m$  is the identity matrix of size  $m$ ) such that [28,29]

$$\mathbf{HM} = \begin{bmatrix} \mathbf{M}_{\text{nz}} \\ \mathbf{0}_{(m-\rho) \times m} \end{bmatrix} \quad (\text{A.1})$$

where  $\mathbf{0}_{p,q}$  is a null matrix of size  $p \times q$  and  $\mathbf{M}_{\text{nz}} \in \mathbb{R}^{\rho \times n}$  has rank  $\rho$ . Matrix  $\mathbf{H}$  is decomposed into two submatrices

$$\mathbf{H} = \begin{bmatrix} \mathbf{K} \\ \mathbf{Z} \end{bmatrix} \quad (\text{A.2})$$

where  $\mathbf{K} \in \mathbb{R}^{\rho \times m}$  and  $\mathbf{Z} \in \mathbb{R}^{(m-\rho) \times m}$ , whose rows represent, respectively, a basis for the orthogonal part and for the kernel of  $\mathbf{M}$ .

The NSD is a particular case of orthogonal decomposition [29] allowing to define a matrix which singles out the full rank part of  $\mathbf{M}$ . Many implementations for this operation are possible, e.g. the Householder transformation [28,29]. In our experience, an effective solution is to implement (A.1) exploiting the QR decomposition [29], using the variant of the QR algorithm returning an upper triangular matrix whose diagonal terms are (in magnitude) in decreasing order.

Notice that the NSD matrix is not unique. In fact, given a unitary matrix  $\mathbf{Q}$  partitioned as

$$\mathbf{Q} = \begin{bmatrix} \mathbf{Q}_{11} & \mathbf{Q}_{12} \\ \mathbf{0}_{m-\rho \times \rho} & \mathbf{Q}_{22} \end{bmatrix} \quad (\text{A.3})$$

where  $\mathbf{Q}_{11}$  and  $\mathbf{Q}_{22}$  are square matrices of size  $\rho \times \rho$  and  $(m-\rho) \times (m-\rho)$ , respectively,  $\mathbf{H}' = \mathbf{QH}$  still satisfies (A.1) (of course with a different  $\mathbf{M}_{\text{nz}}$ ).

#### A.1.2. Reduced row echelon form

The RREF is a reduction technique based on a pivoting strategy, typically used for the solution of linear systems with non-full rank (or, in general, with a rectangular system matrix). The RREF  $\mathbf{P}$  of  $\mathbf{M}$  has two important features [29]: the last  $m - \rho$  rows of  $\mathbf{P}$  are zero,

and for each row of  $\mathbf{P}$  the position of the first non-null element (starting from left) is the row pivot. We collect all the pivots in the set  $j_M$ , which has the following properties [29]:

1.  $j_M$  has  $\rho$  elements
2.  $j_M$  defines a basis for the space spanned by  $\mathbf{M}$ , meaning that

$$\text{span} \left\{ \{ \mathbf{M}(:, j) \}_{j=1}^n \right\} = \text{span} \left\{ \{ \mathbf{M}(:, j_M(j)) \}_{j=1}^\rho \right\}$$

where  $\mathbf{M}(:, j)$  is the  $j$ -th column of  $\mathbf{M}$ . We make use of the pivoting vector  $j_M$  (i.e. we do not require the full  $\mathbf{P}$ ), and of its complement  $j_{\bar{M}} = \{1, \dots, n\} \setminus j_M$ . According to our experience the best selection approach is based again on the QR factorization [29] returning an upper triangular matrix whose diagonal terms are (in magnitude) in decreasing order.

#### A.2. Determination of the constant part of the kernel of a periodic matrix

Let us consider a  $T$  periodic matrix  $\mathbf{M}(t) \in \mathbb{R}^{m \times n}$ , where  $m \leq n$ . For the sake of simplicity, we exploit the exponential form of Fourier series and order the collection of harmonic components as in (18). Let us denote as  $\tilde{\mathbf{M}}_h$  the  $m \times n$  complex matrix representing the  $h$ -th Fourier component of  $\mathbf{M}(t)$ .

**Theorem 1.** *Let  $\mathbf{M}(t) \in \mathbb{R}^{m \times n}$  ( $m \leq n$ ) with rank  $\rho$  independent of time (thus, the size  $m - \rho$  of the kernel of  $\mathbf{M}(t)$  is independent of time), whose Fourier representation is ordered as in (18). Let  $\mathbf{Z}_\perp \in \mathbb{R}^{m-\rho_\perp \times m}$  ( $\rho_\perp \geq \rho$ ) be the constant part of the nullspace of  $\mathbf{M}(t)$ . Then*

$$\mathbf{Z}_\perp \tilde{\mathbf{M}}_h = \mathbf{0}_{m-\rho_\perp \times n} \quad \forall h \in \mathbb{Z}.$$

**Proof.** Since the rank of  $\mathbf{M}(t)$  is constant, it is possible to find a unitary matrix  $\mathbf{H}(t) = [\mathbf{K}^T(t), \mathbf{Z}^T(t)]^T$  such that (A.1) holds, e.g. using the NSD algorithm in Appendix A.1.1. As noted in Appendix A.1.1,  $\mathbf{H}$  is not uniquely defined since it can be transformed into another unitary matrix  $\mathbf{H}'(t)$  using  $\mathbf{H}' = \mathbf{QH}$ , where  $\mathbf{Q}$  is again a unitary transformation as in (A.3). Therefore, if a nontrivial constant part of the nullspace of  $\mathbf{M}(t)$  exists, a unitary transformation  $\mathbf{Q}_{22}(t)$  exists such that

$$\mathbf{Q}_{22}(t) \mathbf{Z}(t) = \begin{bmatrix} \mathbf{Z}_{\parallel}(t) \\ \mathbf{Z}_\perp \end{bmatrix} \quad (\text{A.4})$$

where  $\mathbf{Z}_\perp \in \mathbb{R}^{m-\rho_\perp \times m}$  is constant and  $\mathbf{Z}_{\parallel}(t) \in \mathbb{R}^{\rho_\perp - \rho \times m}$ . Since  $\mathbf{H}$  is unitary,  $\mathbf{Z}$  is pseudo-unitary (i.e.  $\mathbf{ZZ}^T = \mathbf{I}_{m-\rho}$ ) as well as  $\mathbf{Z}_\perp$  and  $\mathbf{Z}_{\parallel}$ , which are also pseudo-orthogonal ( $\mathbf{Z}_\perp \mathbf{Z}_{\parallel}^T = \mathbf{0}$  and  $\mathbf{Z}_{\parallel} \mathbf{Z}_{\perp}^T = \mathbf{0}$ ). In other words, a unitary transformation  $\mathbf{H}'(t)$  exists such that

$$\begin{bmatrix} \mathbf{K}'(t) \\ \mathbf{Z}_{\parallel}(t) \end{bmatrix} \mathbf{M}(t) = \begin{bmatrix} \mathbf{M}_{\text{nz}}(t) \\ \mathbf{0} \\ \mathbf{0} \end{bmatrix}. \quad (\text{A.5})$$

Expressing (A.5) in frequency domain we find

$$\begin{bmatrix} \tilde{\mathbf{K}}' \\ \tilde{\mathbf{Z}}_{\parallel} \\ \tilde{\mathbf{Z}}_\perp \end{bmatrix} \tilde{\mathbf{M}} = \begin{bmatrix} \tilde{\mathbf{M}}_{\text{nz}} \\ \mathbf{0} \\ \mathbf{0} \end{bmatrix} \quad (\text{A.6})$$

where, since  $\mathbf{Z}_\perp$  is constant,  $\tilde{\mathbf{Z}}_\perp$  is block diagonal where each diagonal block is  $\mathbf{Z}_\perp$ . Therefore, the lower third part of (A.6) yields the required result.  $\square$

Based on Theorem 1 we propose an algorithm able to quickly recover  $\mathbf{Z}_\perp$  starting from the Fourier components  $\tilde{\mathbf{M}}_h$ . Let us denote

as  $\mathbf{H}_h = [\mathbf{K}_{\parallel,h}^T \mathbf{Z}_{\perp,h}^T]^T$  (the size of  $\mathbf{Z}_h$  is  $m - \rho_h \times n$ ) the result of the NSD applied to  $\mathbf{M}_h$ , so that because of [Theorem 1](#) a unitary  $\mathbf{U}_h$  (size  $m - \rho_h \times m - \rho_h$ ) exists such that  $\mathbf{U}_h \mathbf{Z}_h = [\mathbf{Z}_{\parallel,h}^T \mathbf{Z}_{\perp,h}^T]^T$ . We proceed as follows:

1. calculate  $\mathbf{Z}_0$  and  $\mathbf{Z}_1$ ;
2. calculate the singular value decomposition (SVD) [29] of  $\mathbf{Z}_0 \mathbf{Z}_1^T$ , i.e. find the unitary matrices  $\mathbf{S}_{01}$  ( $m - \rho_0 \times m - \rho_0$ ) and  $\mathbf{D}_{01}$  ( $m - \rho_1 \times m - \rho_1$ ) such that

$$\mathbf{Z}_0 \mathbf{Z}_1^T = \mathbf{S}_{01} \mathbf{V}_{01} \mathbf{D}_{01}$$

where  $\mathbf{V}_{01}$  ( $m - \rho_0 \times m - \rho_1$ ) is diagonal;

3. choose the rows of  $\mathbf{Z}_{\perp}$  as the rows of  $\mathbf{S}_{01}^T \mathbf{Z}_0$  that, multiplied times  $\mathbf{Z}_1^T \mathbf{D}_{01}^T$ , yield  $[0, \dots, 0, 1, 0, \dots, 0]$  as a result (where the 1 is in  $j$ -th position in the vector where  $j = 1, \dots, \rho_{\perp}$ );
4. repeat the previous steps with  $\mathbf{Z}_0$  and  $\mathbf{Z}_2$  to verify the numerical precision of the determined  $\mathbf{Z}_{\perp}$ .

The consistency of step 3 can be easily verified decomposing

$$\mathbf{S}_{01}^T \mathbf{Z}_0 = \begin{bmatrix} \mathbf{S}_{01,nz}^T \mathbf{Z}_{0,nz} \\ \mathbf{Z}_{\perp} \end{bmatrix} \quad \mathbf{D}_{01} \mathbf{Z}_1 = \begin{bmatrix} \mathbf{D}_{01,nz} \mathbf{Z}_{1,nz} \\ \mathbf{Z}_{\perp} \end{bmatrix} \quad (\text{A.7})$$

where  $\mathbf{S}_{01,nz}$  and  $\mathbf{D}_{01,nz}$  are the unitary matrices of the SVD of  $\mathbf{Z}_{0,nz} \mathbf{Z}_{1,nz}$ . In fact, from (A.7) follows

$$\begin{aligned} \mathbf{S}_{01}^T \mathbf{Z}_0 \mathbf{Z}_1^T \mathbf{D}_{01}^T &= \begin{bmatrix} \mathbf{S}_{01,nz}^T \mathbf{Z}_{0,nz} \mathbf{Z}_{1,nz} \mathbf{D}_{01,nz} & \mathbf{S}_{01,nz}^T \mathbf{Z}_{0,nz} \mathbf{Z}_{\perp}^T \\ \mathbf{Z}_{\perp} \mathbf{Z}_{1,nz} \mathbf{D}_{01,nz} & \mathbf{Z}_{\perp} \mathbf{Z}_{\perp}^T \end{bmatrix} \\ &= \begin{bmatrix} \mathbf{V}_{01,nz} & \mathbf{0}_{(m-\rho_0-\rho_{\perp}) \times \rho_{\perp}} \\ \mathbf{0}_{\rho_{\perp} \times (m-\rho_1-\rho_{\perp})} & \mathbf{I}_{\rho_{\perp}} \end{bmatrix}. \end{aligned}$$

## References

- [1] Farkas M. Periodic motions. New York: Springer-Verlag; 1994.
- [2] Guckenheimer J, Holmes P. Nonlinear oscillations, dynamical systems, and bifurcations of vector fields. New York: Springer-Verlag; 1983.
- [3] Demir A, Mehrotra A, Roychowdhury J. Phase noise in oscillators: a unifying theory and numerical methods for characterization. *IEEE Trans Circuits Syst I: Fundam Theory Appl* 2000;57(May (5)):655–74.
- [4] Demir A. Phase noise and timing jitter in oscillators with colored-noise sources. *IEEE Trans Circuits Syst I: Fundam Theory Appl* 2002;49(December (12)):1782–91.
- [5] Srivastava S, Roychowdhury J. Analytical equations for nonlinear phase errors and jitter in ring oscillators. *IEEE Trans Circuits Syst I: Regul Pap* 2007;54(October (10)):2321–9.
- [6] Carbone A, Palma F. Considering noise orbital deviations on the evaluation of power density spectrum of oscillators. *IEEE Trans Circuits Syst Express Briefs* 2006;53(6):438–42.
- [7] Traversa FL, Bonani F. Asymptotic stochastic characterization of phase and amplitude noise in free-running oscillators. *Fluctuation Noise Lett* 2011;10(2):207–21, doi: 10.1142/S021947751100048X.
- [8] Traversa FL, Bonani F. Oscillator noise: a nonlinear perturbative theory including orbital fluctuations and phase-orbital correlation. *IEEE Trans Circuits Syst I: Regul Pap* 2011, doi: 10.1109/TCSI.2011.2123531.
- [9] Lust K. Improved numerical Floquet multipliers. *Int J Bifurcation Chaos* 2001;11(September (9)):2389–410.
- [10] Traversa FL, Bonani F, Donati Guerrieri S. A frequency-domain approach to the analysis of stability and bifurcations in nonlinear systems described by differential-algebraic equations. *Int J Circuit Theory Appl* 2004;36(4):421–39.
- [11] Brambilla A, Gruosso G, Storti Gajani G. Determination of Floquet exponents for small-signal analysis of nonlinear periodic circuits. *IEEE Trans Computer-Aided Design Integr Circuits Syst* 2009;28(March (3)):447–51.
- [12] Traversa FL, Cappelluti F, Bonani F, Ghione G. Assessment of thermal instabilities and oscillations in multifinger heterojunction bipolar transistors through a harmonic-balance-based CAD-oriented dynamic stability analysis technique. *IEEE Trans Microw Theory Tech* 2009;December (57)(12):3461–8.
- [13] Cappelluti F, Traversa FL, Bonani F, Donati Guerrieri S, Ghione G. Rigorous, HB-based nonlinear stability analysis of multi-device power amplifier. In: European microwave integrated circuits conference. 2010. p. 90–3.
- [14] Demir A. Floquet theory and non-linear perturbation analysis for oscillators with differential-algebraic equations. *Int J Circuit Theory Appl* 2000;28:163–85.
- [15] Kundert KS, Sangiovanni-Vincentelli A, White JK. Steady-state methods for simulating analog and microwave circuits. Boston: Kluwer Academic Publisher; 1990.
- [16] Kuznetsov YA. Elements of applied bifurcation theory. 2nd ed. New York: Springer-Verlag; 1998.
- [17] Brambilla A, Storti Gajani G. Computation of all Floquet eigenfunctions in autonomous circuits. *Int J Circuit Theory Appl* 2008;36:717–37.
- [18] Kundert KS. Introduction to RF simulation and its application. *IEEE J Solid-State Circuits* 1999;34(September):1298–319 [The Mathworks, Inc.]
- [19] Rizzoli V, Masotti D, Mastri F, Montanari E. System-oriented harmonic-balance algorithms for circuit-level simulation. *IEEE Trans Computer-Aided Design Integr Circuits Syst* 2011;30(February (2)):256–69.
- [20] Traversa FL, Bonani F. Frequency domain evaluation of the adjoint Floquet eigenvectors for oscillator noise characterization. *IET Circuits Devices Syst* 2011;5(1):46–51.
- [21] Feldmann P, Melville RC, Long D. Efficient frequency domain analysis of large nonlinear analog circuits. In: In IEEE Custom Integr Circuits Conf. 1996. p. 461–4.
- [22] Roychowdhury J, Long D, Feldmann P. Cyclostationary noise analysis of large RF circuits with multitone excitations. *IEEE J Solid-State Circuits* 1998;33(3):324–36.
- [23] Golub GH, van Loan CF. Matrix computations. 3rd ed. Baltimore: The Johns Hopkins University Press; 1996.
- [24] The Mathworks Inc.: Matlab version r2010b; 2010.
- [25] LAPACK – Linear Algebra Package; 2010. <http://www.netlib.org/lapack/>.
- [26] Sweet AA. Designing bipolar transistor radio frequency integrated circuits. Norwood: Artech House; 2008.
- [27] Demir A, Roychowdhury J. A reliable and efficient procedure for oscillator ppv computation, with phase noise macromodeling applications. *IEEE Trans Computer-Aided Design Integr Circuits Syst* 2003;22(February (2)):188–97.
- [28] Stoer J, Bulirsch R. Introduction to numerical analysis. 3rd ed. New York: Springer-Verlag; 2002.
- [29] Meyer CD. Matrix analysis and applied linear algebra. SIAM: Society for Industrial and Applied Mathematics; 2000.

**Fabio L. Traversa** was born in Bari, Italy, in 1979. He received the Laurea degree in Nuclear Engineering, and the PhD degree in Physics from Politecnico di Torino, Italy, in 2004 and 2008, respectively. During 2008 he was a researcher fellow with the Electronics Department of the same institution, and since 2009 he is a Postdoctoral researcher at the Departament d'Enginyeria Electrònica, Universitat Autònoma de Barcelona, Spain. His research interests are mainly devoted to the physics-based simulation of transport in nano-devices, with special emphasis on the analysis and simulation of quantum correlations. Furthermore, he is also interested into the stability analysis of nonlinear circuits and systems, and into the noise analysis of nonlinear circuits.

**Fabrizio Bonani** was born in Torino, Italy, in 1967. He received the Laurea degree, *cum laude*, and the PhD degree in Electronic Engineering from Politecnico di Torino, Italy, in 1992 and 1996, respectively. Since 1995 he has been with the Electronics Department of the same institution, where he currently is an Associate Professor of Electronics. His research interests are mainly devoted to the physics-based simulation of semiconductor devices, with special emphasis on the noise analysis of field-effect and bipolar transistors, to the thermal analysis of power devices and circuits, and to the simulation and design of power semiconductor devices. He is also interested into the stability analysis of nonlinear circuits and systems, and into the noise analysis of nonlinear circuits.

From October 94 to June 95 he has been with the ULSI Technology Research Department of Bell Laboratories in Murray Hill (NJ) as a consultant, working on physics-based noise modelling of electron devices. From August to October 2008 he was Visiting Scientist at the Ferdinand-Braun-Institut für Höchstfrequenztechnik, Berlin, Germany, developing compact noise models for linear and nonlinear applications.

Prof. Bonani is Senior Member of IEEE, and the vice-chair of the MTT-14 Technical Committee on Low-Noise Techniques. He serves in the Modeling and Simulation committee of the International Electron Device Meeting for years 2010–2011.